Università di Foggia

Corso di Dottorato in
Scienze e Tecnologie innovative per la salute e l'invecchiamento attivo
XXXVIII ciclo

PRECISION MEDICINE FOR HEAD AND NECK CANCER

Chemosensitivity guided therapy and emerging therapeutic agents

Tutor
Prof. Giorgio Mori

Dottoranda
Dott.ssa Francesca Spirito

Anno Accademico 2024/2025

HEAL ITALIA – Health Extended Alliance for Innovative Therapies, Advanced Lab-research and Integrated Approaches of Precision Medicine - Tematica di Ricerca: "Prevention Strategies" - CUP D73C22001230006, ammesso a finanziamento a valere sull'Avviso D.D. n. 341/2022 Investimento 1.3 - Avviso "Partenariati Estesi"

PRECISION MEDICINE FOR HEAD AND NECK CANCER: CHEMOSENSITIVITY GUIDED THERAPY AND EMERGING THERAPEUTIC AGENTS

INDEX

ABSTRACT

Head and neck squamous cell carcinoma (HNSCC) is the 6th common malignancy worldwide, and it is characterized by high recurrence and mortality rates. Despite advances in diagnosis

and treatment, the five-year survival rate remains poor. Precision medicine approaches integrating functional assays, molecular profiling, and novel therapeutic agents represent a promising strategy to overcome treatment resistance and improve therapeutic decision-making.

This thesis aimed to develop and evaluate an integrated precision-oncology framework for HNSCC combining functional chemosensitivity testing, transcriptomic profiling, and preclinical evaluation of bioactive compounds. Patient-derived tumor samples were used to establish primary cultures of bulk tumor cells and cancer stem cell (CSC)–enriched populations.

For functional drug testing, biopsy specimens were divided into diagnostic and research samples. Primary cultures and CSC-enriched spheroids were generated using a rotating bioreactor and exposed to standard chemotherapeutic agents, with cell viability assessed to determine patient-specific drug sensitivity. Transcriptomic profiling was performed using bulk mRNA sequencing, followed by differential expression and pathway enrichment analyses to identify transcriptional programs associated with CSCs and therapeutic resistance.

The therapeutic potential of two bioactive compounds was investigated. Polydatin was tested on HNSCC cells and healthy gingival cells to assess effects on viability and oxidative stress. Benzyl Isothiocyanate (BITC) was evaluated as a chemosensitizing agent in therapy-resistant HNSCC cell lines treated with cisplatin and radiotherapy, with analyses of apoptosis, reactive oxygen species modulation, and mitochondrial function.

Chemosensitivity assays revealed inter-patient variability within CSC populations. Transcriptomic analyses demonstrated differences between 2D and 3D cultures, with CSC-enriched models activating pathways related to stemness and aggressiveness. Polydatin selectively reduced tumor cell viability while sparing healthy cells, whereas BITC enhanced

sensitivity to chemo-radiotherapy. Overall, these findings support the translational potential of precision medicine approaches for improving therapeutic efficacy and reducing treatment-related toxicity in HNSCC.

1. BACKGROUND

1.1 Head and neck cancer

Head and neck squamous cell carcinoma (HNSCC) comprises a heterogeneous group of epithelial malignancies arising from the mucosal surfaces of the upper aerodigestive tract. These tumors originate from the stratified squamous epithelium lining the oral cavity, pharynx, larynx, lips, sinonasal tract, and, less frequently, the salivary glands.[1] Collectively, head and neck cancers represent a major global health burden, accounting for 800,000 new cases diagnosed worldwide annually.[2]

Approximately 90% of head and neck malignancies are classified as squamous cell carcinomas, reflecting their common epithelial origin.[1]

HNSCC is characterized by high incidence, significant morbidity, and poor clinical outcomes. A major clinical challenge lies in the fact that many patients are diagnosed at advanced stages of disease, when tumors have already acquired aggressive features and therapeutic options are limited. Consequently, prognosis remains unfavorable[3], with five-year survival rates that have shown only modest improvement over recent decades despite advances in treatments.[2,4] High rates of local recurrence, regional lymph node metastasis, and treatment resistance further contribute to the substantial mortality associated with this disease.[5]

This complex clinical behavior reflects the intrinsic biological heterogeneity of HNSCC, which encompasses diverse cellular subpopulations, adaptive survival mechanisms, and variable responses to therapy.[6] Understanding the shared and distinct features of HNSCC across anatomical sites is therefore essential for the development of more effective, personalized therapeutic strategies.[7]

1.1.1 Epidemiology

HNSCC predominantly affects older adults, with the highest incidence observed in the fifth and sixth decades of life.[8] However, epidemiological trends over recent decades indicate a concerning increase in incidence among younger populations, particularly among caucasian women aged between 18 and 44 years. This shift suggests evolving etiological patterns and highlights the dynamic nature of HNSCC epidemiology.[9]

Historically, HNSCC has shown a strong male predominance, with a male-to-female incidence ratio of approximately 2:1 across most ethnic groups. Nevertheless, this gender gap has progressively narrowed over the past fifty years, largely attributable to increased exposure of women to established risk factors such as tobacco use and alcohol consumption.[10,11] These changes underscore the influence of sociocultural and behavioral factors on disease distribution.

At a global level, head and neck cancers (HNCs) represent a substantial public health burden. According to GLOBOCAN 2022 estimates, HNC accounted for approximately 940,000 new cases and 480,000 deaths worldwide, ranking as the seventh most prevalent type of cancer globally in terms of incidence and mortality.[10,11] The geographic distribution of HNSCC is highly heterogeneous, reflecting regional differences in lifestyle, environmental exposures, and socioeconomic factors. High incidence rates have been reported in the Indian subcontinent, where betel quid

chewing and smokeless tobacco use are widespread, accounting for up to 80% of all HNSCC cases.[2,12]

In the United States, HNSCC accounts for approximately 3–4% of all cancer diagnoses and nearly 2% of cancer-related deaths. Although advancements in diagnostic techniques and therapeutic strategies have been achieved, more than 60% of patients continue to present with locally or regionally advanced disease at the time of diagnosis. [4] As a result, overall survival rates have shown only marginal improvement over the past three decades. Patients with locally advanced, recurrent, or metastatic HNSCC face a particularly poor prognosis, with median survival ranging from 6 to 15 months despite multimodal treatment approaches. [13]

In Italy, epidemiological data indicate a substantial disease burden, with approximately 2.343 new head and neck cancer diagnoses estimated in 2024, the majority occurring in men.[14] Mortality remains high, with over 4,000 deaths reported annually. [15] Incidence rates are notably higher in northern regions compared to central and southern areas, a distribution likely influenced by industrial exposure patterns and lifestyle-related risk factors. Current estimates indicate a five-year survival rate of 13% in men and 22% in women.[14] This picture remains unsatisfactory and emphasizes the urgent need for improved prevention, early detection, and more effective therapeutic strategies.

Overall, the persistent high incidence, late-stage diagnosis, and limited survival gains associated with HNSCC underscore the substantial clinical burden of this disease. These epidemiological challenges provide a strong rationale for the development of innovative, personalized treatment approaches aimed at improving patient outcomes and reducing disease-related mortality.

1.1.2 Etiology and risk factors

HNSCC arises through a complex, multifactorial process involving the interaction of environmental, behavioral, infectious, and host-related factors.[1] Although tobacco use and alcohol consumption remain the most significant and well-established risk factors for HNSCC development, increasing evidence highlights the contribution of additional etiological agents, underscoring the biological heterogeneity of the disease.[16]

Tobacco

Tobacco smoking is the single most important risk factor for HNSCC and has been unequivocally classified as carcinogenic to humans by the International Agency for Research on Cancer (IARC).[17,18] Epidemiological studies indicate that up to 80% of patients diagnosed with oral squamous cell carcinoma (OSCC), and a substantial proportion of HNSCC overall, are current or former smokers.[16] The risk of developing HNSCC is strongly dose-dependent, with heavy smokers exhibiting a markedly increased risk compared to moderate smokers, and individuals consuming large quantities of cigarettes daily showing a 5–25-fold increased risk compared to non-smokers.[10]

The carcinogenic effects of tobacco are primarily mediated by combustion-derived compounds, including nitrosamines, polycyclic aromatic hydrocarbons such as benzo[a]pyrene, and aromatic amines.[19] These substances act as pro-carcinogens that undergo metabolic activation by oxidative enzymes, generating reactive intermediates capable of forming covalent DNA adducts and inducing mutagenic lesions.[20] In addition to these genotoxic effects, nicotine and its metabolites have been shown to exert pro-tumorigenic activity by activating nicotinic acetylcholine

receptors, thereby stimulating signaling pathways involved in cell proliferation, survival, and angiogenesis.[21]

Nicotine-mediated activation of epidermal growth factor (EGF) release and subsequent epidermal growth factor receptor (EGFR) signaling promotes mitogenic and anti-apoptotic pathways, while the induction of catecholamine release leads to β-adrenergic receptor activation and further amplification of oncogenic signaling cascades.[22] Moreover, activation of nicotinic receptors has been implicated in the induction of epithelial-to-mesenchymal transition (EMT), a process associated with enhanced migratory capacity, invasive behavior, and acquisition of malignant phenotypes.[23] Beyond chemical carcinogenesis, thermal irritation of the mucosa caused by tobacco smoke may act as a cofactor in tumor initiation, as suggested by the markedly increased risk observed in populations practicing reverse smoking.[24] Smokeless and chewing tobacco products are also strongly associated with site-specific HNSCC development, particularly in regions of direct mucosal contact.[17]

Alcohol

Alcohol consumption represents a major independent risk factor for HNSCC and acts synergistically with tobacco, resulting in a multiplicative rather than additive increase in cancer risk.[25] Epidemiological data suggest that the combined exposure to tobacco and alcohol can increase the risk of oral cancer by up to 100-fold, with heavy smokers and drinkers experiencing a substantially higher incidence than expected from the individual effects of either agent alone.[26]

Ethanol contributes to carcinogenesis through both local and systemic mechanisms. Locally, alcohol increases the permeability of the oral mucosa by disrupting epithelial

lipid components, leading to epithelial atrophy and facilitating the penetration of tobacco-derived carcinogens. Systemically, chronic alcohol abuse impairs innate and adaptive immune responses, increasing susceptibility to infections and malignant transformation.[27] Furthermore, acetaldehyde, the primary metabolite of ethanol, is classified as a carcinogenic compound due to its ability to form DNA adducts and interfere with DNA repair mechanisms, thereby promoting genomic instability.[28]

Other Etiological Factors

In addition to tobacco and alcohol, several other factors contribute to HNSCC pathogenesis. Human papillomavirus (HPV) infection, particularly with high-risk oncogenic strains such as HPV-16 and HPV-18, plays a pivotal role in a distinct subset of HNSCC, predominantly affecting the oropharynx.[29] HPV-positive HNSCCs most commonly arise in the tonsils and base of the tongue and account for up to 75% of oropharyngeal squamous cell carcinomas, while HPV-driven tumors are relatively rare in non-oropharyngeal sites.[29]

Other infectious agents have been proposed as potential contributors to oral carcinogenesis, including Herpes Simplex Virus (HSV) and Epstein–Barr Virus (EBV). Elevated EBV titers have been reported in a high proportion of patients with oral cancer and in individuals presenting with potentially malignant oral disorders.[30] Fungal infections, particularly those caused by Candida albicans, have also been associated with malignant transformation of the oral mucosa. Several mechanisms have been proposed to explain Candida-mediated carcinogenesis, including chronic inflammation, production of carcinogenic metabolites, and induction of epithelial dysplasia.[31]

Additional predisposing factors include nutritional deficiencies, such as inadequate intake of vitamins C and E, carotenoids, vitamin A, riboflavin, folates, and iron, as well as exposure to ultraviolet radiation, particularly in lip carcinomas.[32] Immunosuppressive conditions, including HIV infection, further increase the risk of HNSCC development by impairing immune surveillance and facilitating oncogenic viral persistence.[33]

1.1.3 Tumor heterogeneity and disease progression

HNSCC is characterized by marked clinical and biological heterogeneity, reflected in its variable patterns of presentation, progression, metastatic behavior, and therapeutic response. This heterogeneity represents a major challenge in disease management and contributes significantly to differences in therapeutic response and clinical outcome among patients. [33]

Recent transcriptomic and integrative genomic analyses have further demonstrated that HNSCC can be stratified into distinct molecular subtypes, each defined by specific signaling pathway activation, immune landscape features, metabolic programs, and predicted drug sensitivities. These molecular classifications suggest that HNSCC does not consist of discrete, unrelated subtypes, but rather reflects a biological continuum of disease evolution. At one end of this spectrum, tumors retain features closer to the normal epithelium, including preserved differentiation programs and partial immune activation. Progressively, tumors acquire proliferative, metabolic, and migratory traits, eventually transitioning toward highly mesenchymal, stem-like, hypoxic, and therapy-resistant phenotypes.[34] This gradual shift reflects increasing biological aggressiveness and loss of epithelial identity. Importantly, these biologically distinct subgroups are not

fully captured by traditional clinicopathological parameters, underscoring the need for molecular and functional approaches to better guide therapeutic decision-making.

1.1.4 Current Therapeutic Strategies and Limitations

Despite significant advances in diagnostic techniques and therapeutic strategies, the prognosis of patients affected by HNSCC remains poor. Early diagnosis continues to represent the most critical determinant of improved survival and clinical outcome; however, a substantial proportion of patients are still diagnosed at advanced stages of disease, when treatment efficacy is limited and morbidity is high.[35]

The current therapeutic management of HNSCC relies on a multimodal approach that includes surgical resection, radiotherapy, and systemic therapy. Platinum-based chemotherapy, most commonly cisplatin, alone or in combination with agents such as carboplatin, 5-fluorouracil, paclitaxel, or docetaxel, represents the backbone of systemic treatment.[36] Treatment strategies may involve a single modality or a combination of approaches, depending on tumor site, size, stage, lymph node involvement, and presence of distant metastases, as well as patient-related factors such as comorbidities, nutritional status, performance status, and treatment tolerance.[37]

In early-stage disease (stages I–II), surgical resection remains the gold standard of care and is often associated with favorable local control rates.[38] Nevertheless, adjuvant radiotherapy, with or without concomitant chemotherapy, is frequently required based on the presence of adverse pathological features.[39] Non-surgical approaches may be preferred in selected cases where surgery is expected to result in significant functional impairment or unacceptable cosmetic outcomes.[40] Elective neck dissection is

commonly recommended in patients with clinically evident lymphadenopathy or a high risk of occult regional metastases.[41]

Locally advanced HNSCC (stages III–IV) typically necessitates combined treatment strategies, often involving surgical resection followed by adjuvant radiotherapy or concurrent chemoradiotherapy.[42] The choice of postoperative treatment is largely driven by unfavorable prognostic factors such as perineural or lymphovascular invasion, extranodal extension, and advanced nodal disease.[43] Radiotherapy may also be employed as a primary treatment modality in selected patients with unresectable tumors or when surgical intervention is contraindicated. For patients who are not eligible for surgery, concurrent chemoradiotherapy represents the current standard of care, while radiotherapy alone may be considered in cases of limited treatment tolerance.[42]

Despite aggressive multimodal treatment, therapeutic success remains limited, particularly in advanced-stage disease.[44] Radiotherapy is highly effective in small, localized tumors, achieving local control in the majority of cases; however, its efficacy progressively declines in advanced tumors. Moreover, conventional treatment strategies are frequently associated with substantial toxicity, high economic costs, and significant long-term functional impairment, profoundly affecting patients' quality of life.[44]

Importantly, treatment decisions are still largely based on clinicopathological parameters and staging systems, which fail to fully account for the biological heterogeneity of HNSCC and the presence of therapy-resistant cellular subpopulations. This limitation contributes to variable treatment responses, high rates of recurrence,

and disease progression, underscoring the urgent need for more personalized and biologically informed therapeutic approaches.

1.2 Cancer Stem Cells (CSCs)

A defining feature of HNSCC, as well as many other solid malignancies, is the presence of marked intratumoral heterogeneity. [45] Tumors are composed of diverse populations of neoplastic cells that differ in their proliferative capacity, differentiation state, invasive behavior, and response to therapy. Traditionally, this heterogeneity has been interpreted through the lens of the clonal evolution model, in which genetic instability and the progressive accumulation of somatic mutations give rise to multiple tumor subclones with variable fitness and adaptability to microenvironmental stimuli.[46]

An alternative and complementary framework has emerged to explain tumor heterogeneity, proposing that cancers are organized as hierarchically structured tissues rather than homogeneous cell populations. According to this model, functional diversity within tumors arises from differentiation processes driven by a distinct subset of cells endowed with stem-like properties.[47] This concept forms the basis of the cancer stem cell (CSC) model, also referred to as the hierarchical model of tumor growth, which contrasts with the purely stochastic view of tumor evolution.

Cancer stem cells are defined by three fundamental properties: long-term self-renewal, the ability to generate heterogeneous progeny through multilineage differentiation, and extensive proliferative potential. These characteristics closely mirror those of normal tissue stem cells, which are responsible for tissue development, maintenance, and regeneration. In physiological settings, stem cell–driven hierarchies are well established, with the hematopoietic system representing the most thoroughly

characterized example, in which rare stem cells give rise to progressively differentiated progenitor and mature cell populations. [49]

Increasing experimental evidence indicates that similar hierarchical organization exists within tumors. In this context, CSCs represent a minor subpopulation capable of sustaining tumor growth and generating phenotypically diverse cancer cell populations, thereby acting as key drivers of intratumoral heterogeneity. Importantly, tumor cell hierarchies are not necessarily fixed.[50] The concept of cellular plasticity has gained prominence, highlighting the ability of non-stem cancer cells to reacquire stem-like properties under specific conditions, such as microenvironmental stress, therapeutic pressure, or genetic and epigenetic alterations. This plastic behavior provides a conceptual bridge between the stochastic and hierarchical models, reconciling genetic evolution with functional organization.[51]

The recognition of CSC-driven hierarchy and plasticity has profound implications for cancer biology and clinical management. By contributing to tumor heterogeneity, therapeutic resistance, and disease recurrence, CSCs have emerged as a critical determinant of treatment failure and poor prognosis. Consequently, understanding CSC biology represents a fundamental step toward the development of more effective, personalized therapeutic strategies, particularly in highly heterogeneous and treatment-refractory tumors such as HNSCC.[52]

1.2.1 Evolution of CSCs model

The cancer stem cell (CSC) hypothesis originates from early concepts of tumor formation dating back to the late nineteenth century. The so-called “embryonal rest hypothesis,” proposed by Rudolf Virchow and Julius Cohnheim, postulated that tumors

could arise from residual embryonic cells that persist in adult tissues and later undergo malignant transformation. Although speculative at the time, this hypothesis laid the conceptual groundwork for the idea that a distinct subset of cells may be responsible for tumor initiation and maintenance. [53]

More than a century later, pivotal experimental evidence supporting cellular hierarchy emerged from studies of the hematopoietic system. In 1961, Till and McCulloch demonstrated the existence of hematopoietic stem cells through clonal assays, providing the first functional proof that a rare population of cells possessed self-renewal and multilineage differentiation capacity.[54] In the same year, Southam and Brunschwig reported that tumor formation following subcutaneous injection of cancer cells into patients occurred only when very large numbers of cells were administered, suggesting that only a small fraction of tumor cells possessed tumor-initiating potential [55]

Subsequent experimental studies reinforced this concept. Transplantation assays in murine lymphoma models revealed that only 1–4% of transplanted cells were capable of forming colonies in recipient spleens. [56] In the 1970s, similar observations were extended to solid tumors. Hamburger and Salmon demonstrated that, in cancers of the lung, ovary, and brain, only one in 1,000 to one in 5,000 isolated tumor cells was capable of forming colonies in vitro. [57] These findings collectively indicated that tumor cell populations are functionally heterogeneous and that only a minority of cells possess extensive proliferative and tumorigenic capacity. [56]

A major breakthrough occurred in 1994, when Lapidot and colleagues provided the first direct evidence of cancer stem cells in human malignancy by identifying leukemia-

initiating cells in acute myeloid leukemia through transplantation of a phenotypically defined subpopulation into immunodeficient mice. They further demonstrated that leukemia-initiating cells were exceedingly rare in patient samples. [58] This concept was definitively validated in 1997 by Bonnet and Dick, who showed that leukemic stem cells expressing a $CD34^{+}CD38^{-}$ phenotype were capable of recapitulating the full cellular heterogeneity of acute myeloid leukemia upon transplantation into immunodeficient mice, fulfilling the functional criteria of stemness. [59]

The CSC hypothesis was subsequently extended to solid tumors. In 2003, Al-Hajj and colleagues identified a tumor-initiating cell population in breast cancer, while Singh and coworkers demonstrated self-renewing, stem-like cells in brain tumors using in vitro assays. [60,61] Over the past decade, CSCs have been identified and isolated in a wide range of solid malignancies, including cancers of the lung, colon, prostate, pancreas, and the head and neck region. Collectively, these studies support the concept that tumor growth and maintenance are driven by a subpopulation of CSCs endowed with long-term self-renewal capacity and tumor-initiating potential.

More recent evidence has further refined this model by demonstrating that stem-like properties can be acquired by non-CSC populations within tumors. Experimental studies using primary tumor-derived cell lines have shown that differentiated cancer cells can regain self-renewal capacity under specific genetic, epigenetic, or microenvironmental conditions. These findings have contributed to reconciling the CSC model with the clonal evolution hypothesis, suggesting that tumor progression is driven by both hierarchical organization and dynamic cellular plasticity. [56]

Together, these observations have reshaped the understanding of tumor biology, establishing CSCs as key drivers of intratumoral heterogeneity, disease progression, and therapeutic resistance. This evolving conceptual framework provides the biological basis for investigating CSC-targeted strategies and functional precision medicine approaches in head and neck squamous cell carcinoma.

1.2.2 Percentage of CSCs and heterogeneity of the tumor

The actual frequency of CSCs within tumors remains a subject of ongoing debate. Early studies across multiple cancer types suggested that CSCs represent a rare subpopulation, often accounting for less than 1–2% of the total tumor cell mass. In this context, CSCs were initially described as a highly restricted fraction of tumor cells uniquely endowed with tumor-initiating capacity.[62]

Key studies in colorectal cancer supported this view. O'Brien and colleagues demonstrated that only one $CD133^+$ cell out of approximately 5.7×10^4 unselected human colon cancer cells was capable of initiating tumor formation following xenotransplantation into immunodeficient mice.[63] Similarly, Todaro et al. reported that approximately 2% of $CD133^+$ cells were responsible for tumor initiation in human colon cancers and exhibited enhanced resistance to conventional therapies, reinforcing the notion of CSCs rarity coupled with therapeutic resistance. [62]

However, subsequent studies challenged the concept that tumor-initiating cells are universally rare. In murine models of leukemia and lymphoma, Kelly et al. demonstrated that tumor-initiating capacity was present in a substantially larger fraction of cancer cells, with at least one in ten cells capable of generating tumors in syngeneic

recipients.[64] In solid tumors, Boiko and colleagues identified $CD271^+$ cells as melanoma stem cells and reported highly variable CSCs frequencies across patients, ranging from 2.5% to as high as 41%.[65]

These findings indicate that CSCs frequency is not a fixed parameter but rather a dynamic feature that varies according to tumor type, disease stage, genetic background, and experimental context. Differences in CSCs abundance may also reflect methodological variables, including the choice of surface markers, tumor dissociation procedures, and transplantation models. Importantly, high CSC frequency does not necessarily contradict the hierarchical model but instead underscores the functional heterogeneity and plasticity of tumor cell populations.[66]

1.2.3 Marker-Based Identification of CSCs: Strengths and Limitations

CSCs have traditionally been identified and characterized through the expression of specific molecular markers, whose selection varies according to tumor type and tissue of origin.[67] To date, no single marker has been shown to unequivocally and universally define CSCs, and accumulating evidence suggests that CSCs exist as overlapping and partially interconvertible subpopulations within a hierarchical and dynamic tumor ecosystem. Consequently, CSCs identification has often relied on the combined use of multiple markers rather than on individual molecular signatures.[68]

In HNSCC, a wide range of putative CSC markers has been described. These include surface proteins such as CD44, CD24, CD133, and c-MET, intracellular enzymes such as aldehyde dehydrogenase (ALDH), and regulatory proteins including Musashi-1.[69] In addition, CSC populations have been shown to express transcription factors classically associated with embryonic stem cell (ESC) pluripotency, such as OCT4, SOX2, and

NANOG. The expression of these markers has been correlated with key CSC-associated properties, including self-renewal capacity, tumor initiation, metastatic potential, and resistance to chemotherapy and radiotherapy.[70]

ESC-associated transcription factors play a central role in maintaining stemness and pluripotency. OCT4, SOX2, and NANOG form a tightly regulated transcriptional network that sustains the undifferentiated state of embryonic stem cells and has been shown to be aberrantly activated in several solid tumors, including HNSCC. [71] In HNSCC, increased expression of these factors has been detected in tumor tissues and peritumoral regions and has been associated with stem-like phenotypes, epithelial–mesenchymal transition (EMT), and aggressive tumor behavior. However, their prognostic significance remains controversial, with some studies reporting associations with early disease stage or improved survival, underscoring the context-dependent nature of marker expression.[72]

Similarly, surface markers commonly used to identify CSCs exhibit significant heterogeneity. CD44, one of the most extensively studied CSC markers in epithelial malignancies, has been associated with poor prognosis, locoregional recurrence, and radioresistance in HNSCC, particularly when specific isoforms such as CD44v6 are expressed.[73] Combinatorial phenotypes, including CD44^high/CD24^low, have been linked to enhanced stemness and EMT features. CD133 expression has been correlated with tumor aggressiveness, disease progression, and poor clinical outcome, while Musashi-1 and ALDH1 expression have been associated with advanced tumor stage, lymph node metastasis, and malignant transformation of potentially premalignant lesions.[74] Overexpression of c-MET has also been implicated in CSC maintenance, angiogenesis, invasion, and unfavorable prognosis across multiple tumor types.[75]

Despite the extensive characterization of CSC-associated markers, several limitations constrain their clinical and experimental utility. Marker expression is often heterogeneous within tumors, varies across disease stages, and can be influenced by microenvironmental conditions and therapeutic pressure. Moreover, many markers associated with CSCs are not exclusive to stem-like tumor cells but are also expressed by normal stem cells or differentiated tumor populations, reducing their specificity. Importantly, marker expression alone does not necessarily reflect functional stemness, tumor-initiating capacity, or therapeutic resistance.[76]

These limitations have increasingly shifted attention toward functional approaches for CSC identification, which focus on biological properties such as self-renewal, survival under stress conditions, three-dimensional growth capacity, and resistance to cytotoxic treatments. In this context, marker-based strategies are now regarded as complementary rather than definitive tools for CSC characterization. Functional selection methods, including three-dimensional culture systems and bioreactor-based models, offer the advantage of enriching for CSC-like populations based on their intrinsic biological behavior rather than predefined molecular labels.[77]

1.2.4 CSCs Enrichment through 3D Culture Systems and Bioreactor-Based Models

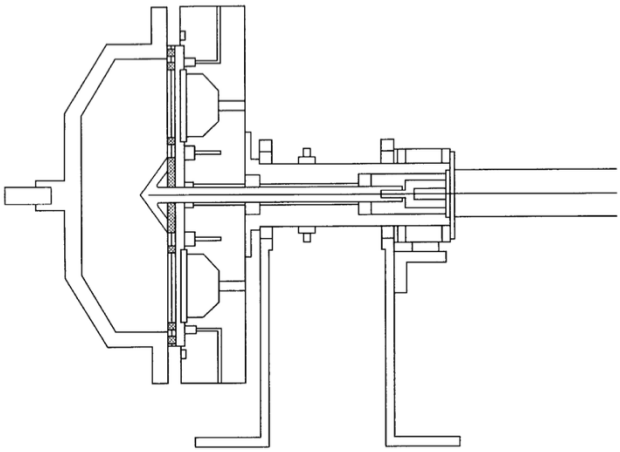

Figure 1. Hydrodynamic Focusing Bioreactor (HFB)

Functional approaches for the enrichment and study of CSCs have gained increasing relevance, particularly in light of the limitations associated with marker-based identification strategies. Among these approaches, three-dimensional (3D) culture systems and bioreactor-based models provide biologically relevant environments that allow selective survival and expansion of tumor cell subpopulations with stem-like properties.[78]

A hydrodynamic focusing bioreactor (HFB) (**Figure 2**), originally developed by the National Aeronautics and Space Administration (NASA) at the Johnson Space Center, represents an advanced platform for the functional selection of CSCs. The HFB consists of a rotating, fluid-filled culture chamber that generates a low-shear, suspension-based environment through hydrodynamic focusing. Unlike conventional static or adherent culture systems, this configuration minimizes shear stress and mechanical forces that can influence cell morphology, adhesion, and biomechanical properties, thereby preserving intrinsic cellular phenotypes.

The bioreactor generates a dynamically controlled hydrodynamic force that regulates the movement, spatial distribution, and retention of cells within the culture chamber while facilitating the removal of air bubbles and cellular debris. When combined with appropriate culture conditions, this system enables selective pressure based on functional cellular traits rather than predefined molecular markers. In this context, cells capable of surviving, self-organizing, and proliferating under non-adherent, low-shear conditions are preferentially maintained, while more differentiated tumor cells undergo apoptosis.

Previous studies have demonstrated the ability of the HFB to enrich for CSC-like populations from multiple tumor cell lines, including selective isolation and expansion of $CD133^{+}$ cancer stem cells accompanied by the preferential elimination of $CD133^{-}$ cells.[77] These findings support the concept that bioreactor-based systems can functionally enrich for tumor-initiating, therapy-resistant cell populations by exploiting their intrinsic biological properties rather than surface marker expression alone.

Importantly, bioreactor-based CSC enrichment models recapitulate key features of the tumor microenvironment, including three-dimensional growth, dynamic nutrient and oxygen gradients, and reduced mechanical constraints. As such, they provide a biologically relevant framework for investigating CSC behavior, therapeutic resistance, and treatment response. This functional selection strategy aligns with precision medicine principles by enabling patient-specific characterization of aggressive and treatment-refractory tumor cell populations, thereby offering a robust platform for translational applications.

1.3 Targeting Cancer Stem Cells through Functional Chemosensitivity Testing: the ChemoID Approach

Current treatment protocols for HNSCC are based on combinations of surgical resection of the primary tumor, cervical lymph node dissection, radiotherapy, and systemic chemotherapy. In locally advanced disease, chemotherapy is commonly administered in combination with radiotherapy, particularly in the presence of adverse pathological features such as extranodal lymph node extension. Despite standardized treatment algorithms, patients with tumors of similar stage and grade often exhibit markedly different clinical responses to chemotherapy.[79]

This inter-patient variability represents a major limitation of conventional treatment strategies. Ineffective anticancer therapy not only fails to control disease progression but also exposes patients to unnecessary toxicity and may promote the selection and expansion of therapy-resistant tumor clones. Standard chemotherapeutic regimens for advanced HNSCC typically include platinum-based agents, either as monotherapy or in combination with other cytotoxic drugs or targeted agents such as epidermal growth factor receptor (EGFR) inhibitors. However, the increasing incidence of drug resistance after only a limited number of treatment cycles has emerged as a critical challenge in the management of head and neck cancer. [80]

In recent years, CSCs have been intensively investigated as key contributors to therapeutic resistance, disease recurrence, and metastatic dissemination across multiple tumor types, including HNSCC.[81-85] Although conventional chemotherapy and radiotherapy can effectively eliminate the majority of rapidly proliferating tumor cells, a small fraction of treatment-resistant cells often survives and retains the ability to regenerate the tumor. [86] This residual population is widely believed to be enriched reflecting intrinsic mechanisms

of resistance, including enhanced drug efflux capacity, efficient DNA damage repair, resistance to oxidative stress, and the ability to adopt a quiescent or slow-cycling state. Cellular plasticity further contributes to this phenomenon by enabling dynamic transitions between stem-like and non-stem-like states in response to therapeutic pressure. [86]

Most currently available anticancer treatments primarily target proliferating tumor cells and dominant molecular pathways represented in the bulk tumor population. As a consequence, therapies that fail to effectively target CSCs may result in transient tumor regression without durable disease control, ultimately leading to recurrence. These limitations highlight the need for therapeutic strategies capable of identifying and eliminating CSC-enriched populations in a patient-specific manner.[87]

In this context, functional chemosensitivity testing has emerged as an alternative and complementary approach to molecular profiling. [83-85] The ChemoID® assay is a functional precision oncology platform designed to evaluate the sensitivity of patient-derived tumor cells, including CSC-enriched populations, to clinically relevant chemotherapeutic agents. By directly measuring tumor cell viability following drug exposure, ChemoID captures the integrated effects of genetic, epigenetic, and microenvironmental factors that collectively determine treatment response. [83-85]

A defining feature of the ChemoID approach is its ability to discriminate between bulk tumor cells and CSC-enriched fractions, enabling the assessment of differential drug sensitivity within distinct functional compartments of the same tumor. This strategy provides clinically actionable information that cannot be inferred from conventional staging or biomarker analysis alone and supports individualized therapeutic decision-making. By focusing on the elimination of therapy-resistant CSC populations, functional

chemosensitivity testing aligns with the principles of precision medicine and represents a promising tool for improving treatment efficacy and reducing recurrence in HNSCC.[88]

1.4 Emerging Therapeutic Agents

The limited efficacy of conventional therapeutic strategies in HNSCC, particularly in the context of therapeutic resistance and disease recurrence, has stimulated increasing interest in complementary and adjuvant approaches capable of targeting multiple oncogenic pathways simultaneously.[89] Among these strategies, naturally occurring plant-derived compounds,[90,91] commonly referred to as phytochemicals, have emerged as promising candidates due to their pleiotropic biological activities and favorable toxicity profiles. When used as adjuvants to standard-of-care chemo- and radiotherapy regimens, phytochemicals may enhance anticancer efficacy by modulating diverse cellular processes involved in tumor survival, adaptation, and resistance.[92]

Acquired chemoresistance and metastatic progression are driven by complex and interconnected molecular mechanisms, often involving oxidative stress regulation, metabolic reprogramming, and activation of compensatory survival pathways. In this context, phytochemicals offer a unique advantage by acting on multiple signaling cascades rather than on a single molecular target, thereby limiting tumor cell plasticity and adaptive escape mechanisms.[93]

Benzyl Isothiocyanate (BITC)

Benzyl isothiocyanate (BITC) is a bioactive phytochemical generated through the hydrolysis of glucotropaeolin, a glucosinolate abundantly present in cruciferous vegetables such as mustard, watercress, broccoli, cabbage, and cauliflower.[94] Isothiocyanates are well-

established chemopreventive agents that have demonstrated potent anticancer activity in a wide range of preclinical models, inhibiting tumorigenesis induced by chemical carcinogens in multiple organs, including lung, colon, liver, pancreas, and mammary tissue.[95]

Mechanistically, isothiocyanates exert dual effects by modulating xenobiotic metabolism and redox homeostasis. They inhibit phase I metabolic enzymes while activating phase II detoxification pathways in healthy tissues, thereby reducing carcinogen-induced damage. In contrast, in cancer cells characterized by elevated basal levels of reactive oxygen species (ROS), isothiocyanates induce excessive oxidative stress, pushing redox balance beyond a tolerable threshold and ultimately triggering cell death.[96]

BITC, in particular, has attracted significant interest as an adjuvant anticancer agent due to its ability to selectively impair tumor cell viability, reduce stemness-associated features, and induce apoptosis.[97] Previous studies, including work from our laboratory, have demonstrated that BITC inhibits migration and invasion of HNSCC-derived cell lines and enhances the cytotoxic effects of conventional chemotherapeutic agents such as cisplatin.[98] At the molecular level, BITC promotes ROS accumulation, leading to oxidative damage of DNA, proteins, and mitochondrial structures, resulting in cell cycle arrest at the G2/M phase and activation of apoptotic pathways.[99]

Polydatin

Polydatin (Pol), the glycosylated form of resveratrol, is an oligostilbene found at high concentrations in the roots of *Polygonum cuspidatum*. Structurally, Pol differs from resveratrol by the presence of a glucoside moiety at the C-3 position, a modification that

enhances its solubility, bioavailability, and metabolic stability, potentially improving its therapeutic efficacy.[100]

Polydatin has been widely studied in both in vitro and in vivo models, where it has demonstrated pleiotropic pharmacological activities, including modulation of oxidative stress, regulation of inflammatory responses, and inhibition of oncogenic signaling pathways. Its antitumor effects have been associated with the regulation of reactive oxygen species and suppression of pathways involved in tumor growth and survival, such as the PI3K/AKT signaling axis. Consistent with these mechanisms, Pol has been shown to induce apoptosis and inhibit proliferation in several malignancies, including hepatocellular carcinoma, osteosarcoma, breast cancer, cervical cancer, and lung cancer.[101]

Despite these promising findings, the role of Polydatin in HNSCC remains largely unexplored. HNSCC cells are characterized by pronounced metabolic plasticity and a strong reliance on glycolytic metabolism to sustain proliferation and survival.[102] Based on these features, Polydatin represents a particularly attractive candidate for targeting metabolic vulnerabilities in HNSCC. By promoting oxidative metabolism and interfering with tumor-specific metabolic adaptations, Pol may disrupt cellular homeostasis and sensitize cancer cells to therapeutic stress.

Taken together, the multitargeted biological activity, favorable pharmacokinetic properties, and low toxicity of BITC and Polydatin support their investigation as emerging therapeutic agents in HNSCC. Their integration with functional chemosensitivity testing and CSC-focused approaches offers a rational framework for the development of personalized, mechanism-driven therapeutic strategies aimed at overcoming resistance and improving clinical outcomes.

1.5 Scope and Objectives of the Study

The increasing biological complexity and therapeutic challenge of HNSCC underscore the need for innovative approaches capable of moving beyond conventional, population-based treatment paradigms. Precision medicine strategies that integrate functional assays, molecular profiling, and novel therapeutic agents offer a promising framework for addressing tumor heterogeneity, treatment resistance, and inter-patient variability in therapeutic response.

The overall objective of this doctoral thesis was to develop and evaluate an integrated precision-oncology framework for HNSCC by combining functional and molecular approaches with the preclinical investigation of emerging therapeutic agents. Specifically, this work aimed to:

1. Assess patient-specific chemosensitivity by performing functional chemosensitivity testing on both bulk tumor cells and cancer stem cell (CSC)–enriched populations derived from patient tumor samples, in order to evaluate differential drug responses within distinct functional compartments of the same tumor.
2. Characterize transcriptomic differences associated with cellular state and culture conditions by conducting bulk RNA sequencing of patient-derived tumor cultures grown as both bulk tumor cells (two-dimensional (2D) condition) and cancer stem cell (CSC)–enriched populations (three-dimensional (3D) condition), with the aim of identifying molecular pathways linked to stemness, therapeutic resistance, and tumor aggressiveness.
3. Evaluate the therapeutic and chemosensitizing potential of bioactive compounds by performing preclinical studies on Polydatin and Benzyl Isothiocyanate (BITC), investigating their effects on tumor cell viability, oxidative stress, and treatment

response, both as standalone agents and BITC in combination with standard chemotherapeutic and radiotherapeutic modalities.

By integrating functional chemosensitivity testing, transcriptomic profiling, and preclinical evaluation of bioactive compounds, this thesis seeks to provide a comprehensive and biologically informed framework for personalized therapeutic decision-making in HNSCC. Ultimately, this work aims to contribute to the development of precision medicine strategies that can improve treatment efficacy while minimizing toxicity and disease recurrence.

2) Materials and Methods

2.1 ChemoID Patient Selection and Inclusion Criteria

Patients older than 18 years with primary HNSCC were eligible for inclusion in this study. All enrolled patients had not received any neoadjuvant chemotherapy or radiotherapy prior to surgical biopsy. Written informed consent was obtained from all participants, and sample collection was performed in accordance with institutional ethical guidelines.

2.2 Chemotherapeutic Agents

The chemotherapeutic agents evaluated using the ChemoID® assay included both single agents and combination regimens commonly employed in the clinical management of HNSCC. The drugs tested were carboplatin, cisplatin, paclitaxel, 5-fluorouracil, bleomycin, epirubicin, methotrexate, cetuximab, and docetaxel. Drug selection and combinations were guided by standard clinical practice.

2.3 Tumor Biopsy Collection and Sample Shipment

The ChemoID® assay was performed in a CLIA-certified and College of American Pathologists (CAP)-accredited clinical laboratory located in West Virginia, USA. To preserve tissue integrity and minimize contamination, a standardized biopsy collection and shipment protocol was implemented.

Prior to biopsy, the oral cavity was disinfected using chlorhexidine mouth rinses. Biopsy specimens were further decontaminated with a povidone–iodine (Betadine) solution, followed by extensive washing with sterile saline to remove residual disinfectant. Two biopsy samples were collected from each patient under sterile operating room conditions. One specimen was fixed in 10% formalin and submitted to the Department of Pathology at the Azienda Ospedaliera Universitaria “San Giovanni di Dio e Ruggi d’Aragona” (Salerno, Italy) for histopathological diagnosis. The second specimen was prepared for shipment to the ChemoID® clinical laboratory.

In cases of highly contaminated or ulcerated tumors, an alternative sampling method was employed using a trocar inserted through the initial biopsy site to obtain deeper tissue samples while minimizing oral microbial contamination. All samples were placed in sterile vials containing proprietary ChemoID® transport medium and shipped the same day via express courier in temperature-controlled polystyrene containers. To protect samples from airport X-ray exposure, a 2.2-mm lead shield was applied around the transport vial. Samples reached the ChemoID® laboratory within 48 hours of collection and were processed immediately upon arrival.

2.4 Primary Tumor Cell Culture

Primary tumor cell cultures were established from fresh biopsy specimens using a semi-automated dissociation protocol. Tissue samples were processed using a gentleMACS™ Dissociator (Miltenyi Biotec, Auburn, CA) with C-Tubes, combining mechanical dissociation with enzymatic digestion using a 50%/0.025% trypsin and Accutase solution (Innovative Cell Technologies, San Diego, CA).

Dissociated cells were plated in 24-, 12-, or 6-well culture plates and maintained in RPMI-1640 medium supplemented with 5% heat-inactivated fetal bovine serum, 50 U/mL penicillin, and 5 mg/mL streptomycin. Cultures were maintained until subconfluence prior to downstream applications.

2.5 Isolation of Cancer Stem Cell–Enriched Populations

CSC–enriched populations were isolated from primary tumor cultures using a hydrodynamic focusing bioreactor (HFB) developed by the National Aeronautics and Space Administration (NASA) at the Johnson Space Center (Celdyne, Houston, TX). The HFB creates a three-dimensional, low-shear culture environment that mimics microgravity conditions through controlled hydrodynamic focusing.

A defined number of primary tumor cells (2×10^6 cells) were cultured in the bioreactor for 7 days at a rotation speed of 25 rpm with 20% airflow in RPMI medium without supplemental growth factors. Cell viability was assessed using Trypan Blue exclusion. Enrichment of CSC-like populations was verified by monitoring the expression of established CSC-associated markers, including integrin, CD44, and CD133.

2.6 In Vitro Growth and Invasion Assays

To compare biological properties between parental HNSCC cells and CSC-enriched populations, cell proliferation and invasive capacity were assessed. Cell growth rates were determined by seeding 30,000 cells/cm^2 and performing cell counts every 24 hours using Trypan Blue staining. Saturation density was assessed by changing medium daily from day 4 onward and counting cells every 48 hours until growth arrest.

Cell invasiveness was evaluated using Matrigel invasion assays. Transwell inserts were coated with Matrigel and allowed to solidify. Cells were seeded in the upper chamber, and chemoattractant medium was placed in the lower chamber. After incubation, cells migrating through the membrane were fixed, stained with 0.2% crystal violet, and counted in multiple microscopic fields.

2.7 ChemoID® Functional Chemosensitivity Assay

The ChemoID® assay was performed in a CLIA-certified and CAP-accredited clinical laboratory at the Cabell Huntington Hospital and Edwards Cancer Center (West Virginia, USA). Equal numbers of bulk tumor cells and CSC-enriched populations were plated in quintuplicate in 96-well plates and incubated at 37 °C. After 24 hours, chemotherapeutic agents were added either as single drugs or in combination for 1 hour. Media were then replaced, and cell viability was assessed 48 hours later using the MTT assay. Drug efficacy was expressed as a continuous cytotoxic index ranging from <10% to 100% cell death, representing predicted therapeutic effectiveness.
All the test phases are summarized in **Figure 2**.

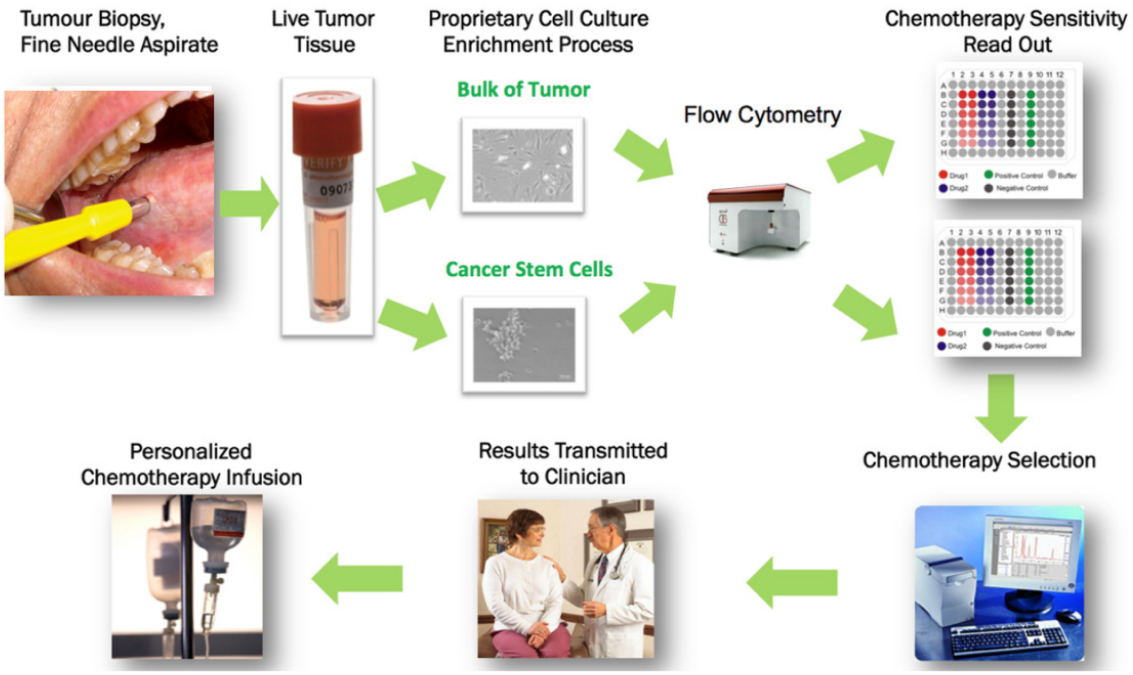

Figure 2. ChemoID test phases.

2.8 ChemoID® Report Generation

Following assay completion, dose–response curves were generated for each drug and drug combination. Results were summarized in a clinical report (**Figure 3**) provided to the treating oncologist, including cytotoxic indices represented graphically using a color-coded system: green (60–100%), yellow (30–60%), and red (<30%).

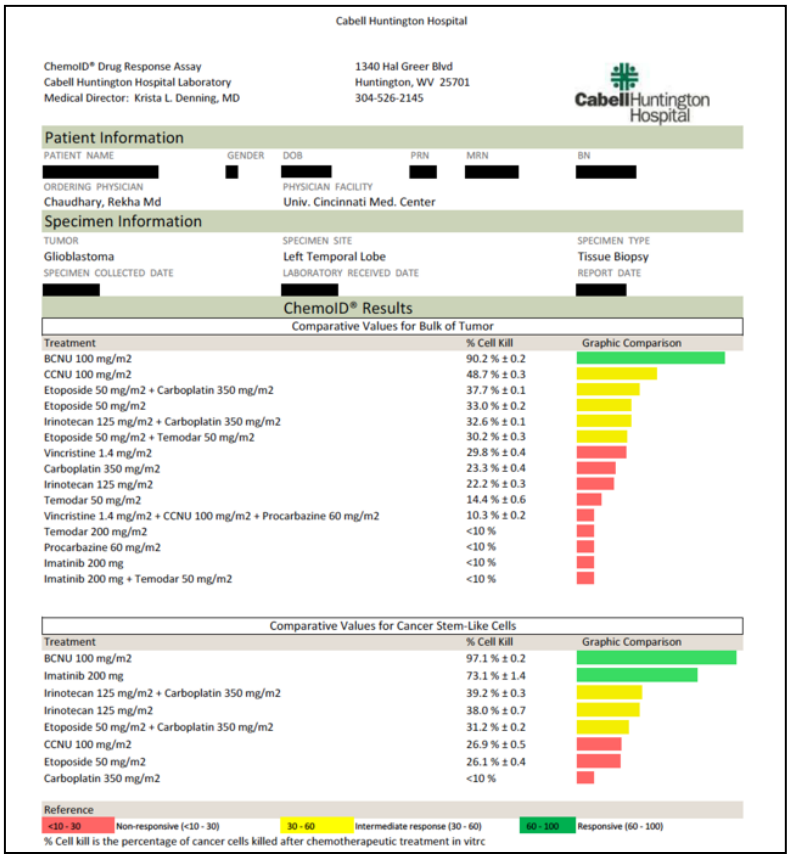

Cabell Huntington Hospital

ChemoID® Drug Response Assay
Cabell Huntington Hospital Laboratory
Medical Director: Krista L. Denning, MD

1340 Hal Greer Blvd
Huntington, WV 25701
304-526-2145

Patient Information

PATIENT NAME	GENDER	DOB	PRN	MRN	BN
[redacted]	[redacted]	[redacted]	[redacted]	[redacted]	[redacted]

ORDERING PHYSICIAN: Chaudhary, Rekha Md
PHYSICIAN FACILITY: Univ. Cincinnati Med. Center

Specimen Information

TUMOR	SPECIMEN SITE	SPECIMEN TYPE
Glioblastoma	Left Temporal Lobe	Tissue Biopsy

SPECIMEN COLLECTED DATE	LABORATORY RECEIVED DATE	REPORT DATE
[redacted]	[redacted]	[redacted]

ChemoID® Results

Comparative Values for Bulk of Tumor

Treatment	% Cell Kill	Graphic Comparison
BCNU 100 mg/m2	90.2 % ± 0.2	
CCNU 100 mg/m2	48.7 % ± 0.3	
Etoposide 50 mg/m2 + Carboplatin 350 mg/m2	37.7 % ± 0.1	
Etoposide 50 mg/m2	33.0 % ± 0.2	
Irinotecan 125 mg/m2 + Carboplatin 350 mg/m2	32.6 % ± 0.1	
Etoposide 50 mg/m2 + Temodar 50 mg/m2	30.2 % ± 0.3	
Vincristine 1.4 mg/m2	29.8 % ± 0.4	
Carboplatin 350 mg/m2	23.3 % ± 0.4	
Irinotecan 125 mg/m2	22.2 % ± 0.3	
Temodar 50 mg/m2	14.4 % ± 0.6	
Vincristine 1.4 mg/m2 + CCNU 100 mg/m2 + Procarbazine 60 mg/m2	10.3 % ± 0.2	
Temodar 200 mg/m2	<10 %	
Procarbazine 60 mg/m2	<10 %	
Imatinib 200 mg	<10 %	
Imatinib 200 mg + Temodar 50 mg/m2	<10 %	

Comparative Values for Cancer Stem-Like Cells

Treatment	% Cell Kill	Graphic Comparison
BCNU 100 mg/m2	97.1 % ± 0.2	
Imatinib 200 mg	73.1 % ± 1.4	
Irinotecan 125 mg/m2 + Carboplatin 350 mg/m2	39.2 % ± 0.3	
Irinotecan 125 mg/m2	38.0 % ± 0.7	
Etoposide 50 mg/m2 + Carboplatin 350 mg/m2	31.2 % ± 0.2	
CCNU 100 mg/m2	26.9 % ± 0.5	
Etoposide 50 mg/m2	26.1 % ± 0.4	
Carboplatin 350 mg/m2	<10 %	

Reference

<10 - 30 Non-responsive (<10 - 30) | 30 - 60 Intermediate response (30 - 60) | 60 - 100 Responsive (60 - 100)

% Cell kill is the percentage of cancer cells killed after chemotherapeutic treatment in vitrc

Figure 3. ChemoID clinical report

2.9 Cell Culture and Sample Preparation for Transcriptomic Analysis

From the panel of the primary tumor cell cultures established from patient biopsies, three representative samples were selected for transcriptomic analysis: patient 9 (612C), patient 5 (547C), and patient 11 (682C). Sample selection was based on culture availability, stability, and expansion capacity under the experimental conditions, ensuring sufficient biological material for downstream genomic analyses.

For each selected sample, cells were expanded under both two-dimensional (2D) (bulk of the tumor) and three-dimensional (3D) (CSCs) culture conditions to allow comparative analysis of transcriptional profiles associated with cellular organization and growth modality.

2.10 Two-Dimensional (2D) Cell Culture Conditions

For 2D cultures, 1×10^6 cells were seeded in duplicate into 100 mm culture dishes containing complete RPMI medium (RPMI-1640 supplemented with 20% fetal bovine serum, 1% penicillin/streptomycin, and 0.1% amphotericin B). Cells were maintained under standard culture conditions (37 °C, 5% CO_2) for 7 days to allow adequate proliferation.

At the end of the culture period, cells were harvested by enzymatic detachment using 0.25% trypsin for 5 minutes. Enzymatic activity was neutralized with complete medium, and cell suspensions were collected for cell counting and viability assessment using Trypan Blue exclusion and a Nexcelom Cellometer system. Following centrifugation (1,000 rpm for 3 minutes), cell pellets were collected and stored at −80 °C until RNA extraction.

2.11 Three-Dimensional (3D) Cell Culture Conditions

For 3D cultures, 2×10^6 cells from each selected sample were seeded into the hydrodynamic focusing bioreactor in complete RPMI medium without the addition of growth factors. Cultures were maintained for 7 days at a rotation speed of 25 rpm with an airflow of 20%, under conditions identical to those used for CSC enrichment.

After the culture period, cells were harvested from the bioreactor, centrifuged (1,000 rpm for 3 minutes), and resuspended in fresh medium for cell counting and viability assessment using Trypan Blue exclusion. Following a second centrifugation step, final cell pellets were collected and stored at −80 °C for transcriptomic analysis.

2.12 RNA Extraction and Bulk mRNA Sequencing

RNA extraction and bulk mRNA sequencing were performed by the Molecular and Genomics Core Facility (MGCF) at the University of Mississippi Medical Center (UMMC).

Total RNA was extracted from frozen cell pellets using the PureLink™ RNA Mini Kit (Invitrogen), following the manufacturer's protocol.

RNA quality control was conducted to assess concentration and integrity, including evaluation of 18S and 28S ribosomal RNA bands and calculation of the RNA Integrity Score (RIS). Only samples with RIS > 8 were considered suitable for sequencing.

Libraries were prepared using the TruSeq Stranded mRNA Library Prep Kit (Illumina, Set-A indexes). Pooled libraries (12–24 samples per pool) were quantified using a Qubit Fluorometer and evaluated for size distribution and quality using the Qiagen QIAxcel Advanced System or Agilent TapeStation. Sequencing was performed on the Illumina NextSeq 2000 platform using a P3 flow cell with paired-end 100 bp reads.

2.13 Sequence Alignment and Differential Gene Expression Analysis

Raw sequencing data underwent quality control using the Illumina BaseSpace Cloud Computing Platform and custom MGCF pipelines. FASTQ files were aligned to the human reference genome (Ensembl/Hg38) using the DRAGEN RNA Pipeline (v3.7.5) or equivalent MGCF workflows.

Differential gene expression analysis was performed using the DRAGEN Differential Expression Application (v3.10.4), which implements the DESeq2 statistical framework. Read counts were normalized across samples, and genes were tested for differential expression between 2D and 3D culture conditions.

To account for multiple hypothesis testing, p-values were adjusted using the Benjamini–Hochberg method to control the false discovery rate (FDR). Genes were considered differentially expressed if they met the following criteria: adjusted p-value (padj) < 0.05 and

absolute $\log_2$ fold change ($|\log_2 FC|$) > 1. Genes with $\log_2 FC > 1$ were classified as upregulated, whereas those with $\log_2 FC < -1$ were classified as downregulated.

2.14 Pathway Enrichment Analysis (PEA)

To investigate the biological significance of differentially expressed genes (DEGs), pathway enrichment analysis (PEA) was performed to identify biological processes and molecular pathways overrepresented among regulated genes. PEA evaluates whether functional gene groups are enriched beyond what would be expected by chance, without implying direct pathway activation or repression.

Lists of significantly upregulated and downregulated genes were analyzed using the EnrichR platform. Gene Ontology (GO) databases were interrogated with a focus on the Biological Process and Molecular Function categories, while Reactome was used to contextualize enriched pathways within curated molecular interaction networks.

Enrichment results were ranked by adjusted p-values, and the top 20 enriched GO terms were visualized as bar plots. Interpretation was based on both the degree of gene overlap and the known biological functions of the contributing genes.

2.15 Gene Set Enrichment Analysis (GSEA)

To complement threshold-based enrichment analyses and capture coordinated transcriptional programs, Gene Set Enrichment Analysis (GSEA) was performed using GSEA v4.3.2 (Broad Institute). Unlike PEA, GSEA evaluates the entire ranked gene list and identifies gene sets that are non-randomly distributed at the extremes of the expression spectrum.

Input files included: (i) a .gct file containing $\log_2$(TPM + 1) expression values, (ii) a .cls file defining experimental conditions (2D vs 3D), (iii) a ranked gene list (.rnk) based on $\log_2$ fold change values, and (iv) a chip annotation file. Analyses were conducted using the Molecular Signatures Database Hallmark gene sets (MSigDB H collection, version 2023.1).

Enrichment results were evaluated using the normalized enrichment score (NES), nominal p-values, and false discovery rate (FDR). Enrichment plots were generated for the most significant gene sets to visualize gene distribution across the ranked expression dataset.

By integrating PEA and GSEA, this study aimed to obtain a comprehensive view of transcriptional alterations associated with culture dimensionality, capturing both strongly regulated pathways and subtle, coordinated gene expression programs.

2.16 Benzyl Isothiocyanate (BITC): Cell Culture, Treatments, and Functional Assays

Cell lines and reagents

Benzyl isothiocyanate (BITC, 98% purity; Cat. No. AC402130250) was purchased from Thermo Scientific Chemicals (Thermo Fisher Scientific, Waltham, MA). Stock solutions of BITC (100 mM) were prepared in dimethyl sulfoxide (DMSO) and diluted in culture medium to a final working concentration of 10 µM. The final DMSO concentration did not exceed 0.01% (v/v) in any experiment. Reduced glutathione (GSH) and cis-diamminedichloroplatinum (II) (cisplatin, CDDP) were purchased from Sigma-Aldrich (St. Louis, MO). Stock solutions of CDDP (1 mg/mL) were prepared in sterile 0.9% saline solution and stored at room temperature in the dark.

Four therapy-resistant HNSCC cell lines were used: HN22 and HN30, derived from primary tumors of the epiglottis and pharynx, respectively, and HN8 and HN31, derived from lymph

node metastases from the same patients. Cell lines were kindly provided by Dr. George Yoo (Karmanos Cancer Center, Wayne State University, Detroit, MI). Cells were maintained as monolayer cultures in Dulbecco's Modified Eagle Medium (DMEM; HyClone, Thermo Scientific) supplemented with 10% fetal bovine serum (FBS), 1% penicillin–streptomycin, and 0.1% amphotericin B, and incubated at 37 °C in a humidified atmosphere with 5% CO_2. Cells were harvested using 0.25% Trypsin–EDTA.

BITC treatment and irradiation protocol

Cells were seeded at a density of 10,000 cells per well in 96-well tissue culture plates in a final volume of 100 µL and allowed to adhere overnight. The following day, culture medium was removed and cells were treated with 10 µM BITC for 1 hour. After treatment, the medium was replaced with fresh complete medium.

For irradiation experiments, plates were placed in a custom-designed in-house phantom system to ensure uniform radiation delivery. The phantom consisted of a water-filled container overlaid with a rice-filled lid to simulate tissue-equivalent scattering conditions. Plates were scanned using a CT simulator (Philips Brilliance Big Bore 16-Slice CT), and radiation planning was performed using the Pinnacle Treatment Planning System (v9.10). Cells were irradiated using a 6 MV photon beam delivered by an Elekta Synergy linear accelerator. Radiation doses of 4 Gy or 8 Gy were administered, while non-irradiated cells served as controls.

Following irradiation, cells were treated with either complete medium alone or medium containing 10 µM cisplatin. After 24 hours, treatment media were removed and replaced

with complete medium. Cell viability and apoptotic responses were assessed at defined time points following treatment.

Cell viability assays

Cell viability following BITC treatment, alone or in combination with radiation and cisplatin, was assessed using multiple complementary assays.

For short- and long-term BITC exposure experiments, cells were seeded at a density of 2.5 × 10^3 cells per well in 384-well plates. Viability was measured using the WST-8 assay (Dojindo Molecular Technologies, Rockville, MD). After incubation with the reagent for 1 hour at 37 °C, absorbance was measured at 450 nm using a SpectraMax M2e plate reader.

For irradiated and combination-treated cells, viability was additionally assessed using the cell-permeant fluorescent probe calcein AM (Thermo Fisher Scientific). Cells were washed with phosphate-buffered saline (PBS) and incubated with 2 μM calcein AM for 45 minutes at room temperature. Fluorescence intensity was measured at excitation/emission wavelengths of 485/530 nm using a SpectraMax M3 spectrophotometer.

Fluorescence imaging

Following fluorescence-based viability measurements, live cells were imaged using an Olympus IX51 fluorescence microscope at 40× magnification to qualitatively assess treatment-induced changes in cell morphology and viability.

Caspase 3/7 activity assay

Apoptotic activity was evaluated by measuring caspase 3/7 activation 72 hours after treatment. Cells were incubated with a caspase 3/7 fluorescent substrate (AAT Bioquest,

Sunnyvale, CA) for 1 hour at room temperature. Fluorescence intensity was measured at excitation/emission wavelengths of 485/530 nm using a SpectraMax M3 spectrophotometer.

As an internal negative control, selected wells received the caspase 3/7 inhibitor Ac-DEVD-CHO (1 μM) 10 minutes prior to substrate addition. Caspase activity was normalized to cell viability values obtained from parallel assays.

Antioxidant rescue experiments

To evaluate the role of oxidative stress in BITC-mediated cytotoxicity, antioxidant rescue experiments were performed using glutathione (GSH). Cells were seeded at 10,000 cells per well in 96-well plates and pretreated with 5 mM GSH for 30 minutes. After pretreatment, cells were exposed to 10 μM BITC for 1 hour. Cell viability was assessed 24 hours later using the WST-8 assay, as described above.

2.17 Polydatin: Cell Culture, Treatments, and Molecular Analyses

Cell lines and reagents

Human oral squamous cell carcinoma cells (HSC2) were used for in vitro experiments. Cells were cultured in Dulbecco's Modified Eagle Medium alpha (DMEM-α; Gibco, Thermo Fisher Scientific, Waltham, MA, USA) supplemented with 10% fetal bovine serum (FBS) and maintained in a humidified incubator at 37 °C with 5% CO_2.

Human gingival fibroblasts (hGF; Lifeline, San Diego, CA, USA) were used as non-tumoral control cells and cultured in Fibroblast Medium (Lifeline) under identical incubation conditions.

Polydatin was kindly provided by Prof. Ravagnan (Institute of Translational Pharmacology, National Research Council of Italy, CNR). The compound was extracted from *Polygonum cuspidatum* following the procedure described in Patent EP1292320B1. Stock solutions were prepared in dimethyl sulfoxide (DMSO) and diluted in culture medium to the desired working concentrations immediately prior to use.

Polydatin treatment and cell viability assay

Cell viability was assessed using the 3-(4,5-dimethylthiazol-2-yl)-2,5-diphenyltetrazolium bromide (MTT) assay (Merck KGaA, Darmstadt, Germany). Cells were seeded in 96-well plates at a density of 5,000 cells per well for HSC2 cells and 15,000 cells per well for hGF cells. After overnight adhesion, cells were treated with Polydatin at concentrations of 250 µM and 500 µM for 24 or 48 hours. Control cells received vehicle (DMSO) alone.

At the end of the treatment period, 10 µL of MTT solution (0.5 mg/mL) was added to each well, followed by incubation for 4 hours at 37 °C. The reaction was stopped by removing the culture medium and adding 100 µL of DMSO to dissolve the formazan crystals. Absorbance was measured at 570 nm using a microplate reader. Cell viability was expressed as a percentage relative to vehicle-treated controls.

RNA extraction and quantitative real-time PCR (qRT-PCR)

Total RNA was extracted from treated and control cells using the RNeasy Mini Kit (Qiagen, Hilden, Germany), following the manufacturer's instructions. RNA concentration and purity were assessed spectrophotometrically. Complementary DNA (cDNA) synthesis was performed using the iScript™ cDNA Synthesis Kit (Bio-Rad, Hercules, CA, USA) according to the manufacturer's protocol, using a Piko 24 thermal cycler (Thermo Fisher Scientific).

Quantitative real-time PCR was carried out using the SsoFast™ EvaGreen Supermix (Bio-Rad) on a CFX96 real-time PCR detection system (Bio-Rad). Amplification was performed for 40 cycles under the following conditions: initial enzyme activation at 95 °C for 30 seconds, followed by denaturation at 95 °C for 5 seconds and annealing/extension at 60 °C for 10 seconds. Primer pairs were designed using Primer-BLAST ([https://www.ncbi.nlm.nih.gov/tools/primerblast/](https://www.ncbi.nlm.nih.gov/tools/primer-blast/))

Gene expression levels were normalized to GAPDH, which was selected as a housekeeping gene due to its stable expression across experimental conditions. Relative gene expression was calculated using the comparative Ct (ΔΔCt) method.

Statistical analysis

Statistical analyses were performed using GraphPad Prism version 9.5 (GraphPad Software, San Diego, CA, USA). Data distribution was assessed using the Shapiro–Wilk test. Results were expressed as median and interquartile range.

For normally distributed data, comparisons between groups were performed using Student's *t*-test or one-way ANOVA followed by Tukey's multiple comparison test. For non-normally distributed data, the Kruskal–Wallis test was used. Differences were considered statistically significant at *p* < 0.05.

3) Results

3.1 Patient cohort included in the ChemoID® study

Based on the predefined eligibility criteria, a total of 11 patients diagnosed with HNSCC were enrolled in this study (**Table 1**) . Patients' age ranged from 47 to 89 years, with a marked predominance of male subjects (10/11 patients), while only one patient was female.

Case	Age	Sex	Site	Origin	Histology	Smoking	Alcohol
1	49	M	Tongue	Mucosa	OSCC	Yes	Yes
2	82	M	Retromolar trigone	Mucosa	OSCC	Yes	Yes
3	78	M	Lower lip	Mucosa	OSCC	Yes	Yes
4	79	M	Alveolar mucosa	Mucosa	OSCC	Yes	Yes
5	61	M	Left anterior tonsillar pillar	Mucosa	OSCC	Yes	Yes
6	50	M	Floor of mouth	Mucosa	OSCC	Yes	Yes
7	75	M	Retromolar trigone	Mucosa	OSCC	Yes	No
8	79	M	Retromolar trigone	Mucosa	OSCC	Yes	No
9	84	F	Tongue	Mucosa	OSCC	No	No
10	47	M	Anterior palatal mucosa	Mucosa	OSCC	Yes	Yes
11	68	M	Maxillary tuberosity	Mucosa	OSCC	Yes	No

Table 1. Patient cohort included in the ChemoID® study

Regarding established risk factors, 10 out of 11 patients were active smokers, and 7 out of 11 reported regular alcohol consumption. In all cases, tumors originated from the oral mucosa, and histopathological evaluation confirmed the diagnosis of oral squamous cell carcinoma.

Tumor localization was heterogeneous across the cohort. The retromolar trigone represented the most frequently involved anatomical site (3/11 cases), followed by the

tongue (2/11 cases). The remaining tumors arose from the alveolar mucosa, anterior palatal mucosa, tuber maxillae, floor of the oral cavity, lower lip, and left anterior tonsillar pillar, each accounting for one case.

Demographic, clinical, and radiographic data were collected from the institutional database of the Department of Oral and Maxillofacial Surgery, San Giovanni di Dio e Ruggi d'Aragona University Hospital (Salerno, Italy).

3.2 ChemoID® assay results in cancer stem cells

The results of the ChemoID® assay performed on cancer stem cells (CSCs) isolated from the tumor biopsies of the 11 OSCC patients are summarized in **Table 2**. The assay evaluated the cytotoxic response of CSCs to a panel of chemotherapeutic agents administered either as single agents or in combination, and results are expressed as the percentage of CSCs killed following treatment. According to predefined thresholds, responses were classified as highly responsive (60–100%), moderately responsive (30–60%), or non-responsive (<30%).

	1	2	3	4	5	6	7	8	9	10	11
Paclitaxel 40 mg/m²	<10%										
Paclitaxel 175 mg/m²	<10%									22,4%	
Carboplatin 70 mg/m²	<10%		<10%	<10%	<10%	<10%	<10%		<10%		
Carboplatin 100 mg/m²	<10%	25.5%	<10%	<10%	<10%	<10%	<10%	18.6%	<10%	11,8%	10.8%
Cisplatin 50 mg/m²	27.0%		52.6%	37.9%	35.3%	67.2%	46.3%		53.4%		
Cisplatin 100 mg/m²	34.2%	73.6%	88.1%	85.3%	42.8%	86.4%	76.8%	78.3%	78.6%	52,1%	42.9%
Docetaxel 75 mg/m²	22.2%	87.4%	29.3%	29.2%	49.2%	54.1%	25.0%	<10%	25.6%	32,0%	<10%
Paclitaxel 40 mg/m²	<10%		32.9%	10.5%	26.2%	<10%	27.9%		<10%		
Paclitaxel 175 mg/m²	<10%	17.1%	26.8%	<10%	46.6%	16.5%	21.0%	55.0%	<10%		<10%

5-Fluorouracil 600 mg/m^2	<10%		<10%	<10%	<10%	<10%	<10%		<10%		
5-Fluorouracil 800 mg/m^2				14.6%	<10%	11.2%	<10%		<10%		
5-Fluorouracil 1000 mg/m^2	<10%	30.0%	<10%	12.5%				28.1%		21,4%	<10%
Bleomycin 15 mg/m^2				<10%				<10%			<10%
Methotrexate 40 mg/m^2										<10%	<10%
Mitomycin 20 mg/m2											25.8%
Cetuximab 400 mg/m^2											<10%
Vinorelbine 25 mg/m^2								26.8%		<10%	
Erlotinib 150 mg								<10%			
Ifosfamide 3000 mg/m^2		65.2%								15.1%	
Gemcitabine 1000 mg/m^2		34.5%						31.0%		<10%	
Gemcitabine 1000 mg/m^2 + Vinorelbine 25 mg/m2								18.5%			
Paclitaxel 40 mg/m^2 + Cisplatin 50 mg/m^2	30.0%		58.0%	53.8%	40.5%	78.3%	43.1%		57.7%		
Paclitaxel 175 mg/m^2 + Cisplatin 100 mg/m^2		77.7%						90.5%			48.6%
Paclitaxel 40 mg/m^2 + Carboplatin 100 mg/m^2	<10%		<10%	22.8%	<10%	17.9%	<10%		<10%		
5-Fluorouracil 600 mg/m^2 + Carboplatin 70 mg/m^2	<10%		<10%	21.4%	<10%	15.9%	<10%	52.5%	<10%		
5-Fluorouracil 800 mg/m^2 + Cisplatin 50 mg/m^2	27.0%		58.0%	42.7%	52.4%	72.3%	63.6%		45.2%		
5-Fluorouracil 1000 mg/m^2 + Cisplatin 100 mg/m^2		70.1%						78.0%			38.9%
Cisplatin 100 mg/m^2 + Docetaxel 75 mg/m^2		93.5%						72.8%			42.5%
Carboplatin 100 mg/m^2 + Docetaxel 75 mg/m^2								26.8%			
Cisplatin 100 mg/m^2 + 5-Fluorouracil 800 mg\m^2 + Docetaxel 75 mg\m^2	94.0%		96.2%	100.0%	90.5%	94.3%	90.6%		58.7%		
Cisplatin 100 mg/m^2 + 5-Fluorouracil 1000 mg\m^2 + Docetaxel 75 mg\m^2		89.3%									48.7%
Cisplatin 100 mg/m^2 + 5-Fluorouracil 600 mg\m^2 + Paclitaxel 175 mg\m^2	47.3%		62.4%	65.9%	61.5%	91.8%	58.5%		71.6%		54.5%
Cisplatin 100 mg/m^2 + 5-Fluorouracil 1000 mg\m^2 + Paclitaxel 175 mg\m^2		74.4%									

Table 2. Response (% of cells killed) of CScs isolated from OSCC patients to different chemotherapeutic agents. Reactive: 60-100%; Average reactive 30-60%; Non-reactive <30%.

Overall, ChemoID® testing revealed substantial inter-patient heterogeneity in chemosensitivity, despite the homogeneous histological diagnosis of OSCC across the cohort. No consistent association was observed between drug response and the anatomical site of tumor origin.

Marked differences in response were observed even among patients with tumors arising from the same anatomical location. For example, Case #1 and Case #9, both diagnosed with squamous cell carcinoma of the tongue, showed divergent sensitivity to cisplatin. While CSCs from Case #9 were highly responsive to cisplatin at 100 mg/m^2 (78.6% cell death), CSCs from Case #1 exhibited only a moderate response (34.2%) to the same treatment.

Similarly, heterogeneity was evident among patients with tumors originating in the retromolar trigone (Cases #2, #7, and #8). Although CSCs from all three patients were sensitive to cisplatin 100 mg/m^2 (73.6%, 76.8%, and 78.3%, respectively), their responses to other agents and combinations differed substantially. CSCs from Case #2 were highly responsive to docetaxel 75 mg/m^2 (87.4%), whereas CSCs from Cases #7 and #8 were non-responsive or weakly responsive to the same agent (25.0% and <10%, respectively). Notably, the most effective treatment combination differed among these patients:

Case #2 showed maximal cytotoxicity with cisplatin 100 mg/m^2 + docetaxel 75 mg/m^2 (93.5%),

Case #7 responded best to cisplatin 100 mg/m^2 + 5-fluorouracil 800 mg/m^2 + docetaxel 75 mg/m^2 (90.6%),

Case #8 exhibited the highest sensitivity to paclitaxel 175 mg/m^2 + cisplatin 100 mg/m^2 (90.5%).

Differences in response were also observed for identical drug combinations across patients. For instance, the combination of 5-fluorouracil 600 mg/m^2 + carboplatin 70 mg/m^2 resulted in a non-responsive profile (<10%) in Case #7, whereas CSCs from Case #8 displayed a moderate response (52.5%) to the same regimen.

When considering treatment modalities, CSCs generally showed greater sensitivity to combination therapies compared to single-agent treatments. In particular, combinations including cisplatin, 5-fluorouracil, and docetaxel consistently produced the highest levels of cytotoxicity across multiple patients, whereas most single agents—especially paclitaxel at lower doses, carboplatin, methotrexate, and cetuximab—were frequently associated with limited or absent CSC killing.

The highest cytotoxic response identified for each individual patient is reported in **Table 3**, which highlights that multidrug regimens were more effective than monotherapies in targeting CSCs in the majority of cases.

N. Case	Drugs	Percentage of cell kill
Case 1	Cisplatin 100 mg/m2 + 5-Fluorouracil 800 mg\m2 + Docetaxel 75 mg\m2	94.0%
Case 2	Cisplatin 100 mg/m2 + Docetaxel 75 mg/m2	93.5%
Case 3	Cisplatin 100 mg/m2 + 5-Fluorouracil 800 mg\m2 + Docetaxel 75 mg\m2	96.2%
Case 4	Cisplatin 100 mg/m2 + 5-Fluorouracil 800 mg\m2 + Docetaxel 75 mg\m2	100.0%
Case 5	Cisplatin 100 mg/m2 + 5-Fluorouracil 800 mg\m2 + Docetaxel 75 mg\m2	90.5%
Case 6	Cisplatin 100 mg/m2 + 5-Fluorouracil 800 mg\m2 + Docetaxel 75 mg\m2	94.3%
Case 7	Cisplatin 100 mg/m2 + 5-Fluorouracil 800 mg\m2 + Docetaxel 75 mg\m2	90.6%
Case 8	Paclitaxel 175 mg/m2 + Cisplatin 100 mg/m2	90.5%
Case 9	Cisplatin 100 mg/m2	78.6%
Case 10	Cisplatin 100 mg/m2	52.1%
Case 11	Cisplatin 100 mg/m2 + 5-Fluorouracil 1000 mg\m2 + Paclitaxel 175 mg\m2	54.5%

Table 3. The highest % of cell kill detected by ChemoID® CSCs testing in each sample.

3.3 Representative clinical case

A 61-year-old male patient (Case #5) was referred to the Department of Oral and Maxillofacial Surgery at San Giovanni di Dio e Ruggi d'Aragona University Hospital (Salerno, Italy) with a large lesion involving the left anterior tonsillar pillar. Clinical examination revealed an extensive ulcerated mass occupying the oropharyngeal region.

Pre-treatment magnetic resonance imaging (MRI) and computed tomography (CT) scans, with and without contrast enhancement, demonstrated a large neoplastic lesion extending from the left retromolar region to the base of the tongue, with cranial extension toward the skull base and involvement of cervical lymph nodes. The mass caused a marked displacement of midline anatomical structures. Due to the extent and infiltration of the lesion, the patient was deemed not eligible for surgical resection (unresectable) (**Figure 4,5**).

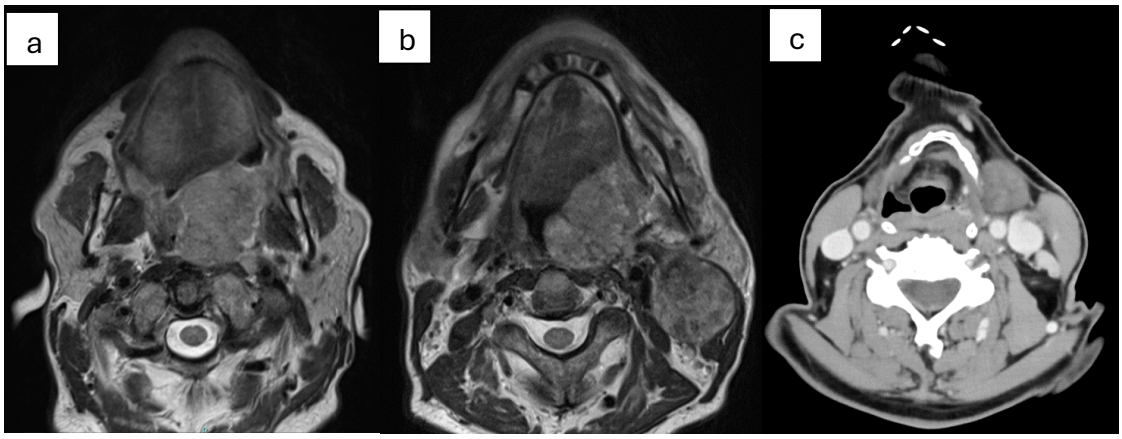

Figure 4. *MRI and CT axial sections before chemotherapy. A) MR image with axial cut in the lingual plane; b) MRI image with axial cut in the mandibular plane; c) CT image with axial cut on the plane of the hyoid bone.*

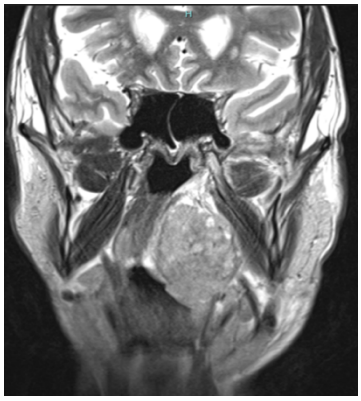

Figure 5. *MRI coronal section before chemotherapy.*

Two biopsy specimens were collected as described in the Materials and Methods section. One specimen was sent to the Department of Pathology for histological diagnosis, while the second specimen was processed for ChemoID® testing. Histopathological analysis confirmed a diagnosis of poorly differentiated, basaloid, infiltrative oral squamous cell carcinoma. Immunohistochemical analysis demonstrated p16 positivity.

ChemoID® testing was performed on both bulk tumor cells and cancer stem cells (CSCs) isolated from the biopsy specimen. The cytotoxic responses to individual

chemotherapeutic agents and combinations are reported in **Table 4**. Among all tested regimens, the combination of cisplatin 100 mg/m^2 + 5-fluorouracil 800 mg/m^2 + docetaxel 75 mg/m^2 produced the highest cytotoxic effect, resulting in 100% cell death in bulk tumor cells and 90.5% cell death in CSCs. Other combinations and single-agent treatments showed lower or moderate efficacy against CSCs.

	Bulk of Tumor	CSCs
Cisplatin 100 mg/m^2 + 5-Fluorouracil 800 mg/m^2 + Docetaxel 75 mg/m^2	**100%**	**90.5%**
Cisplatin 100 mg/m^2 + 5-Fluorouracil 600 mg/m^2 + Paclitaxel 175 mg/m^2	**51.5%**	**61.5%**
5-Fluorouracil 800 mg/m^2 + Cisplatin 50 mg/m^2	**30.1%**	**52.4%**
Docetaxel 75 mg/m^2	**16.4%**	**49.2%**
Paclitaxel 175 mg/m^2	**29.9%**	**46.6%**
Cisplatin 100 mg/m^2	**40.5%**	**42.8%**
Paclitaxel 40 mg/m^2 + Cisplatin 50 mg/m^2	**41.5%**	**40.5%**
Cisplatin 50 mg/m^2	**35.5%**	**35.3%**
Paclitaxel 40 mg/m^2	**<10%**	**26.2%**
Carboplatin 70 mg/m^2	**15.9%**	**<10%**
Carboplatin 100 mg/m^2	**<10%**	**<10%**
5-Fluorouracil 600 mg/m^2	**11.5%**	**<10%**
5-Fluorouracil 800 mg/m^2	**<10%**	**<10%**
Paclitaxel 40 mg/m^2 + Carboplatin 100 mg/m^2	**14.8%**	**<10%**
5-Fluorouracil 600 mg/m^2 + Carboplatin 70 mg/m^2	**10.2%**	**<10%**

Table 4. Response (% of cells killed) of CSCs isolated from the OSCC sample (case no. 5) to different chemotherapeutic agents. Reactive: 60-100%; Average reactive 30-60%; Non-reactive <30%.

Based on these results, the patient was treated with cisplatin 100 mg/m^2, 5-fluorouracil 800 mg/m^2, and docetaxel 75 mg/m^2, corresponding to the regimen with the highest CSC-directed cytotoxicity identified by the ChemoID® assay.

Radiological assessment performed two months after the initiation of chemotherapy revealed a marked regression of the primary tumor mass, as documented by post-treatment CT and MRI imaging, demonstrating a substantial reduction in tumor volume and local disease burden (**Figure 6,7**).

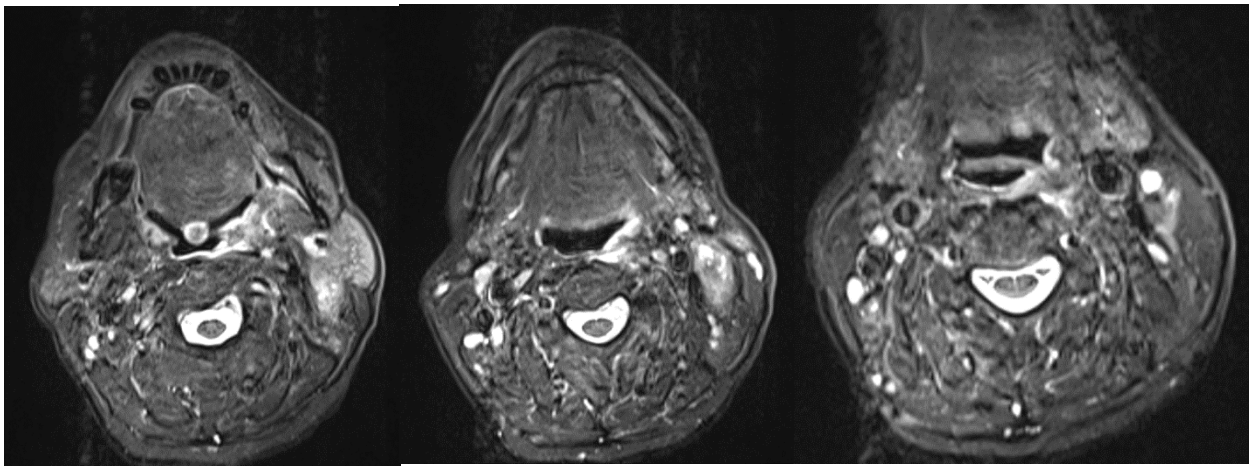

Figure 6. *Post-chemotherapy CT coronal sections. a) CT image with coronal cut on the dorsal plane of the tongue; b) CT image with coronal cut in the mandibular plane; c) CT image with coronal cut in the plane of the hyoid bone.*

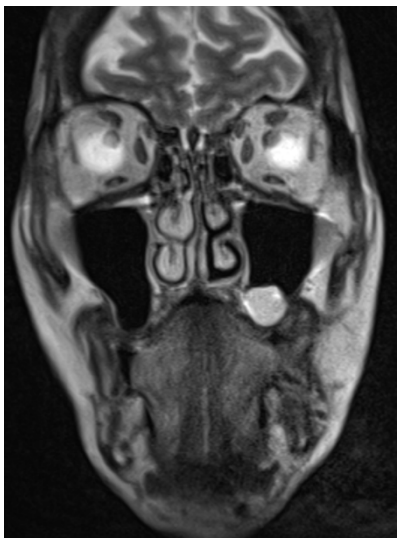

Figura 4. *Post-chemotherapy CT coronal section*

3.4 Transcriptomic profiling of patient-derived cultures under 2D and 3D conditions

Cell yield and viability in 2D and 3D cultures

For the three selected patient-derived samples (547C, 612C, and 682C), cell counts were obtained after 7 days of culture, under both 2D and 3D conditions. For each sample, the total number of cells and the fraction of viable cells were determined using Trypan Blue exclusion and the Nexcell Cellometer.

As shown in **Table 5,** 2D cultures yielded a higher proportion of viable cells across all three samples, with viability consistently above 80% (ranging from 82.5% to 90.2%). In contrast, 3D cultures displayed markedly reduced viability, ranging from ~24.95% (682C) to ~43% (612C). Although the total number of cells obtained in 3D was of the same order of magnitude as in 2D, the fraction of live cells was substantially lower, as previously shown [103]. This observation suggests that the bioreactor culture system imposes a selection on the cells. While most cells do not survive in the dynamic 3D environment, a subpopulation with stem-like properties is maintained. This selective survival is consistent with the hypothesis that 3D conditions enrich for tumor stem cells, which are more resistant to stress and capable of sustaining long-term tumor growth.

Sample	Condition	Live cells	Total cells	Viability %
682C	2D	2.31×10^6	2.8×10^6	82.5
682C	3D	2.52×10^5	2.31×10^6	24.95
612C	2D	2.11×10^6	2.34×10^6	90.17
612C	3D	5.96×10^5	1.38×10^6	43.19
547C	2D	2.95×10^6	3.55×10^6	83.1
547C	3D	7.58×10^5	2.05×10^6	36.98

Table 5. Cell counts and viability in 2D and 3D cultures.

Data preparation for functional analyses

Transcript abundance was estimated using Salmon, a bioinformatics tool that estimates the relative abundance of transcripts or genes from sequencing files (.fastq). It enables the quantification of gene expression in each sample, producing as output an expression matrix containing values such as TPM (Transcripts Per Million), estimated read counts, and other indicators useful for transcriptomic analysis. The transcriptomic dataset used for downstream functional analyses was derived from quantification results generated with Salmon, using the aggregated expression values from the three HNSCC patient-derived samples. From the differential expression analysis, a table with gene-level results was produced, including $\log_2$ fold change, adjusted p-values, and average expression. In total, 14,251 genes were tested.

To prepare the gene list for Pathway Enrichment Analysis (PEA), genes with an adjusted p-value < 0.05 and an absolute $\log_2$ fold change < and > 1 were retained. This filtering step resulted in 528 upregulated genes (higher in 2D) and 665 downregulated genes (higher in 3D), which were used as input for EnrichR.

For Gene Set Enrichment Analysis (GSEA), transcript-level quantification values were organized into a GSEA-compatible format. The matrix included expression values for 14,251 genes across six biological replicates (three per condition), with rows representing genes (identified by Ensembl IDs) and columns representing individual samples. Expression values were transformed as $\log_2(\text{TPM} + 1)$, as required by GSEA.

This dual approach allowed for capturing both strong signals (via EnrichR) and coordinated but potentially subtle shifts in gene expression (via GSEA), thus providing complementary insights into the biological pathways affected by the culture condition.

Pathway Enrichment Analysis (PEA) – 2D condition

Using the list of genes differentially expressed between 2D and 3D culture conditions (528 upregulated in 2D and 665 upregulated in 3D), the PEA was performed using the EnrichR platform. EnrichR is a web-based gene set enrichment tool that compares input gene lists against a wide array of annotated biological libraries - including Gene Ontology (GO) pathways and Reactome - and assesses statistical overrepresentation of specific pathways in the input set.

The differentially expressed genes ($log_2FC > 1$, padj < 0.05) in 2D revealed significant enrichment in GO terms (**Figure 8**) related to:

- Extracellular matrix (ECM) remodeling:
    - Extracellular Matrix Organization (GO:0030198)
    - External Encapsulating Structure Organization (GO:0045229)
    - Extracellular Structure Organization (GO:0043062)
    - Collagen catabolic process (GO:0030574)
- Cellular proliferation and signaling:
    - Negative regulation of canonical Wnt signaling pathway (GO:0090090)
    - Negative regulation of Wnt signaling Pathway (GO:0090090)
    - Negative regulation of cell population proliferation (GO:0008285)
    - Regulation of ERK1/ERK2 cascade (GO:0070372)

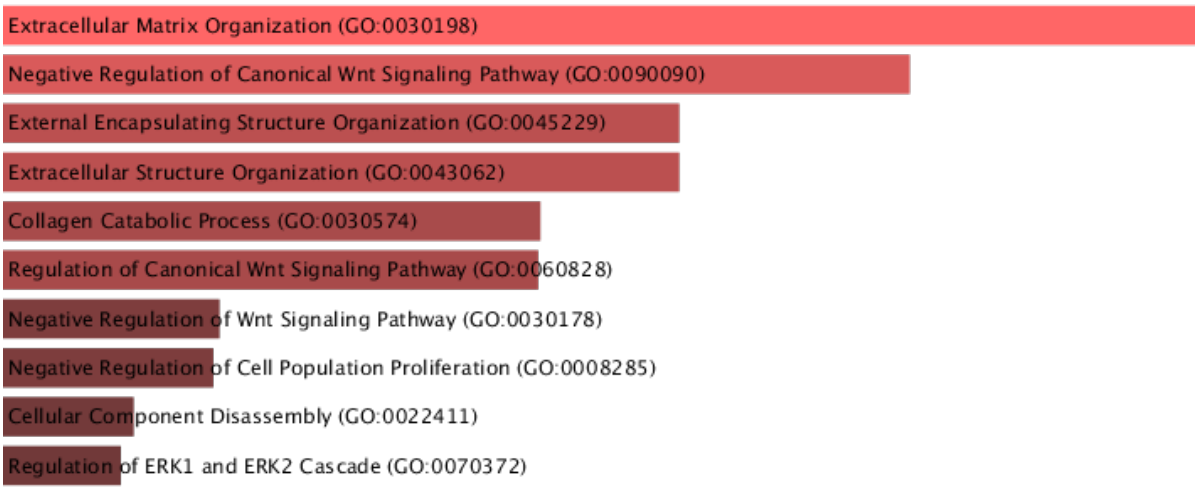

Figure 8. Top 10 enriched Gene Ontology – Biological Process terms identified by EnrichR among genes upregulated in 2D cultures. Terms are sorted by adjusted p-value (Benjamini–Hochberg correction). Processes related to extracellular matrix remodeling and signaling regulation are most significantly overrepresented.

These pathways indicate a transcriptional program driven by matrix degradation, proliferation signals, and suppression of developmental pathways like Wnt, aligning with the literature that describes 2D cultures as promoting high proliferation, structural instability, and loss of diverse phenotypes. [104-106]

Reactome enrichment analysis of the 2D condition confirmed that overexpressed genes were strongly enriched in pathways related to extracellular matrix (ECM) remodeling and signaling regulation (**Figure 9**).

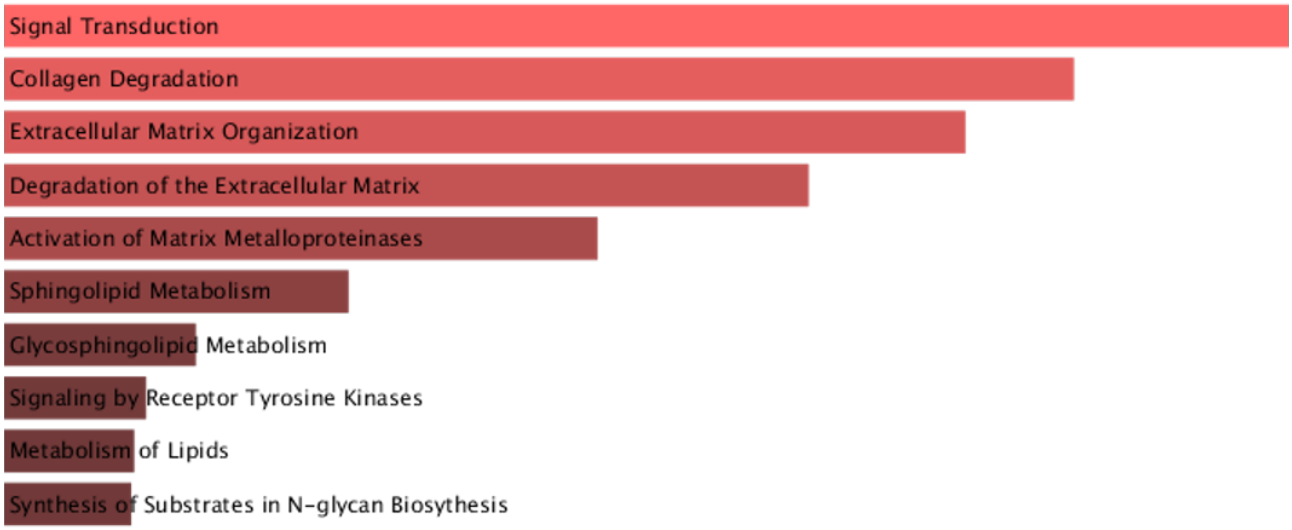

Figure 9. Enrichr-REACTOME. Pathway enrichment analysis- UPREGULATED in 2D vs 3D

By manually uploading the overexpressed gene lists into the Reactome portal (**Figure 10-11**), it was possible to map the position of these genes within the corresponding pathways. This confirmed that the 2D condition is characterized by disorganized ECM remodeling, activation of metalloproteinases, and proliferation-related signaling.

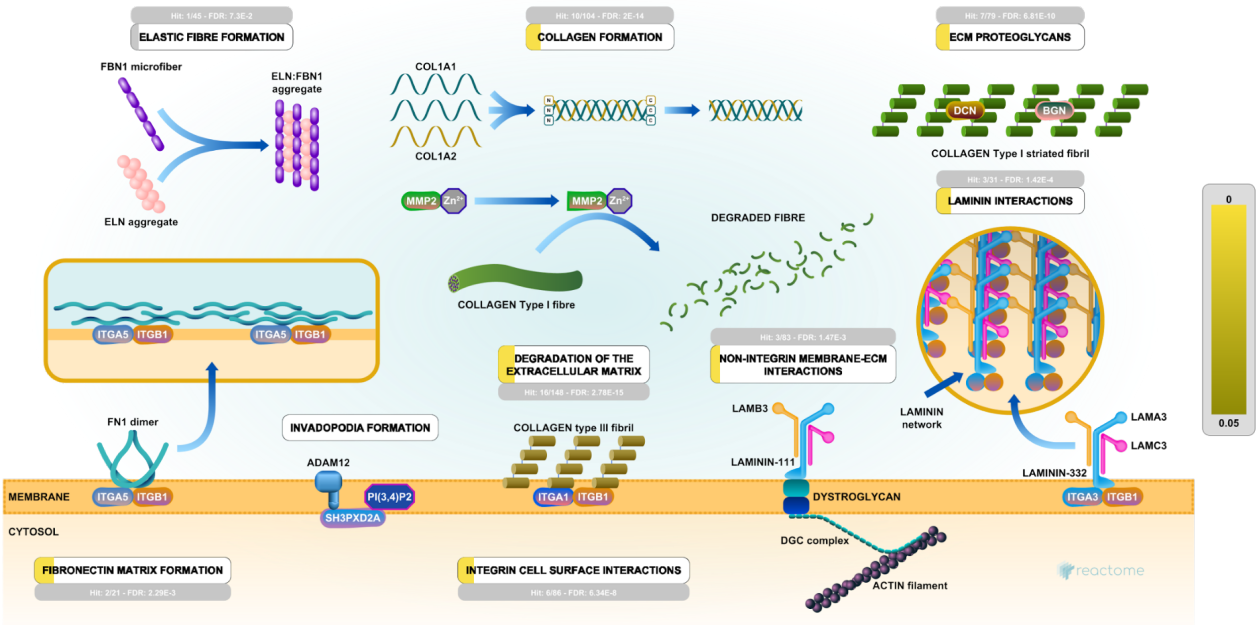

Figure 10. Pathway "Extracellular matrix organization". Exported from *Reactome Pathway Database* (https://reactome.org), licensed under CC BY 4.0.

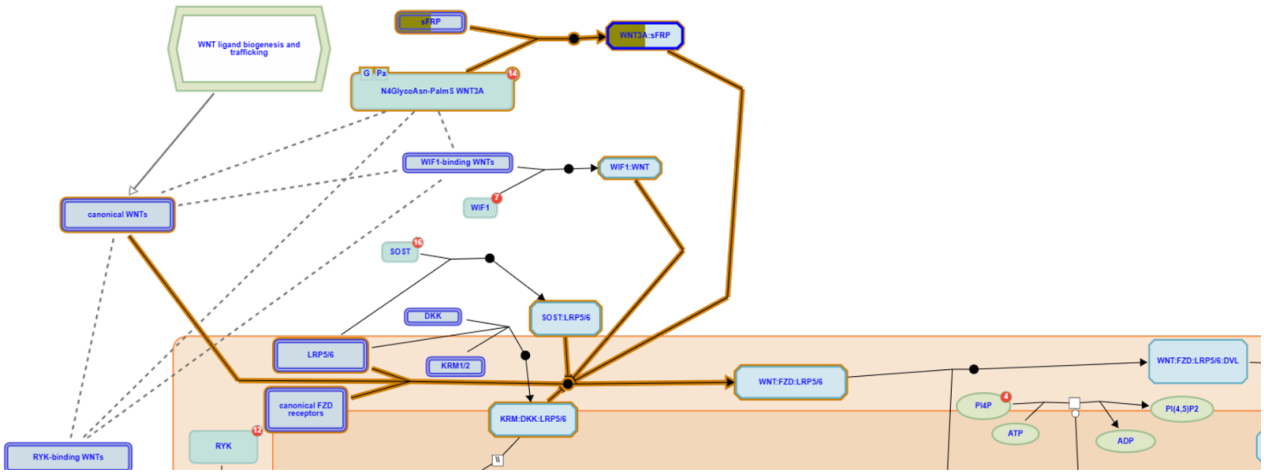

Figure 11. Visualization of "Canonical Wnt signaling pathway" showing genes overexpressed in 2D condition (highlighted in yellow). Source: *Reactome Pathway Database* (https://reactome.org).

Pathway Enrichment Analysis (PEA) – 3D condition

Pathway Enrichment Analysis (PEA) of the genes upregulated in the 3D cultures ($log_2FC < -1$, $padj < 0.05$) revealed significant enrichment in several biological processes related to cell cycle regulation, migration, proliferation, and response to external stimuli (**Figure 12**).

Among the most enriched terms were:

- Regulation of cell migration (GO:0030334)
- Positive regulation of cell cycle process (GO:0090068) and mitotic sister chromatid segregation (GO:0000070):
- Positive regulation of cell population proliferation (GO:0008284)
- Cellular response to hormone stimulus (GO:0032870
- Motor neuron axon guidance (GO:0008045)

Overall, 3D cultures showed overexpression of genes related to pathways linked to cell proliferation, mitotic control, and migration, consistent with a condition that better mimics tumor aggressiveness and heterogeneity compared to 2D cell cultures. The enrichment of axon guidance pathways in 3D-grown tumor cells suggests a shift toward neural-like signaling mechanisms, a phenomenon increasingly recognized as part of tumor cell plasticity[107]. Cellular plasticity is now considered a functional hallmark of cancer, allowing tumor cells to evade terminal differentiation and acquire new phenotypic states that enhance adaptability and survival. Tumor cells may dedifferentiate into progenitor-like cells, inhibit differentiation to maintain a partially undifferentiated phenotype, or even transdifferentiate into lineages of distinct origin[108]. Recent evidence shows that cancer cells can acquire neuronal characteristics, supporting a novel form of plasticity in which malignant cells adopt features typical of neural lineages [107]. Neurons are defined by the expression of lineage-specific genes, the ability to form long cytoplasmic projections (axons) guided by environmental cues, and their capacity to secrete molecules and propagate electrochemical signals. Analogously, tumor cells can exploit similar cytoskeletal mechanisms to promote migration and invasion [109]. The activation of axon guidance pathways observed in the 3D model may therefore reflect this neural-like reprogramming, whereby tumor cells adopt signaling and structural strategies reminiscent of neurons to enhance motility, invasion, and metastatic potential [107]. This finding reinforces the concept that 3D cultures better reproduce the biological complexity of tumors, including their capacity for phenotypic plasticity and microenvironmental adaptation, which are key determinants of malignancy and therapeutic resistance.

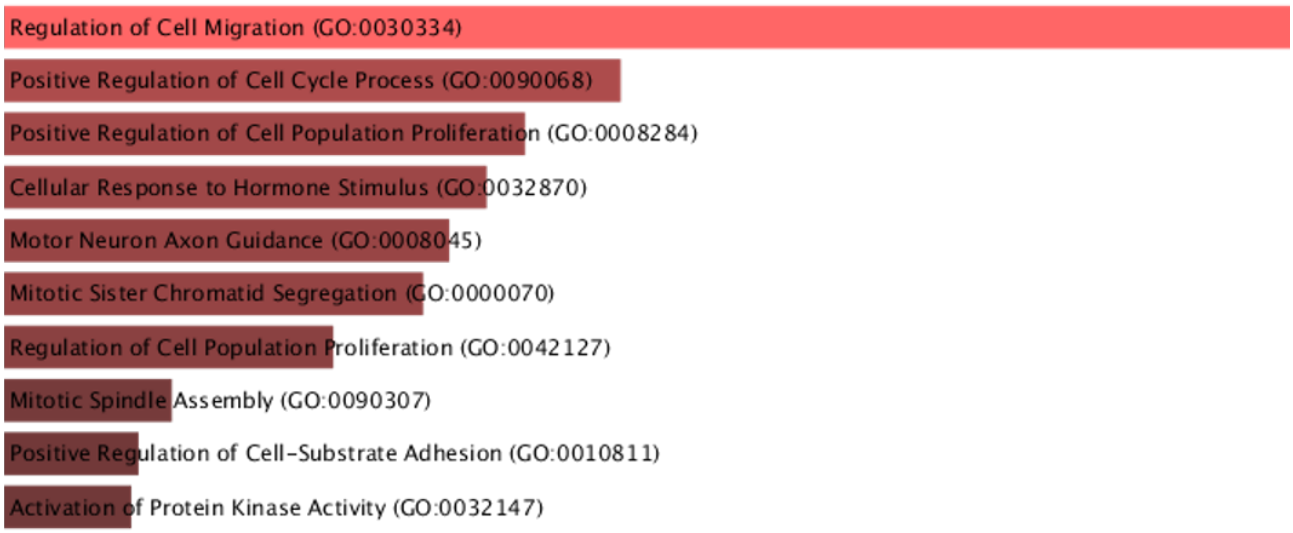

Figure 12. Top 10 enriched Gene Ontology – Biological Process terms identified by EnrichR among genes upregulated in 3D cultures. Terms are sorted by adjusted p-value (Benjamini–Hochberg correction). Processes related to Regulation of Cell Migration and Positive Regulation of Cell Cycle Process.

To further investigate the functional categories enriched in the 3D condition, genes overexpressed in 3D ($log_2FC < –1$, $padj < 0.05$) were analyzed using Reactome database through the EnrichR platform (**Figure 13**). The enrichment analysis revealed a strong association with pathways related to extracellular matrix (ECM) organization, growth factor signaling, and cell cycle regulation:

- Elastic Fibre Formation
- Ethanol Oxidation
- TGFBR3 Regulates TGF-β Signaling
- eNOS Activation
- Alternative Complement Activation
- Reelin Signaling Pathway

The top-ranking pathway, Elastic Fibre Formation, suggests active remodeling of the extracellular matrix (ECM), consistent with a mesenchymal or invasive cellular phenotype. The enrichment in TGF-β signaling further supports the involvement of developmental and migratory programs, often associated with epithelial–mesenchymal transition (EMT) and stem-like traits.

According to recent research about Reelin's functions, it seems to be involved in processes such as cell proliferation, migration, and vascular development. [110] This suggests the potential of the cancer stem cells in increasing tumor aggressiveness, metastatic potential through unexpected pathways.

Additional enriched pathways related to angiogenesis, like eNOS activation [111,112] are consistent with adaptation to hypoxia and nutrient gradients in 3D microenvironments.

Furthermore, the Complement Activation has been shown to be related to cell dedifferentiation, proliferation, and migration, in addition to reducing apoptosis and enhancing tumor growth and increasing metastasis [113].

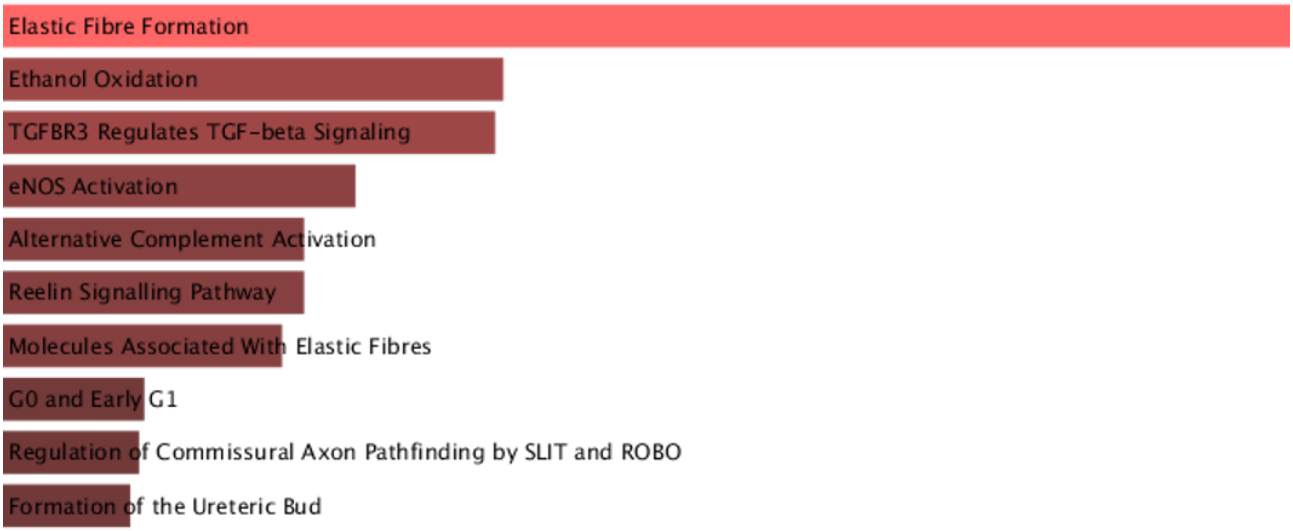

Figure 13. Enrichr-REACTOME. Pathway enrichment analysis- UPREGULATED in 3D vs 2D

Gene Set Enrichment Analysis (GSEA, Hallmark collection)

GSEA performed using the Hallmark gene set collection (MSigDB) revealed a marked transcriptional divergence between the two conditions (**Figure 14**).

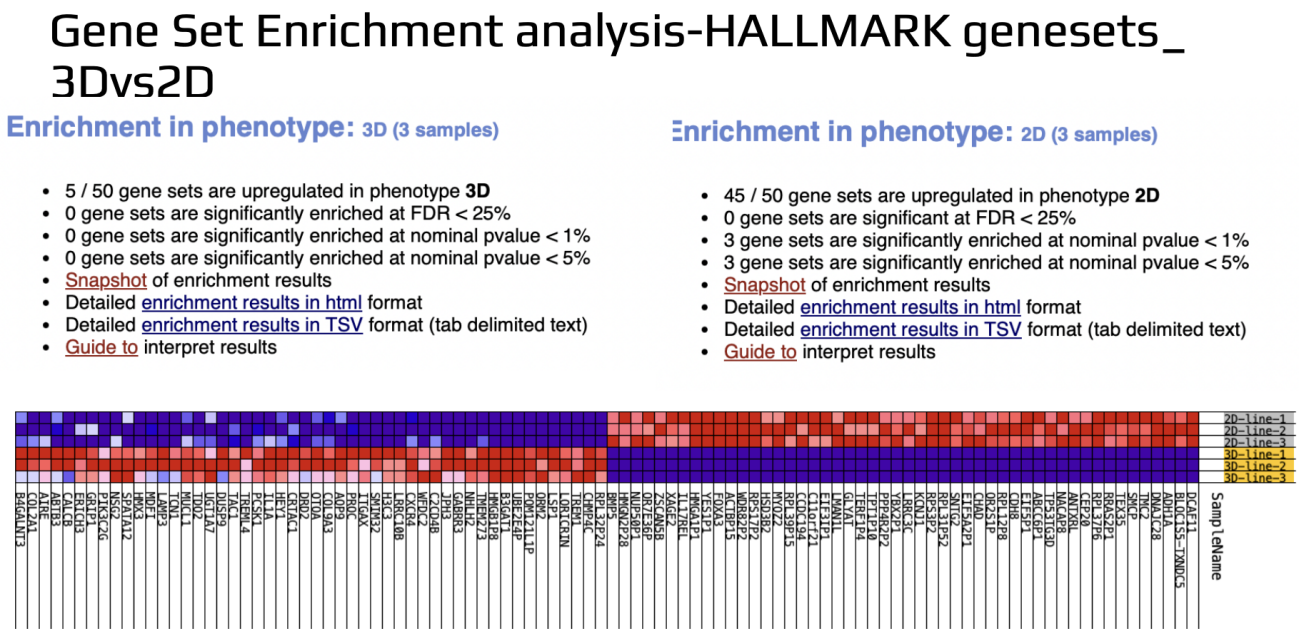

Figure 14. Gene Set Enrichment Analysis, 3D vs 2D condition.

In the 2D condition, a strong enrichment of gene sets related to cell cycle progression, DNA replication, and stress signaling was observed (**Figure 15**):

- E2F targets and G2M checkpoint indicated active cell cycle progression and mitotic division.[114]
- MYC targets V1 highlighted upregulation of oncogenic transcriptional programs driving uncontrolled proliferation.[114]
- DNA repair enrichment reflected replicative stress and genomic instability.
- Interferon-α and -γ responses suggested activation of inflammatory and stress-related pathways.

- Peroxisome pointed to oxidative stress and ROS detoxification mechanisms.
- Apical junction enrichment indicated a partial attempt of 2D monolayers to maintain cell–cell adhesion in a flat, artificial environment.

These results underscore that 2D cultures are characterized by hyperproliferative and stress-associated transcriptional programs, consistent with their artificial and unstable growth environment.

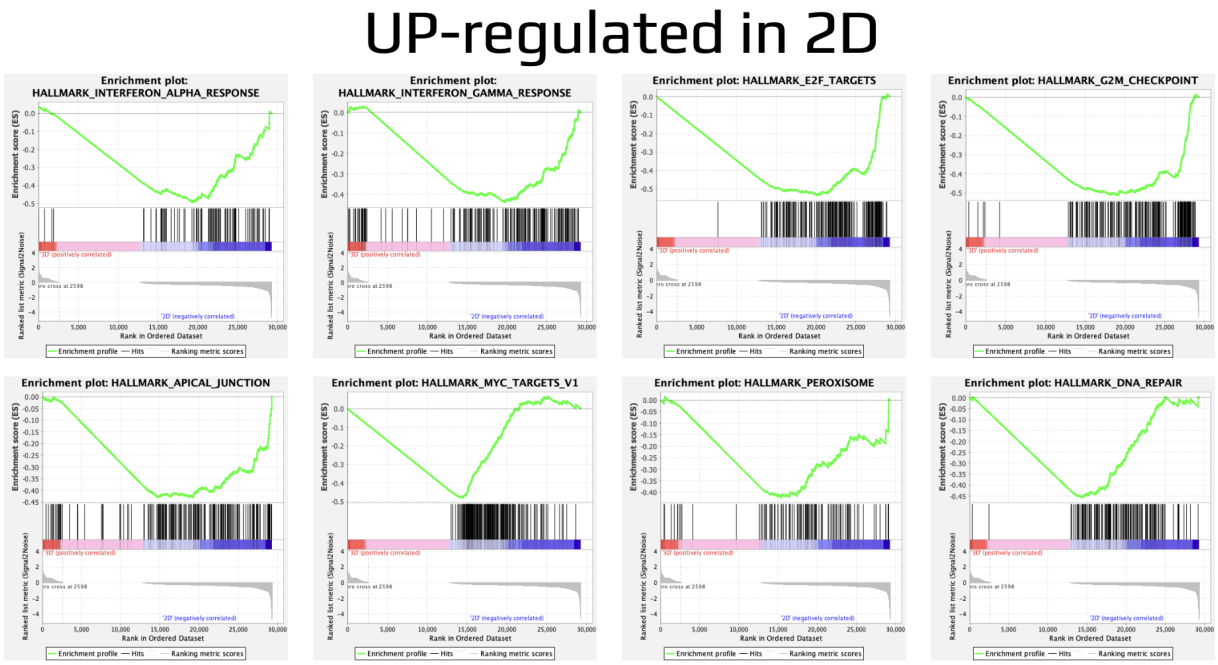

Figure 15. Gene Set Enrichment Analysis, Enriched genes in 2D condition.

In contrast, only a limited number of gene sets were enriched in 3D, but they highlighted key developmental and stemness-associated pathways:

- Wnt/β-catenin signaling (**Figure 16**): a pathway crucial for cancer stem cell (CSC) maintenance in multiple tumor types, including HNSCC, breast, liver, colon and melanoma.[115]

- TNFα signaling via NF-κB (**Figure 17**): known to enhance CSCs properties such as CD44 upregulation and self-renewal capability [116], as well as to promote epithelial-mesenchymal transition (EMT), enhancing migration and invasion.[117]
- Hedgehog signaling (**Figure 18**): regulating proliferation, differentiation, and structural growth is recognized as a driver of CSC expansion and tumor progression.[118]

These enrichments suggest that in 3D, cells activate developmental and stemness-related signaling pathways, more closely mimicking in vivo tumor microenvironments.

In conclusion, 2D cultures are characterized by uncontrolled proliferation, DNA replication stress, and inflammatory/oxidative responses, indicative of an artificial system.

3D cultures overexpressed pathway, although fewer of them were significantly enriched, are involved in developmental and CSC-associated signaling (Wnt, TNFα/NF-κB, Hedgehog), reflecting a more physiological and tumor-relevant state that may sustain stemness, plasticity, and microenvironmental adaptation.

UP-regulated in 3D – HALLMARK_ wnt_beta_catenin_signaling

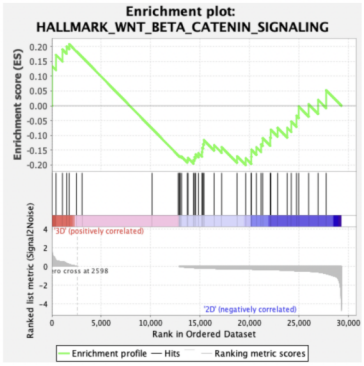

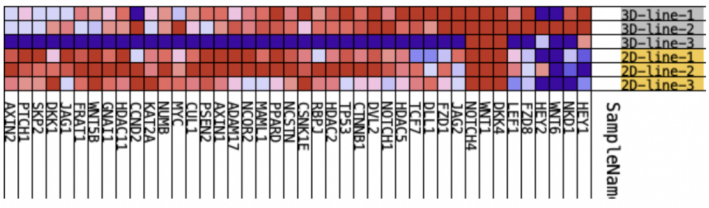

	SYMBOL	TITLE	RANK IN GENE LIST	RANK METRIC SCORE	RUNNING ES	CORE ENRICHMENT
1	HEY1	hes related family bHLH transcription factor with YRPW motif 1 [Source:HGNC Symbol;Acc:HGNC:4880]	27	1.718	0.1338	Yes
2	NKD1	NKD inhibitor of WNT signaling pathway 1 [Source:HGNC Symbol;Acc:HGNC:17045]	420	0.657	0.1719	Yes
3	WNT6	Wnt family member 6 [Source:HGNC Symbol;Acc:HGNC:12785]	1077	0.523	0.1904	Yes
4	HEY2	hes related family bHLH transcription factor with YRPW motif 2 [Source:HGNC Symbol;Acc:HGNC:4881]	1503	0.312	0.2003	Yes
5	FZD8	frizzled class receptor 8 [Source:HGNC Symbol;Acc:HGNC:4046]	1760	0.207	0.2078	Yes

Figure 16. Gene Set Enrichment Analysis, Wnt/β-catenin signaling enriched in 3D condition

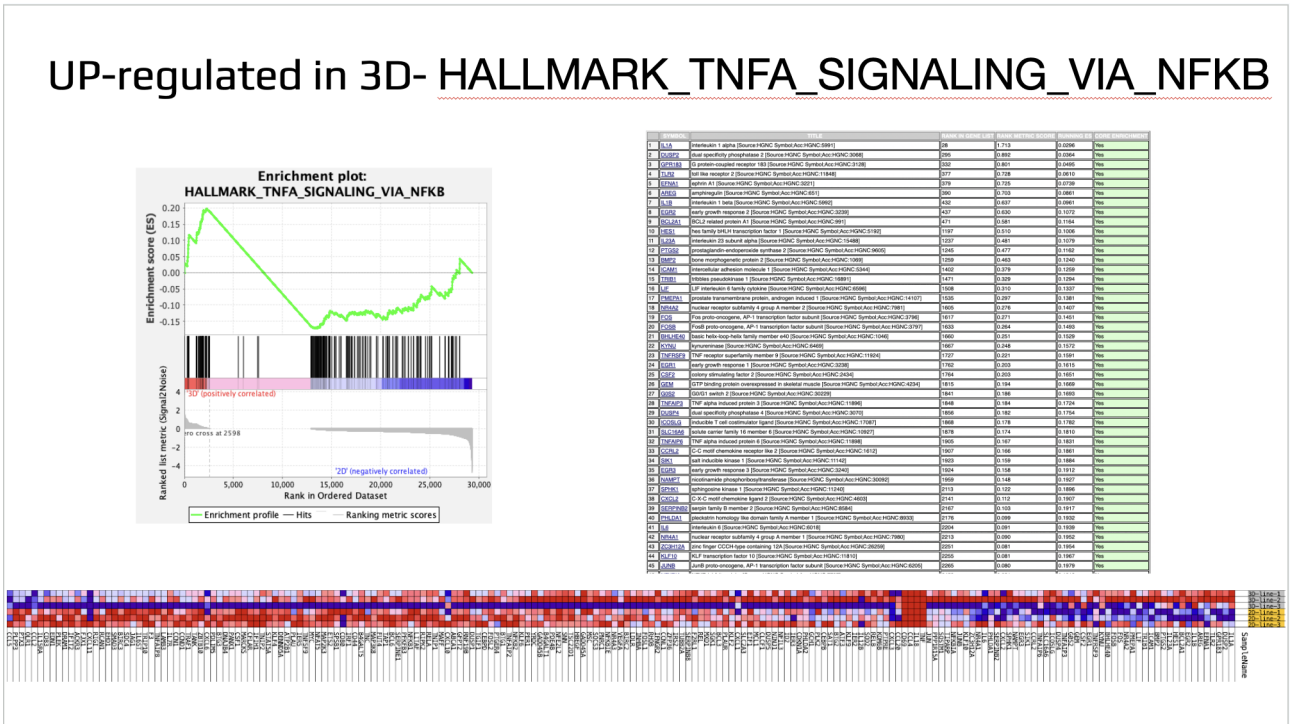

Figure 17. Gene Set Enrichment Analysis, TNFα signaling via NF-κB enriched in 3D condition

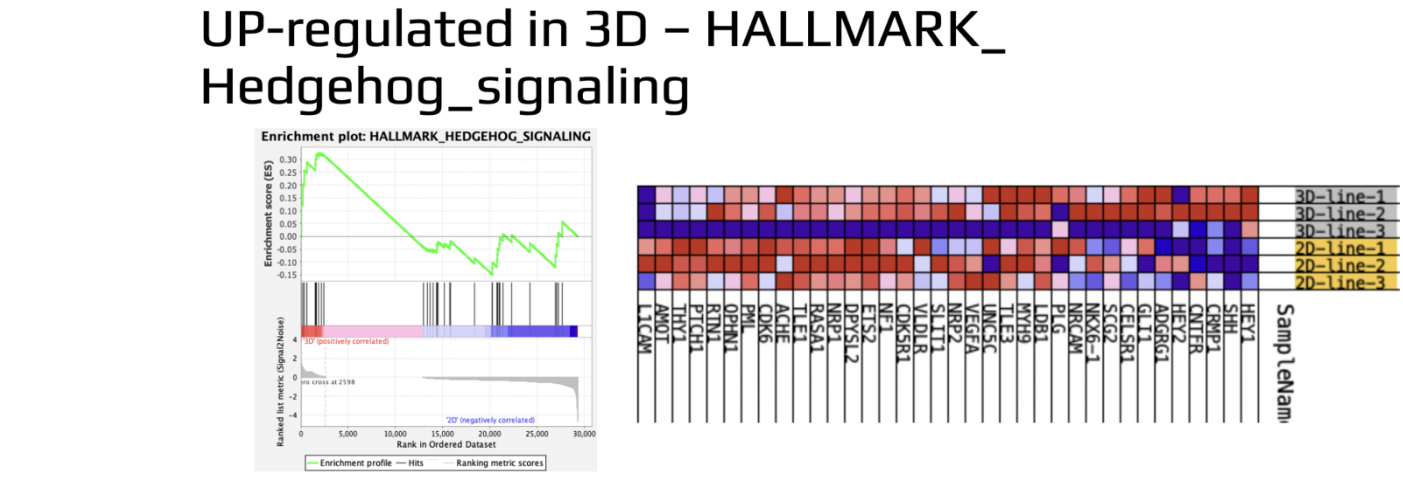

	SYMBOL	TITLE	RANK IN GENE LIST	RANK METRIC SCORE	RUNNING ES	CORE ENRICHMENT
1	HEY1	hes related family bHLH transcription factor with YRPW motif 1 [Source:HGNC Symbol;Acc:HGNC:4880]	27	1.718	0.1291	Yes
2	SHH	sonic hedgehog signaling molecule [Source:HGNC Symbol;Acc:HGNC:10848]	201	1.041	0.2020	Yes
3	CRMP1	collapsin response mediator protein 1 [Source:HGNC Symbol;Acc:HGNC:2365]	348	0.783	0.2562	Yes
4	CNTFR	ciliary neurotrophic factor receptor [Source:HGNC Symbol;Acc:HGNC:2170]	621	0.545	0.2881	Yes
5	HEY2	hes related family bHLH transcription factor with YRPW motif 2 [Source:HGNC Symbol;Acc:HGNC:4881]	1503	0.312	0.2816	Yes
6	ADGRG1	adhesion G protein-coupled receptor G1 [Source:HGNC Symbol;Acc:HGNC:4512]	1542	0.293	0.3025	Yes
7	GLI1	GLI family zinc finger 1 [Source:HGNC Symbol;Acc:HGNC:4317]	1632	0.264	0.3195	Yes
8	CELSR1	cadherin EGF LAG seven-pass G-type receptor 1 [Source:HGNC Symbol;Acc:HGNC:1850]	1863	0.180	0.3252	Yes

Figure 18. Gene Set Enrichment Analysis, Hedgehog signaling enriched in 3D condition

3.5 Functional evaluation of Benzyl Isothiocyanate (BITC) in HNSCC cell models

3.5.1 BITC Sensitizes HN22, HN8, HN30, and HN31 HNSCC cancer cells to the Cytotoxic Effects of Chemo- and Radiation Therapies

To evaluate whether BITC enhances the cytotoxic effects of standard treatments, HNSCC cell lines were pretreated with 10 μM BITC for 1 hour and subsequently exposed to cisplatin (CDDP, 10 μM), ionizing radiation (4 Gy or 8 Gy), or their combinations. Cell viability was assessed at 72 hours following treatment.

In the HN22 cell line, treatment with cisplatin or radiation alone did not result in significant reductions in viability compared to untreated controls, confirming the intrinsic resistance of this cell line. However, pretreatment with BITC markedly enhanced sensitivity to combined modalities. The most pronounced reduction in cell viability was observed following BITC pretreatment combined with 8 Gy radiation and cisplatin, which was significantly more effective than any single or dual treatment **(Figures 19,20).**

A similar pattern was observed in the paired metastatic-derived cell lines HN8, HN30, and HN31. In these models, BITC pretreatment followed by 4 Gy or 8 Gy radiation in combination with cisplatin resulted in a significant decrease in cell viability compared to radiation or chemotherapy alone **(Figures 21,22).** Across all tested cell lines, the triple combination of BITC pretreatment, 8 Gy radiation, and cisplatin consistently produced the greatest cytotoxic effect.

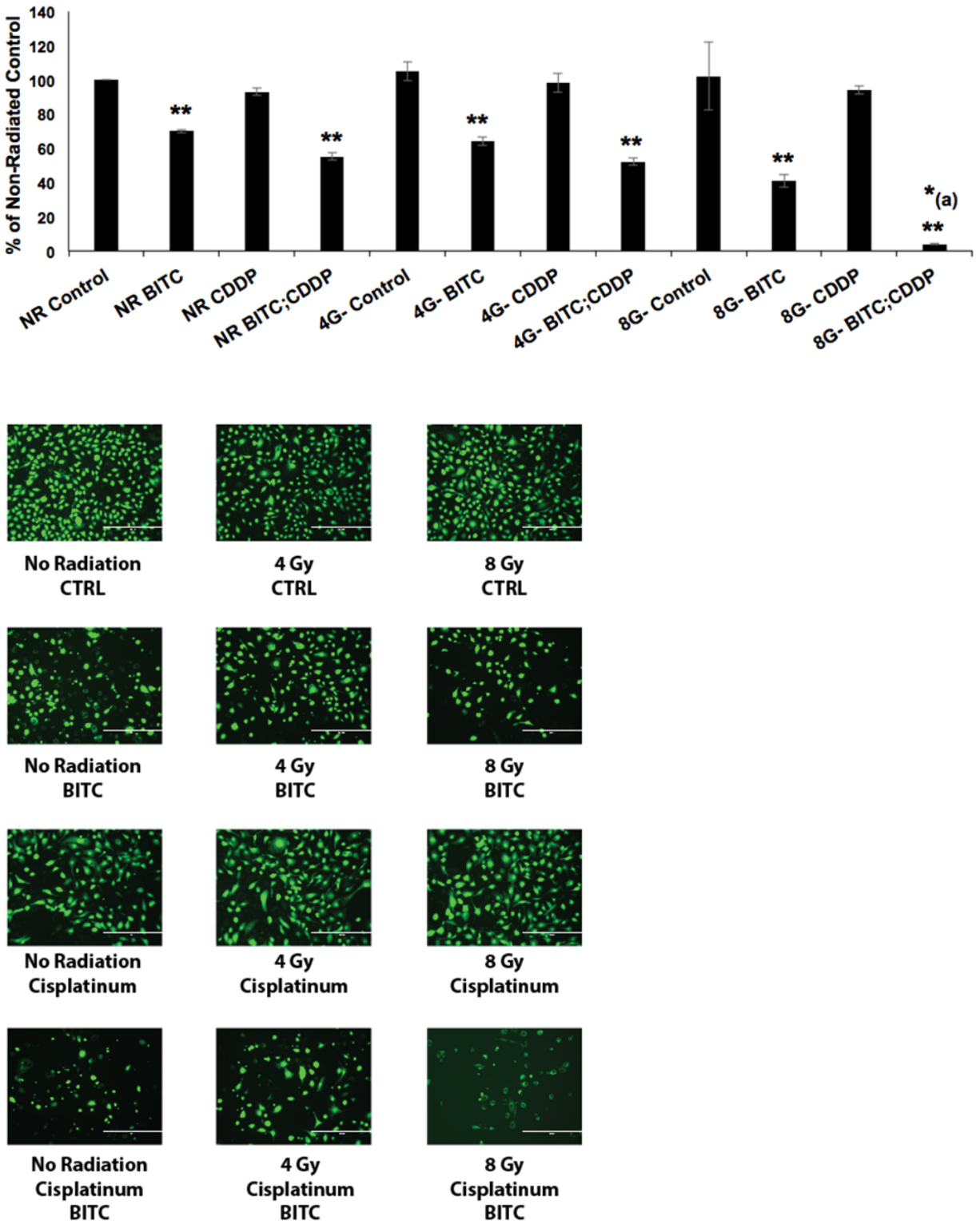

Figure 19. HN22 - 72 Hours

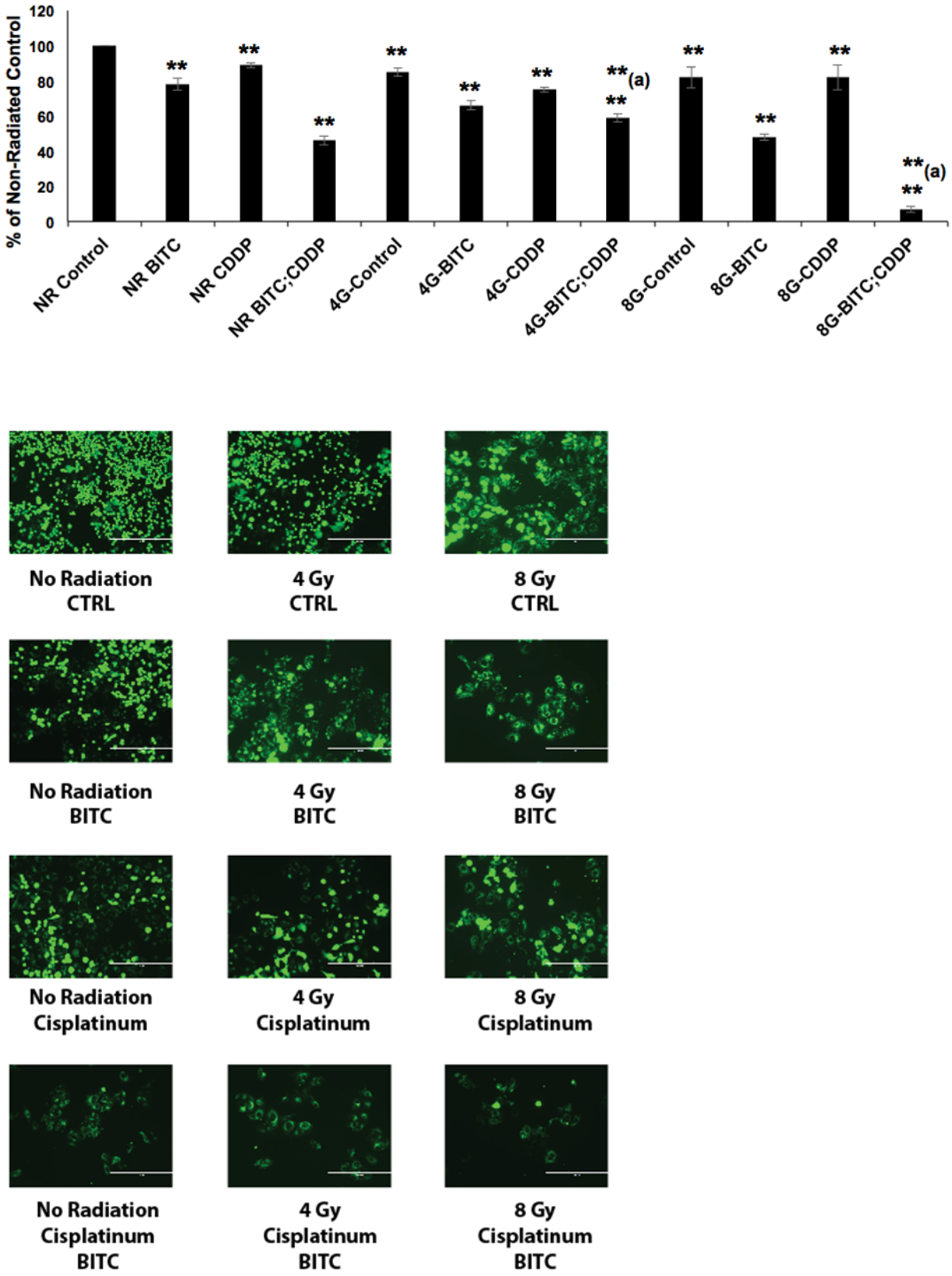

Figure 20. HN8 - 72 Hours

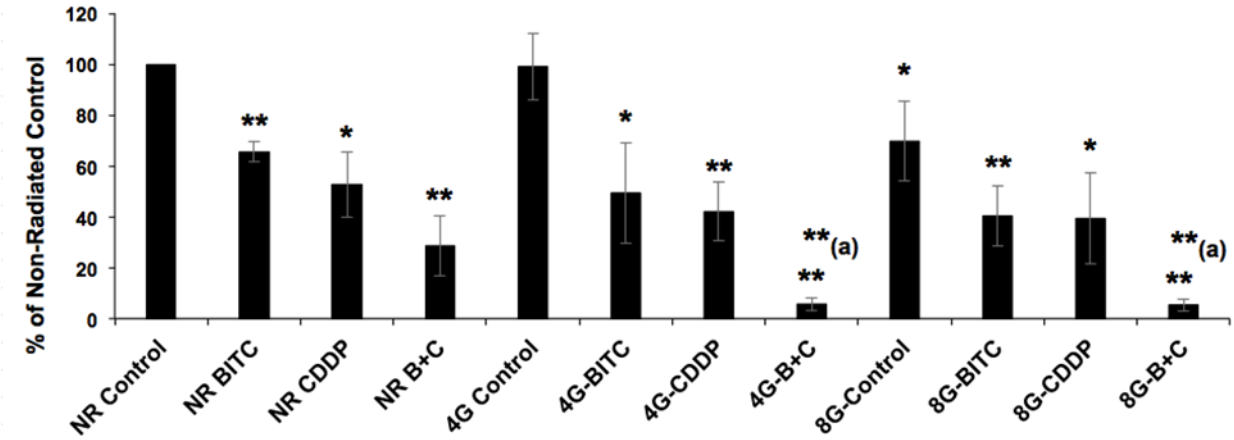

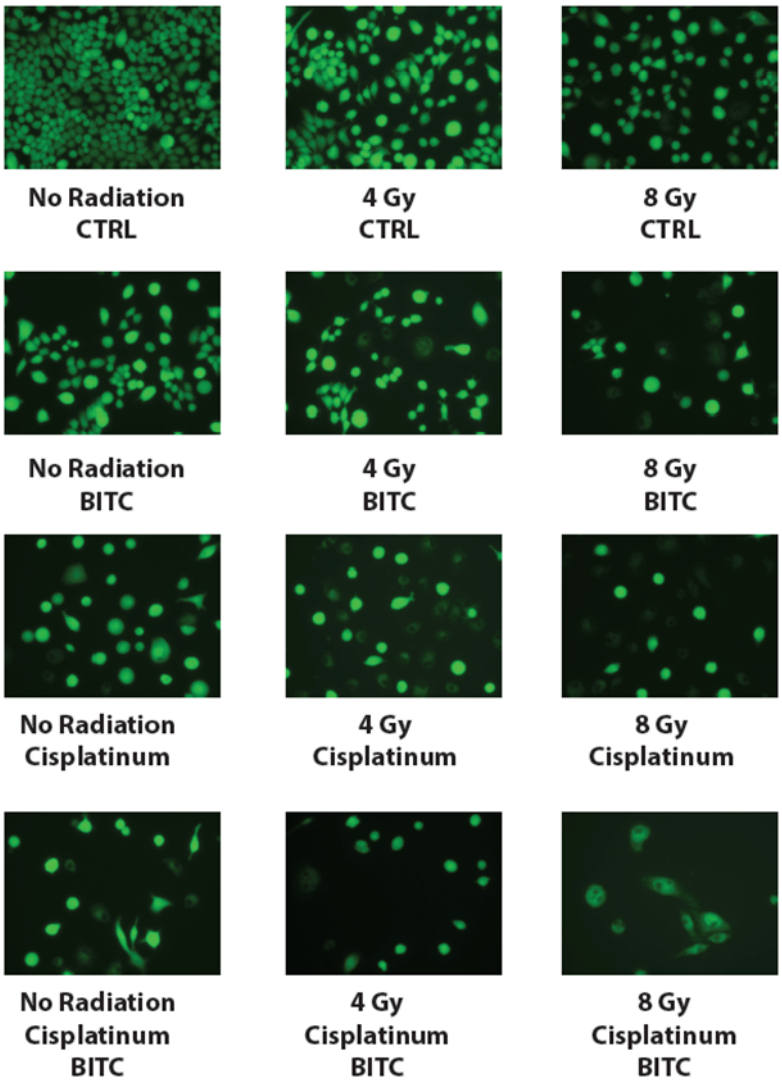

Figure 21. HN30 - 72 Hours

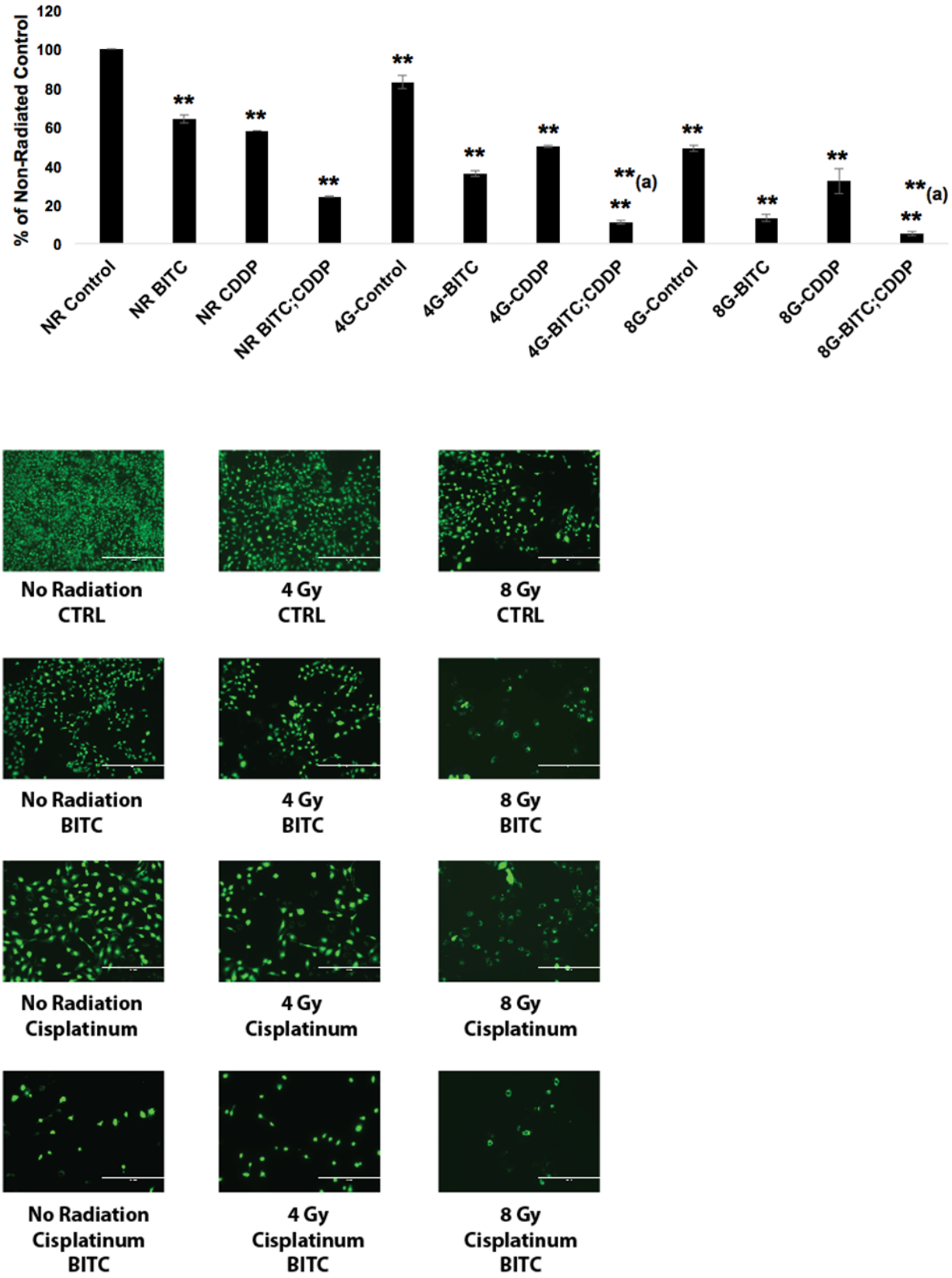

Figure 22. HN31 - 72 Hours

Figure 19-22. Decreased viability of HN22, HN8, HN30 and HN31 cancer cells at 72 hours after receiving a 1-hour BITC treatment before radiation and cisplatin (CDDP) therapies. Cell viability was assessed by spectrophotometric measurements after 72 hours after BITC treatment using Calcein AM dye. Three sets of treatment groups were used. Cells received 10μM BITC for 1-hour only, 10μM CDDP alone for 24 hours, or 1-hour 10μM BITC followed by 10μM CDDP for 24 hours. Control cells received DMSO. One set of treatment groups did not receive radiation (NR), a second set received 4 Gray of radiation, and a third set received 8 Gray of radiation. Data for the graph is the average of three separate experiments. Error bars represent standard deviation (*$p \leq 0.05$, **$p \leq 0.001$, are significantly different from NR Control). (*a = significantly different from NR BITC; CDDP $p \leq 0.05$).

3.5.2 BITC enhances apoptotic cell death via caspase 3/7 activation

To determine whether the observed reduction in cell viability was associated with apoptotic cell death, caspase 3/7 activity was measured 72 hours after treatment.

In HN22 cells, a significant increase in caspase 3/7 activity was detected following treatment with cisplatin alone and with the combination of cisplatin and BITC in non-irradiated conditions (**Figure 23A**). Upon exposure to radiation, caspase activation was further increased, with the highest levels observed in cells treated with the triple combination of BITC, cisplatin, and 8 Gy radiation, corresponding to an approximately 36-fold increase relative to control.

In HN8 cells, caspase 3/7 activity was significantly elevated following cisplatin and BITC treatment in the absence of radiation. Radiation exposure further amplified apoptotic

signaling, with the triple combination producing a >46-fold increase in caspase activity (**Figure 23B**).

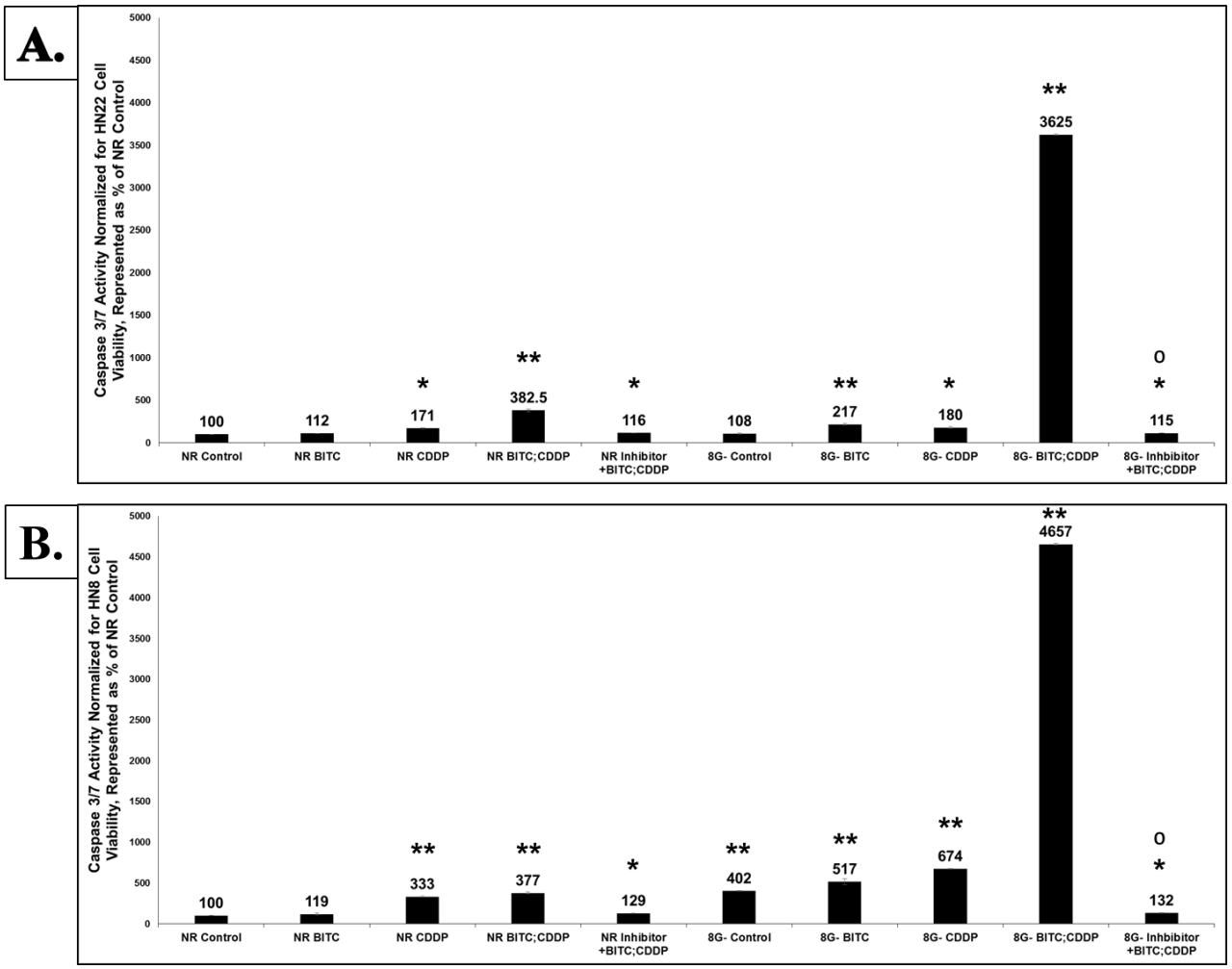

Figure 23. Apoptosis - Caspase 3/7 Activity HN22 and HN8

Similarly, in HN30 and HN31 cell lines, all treatment conditions induced significant increases in caspase 3/7 activity. The strongest apoptotic response was again observed following combined BITC, cisplatin, and 8 Gy radiation, resulting in approximately 17-fold and 19-fold increases, respectively (**Figure 24**).

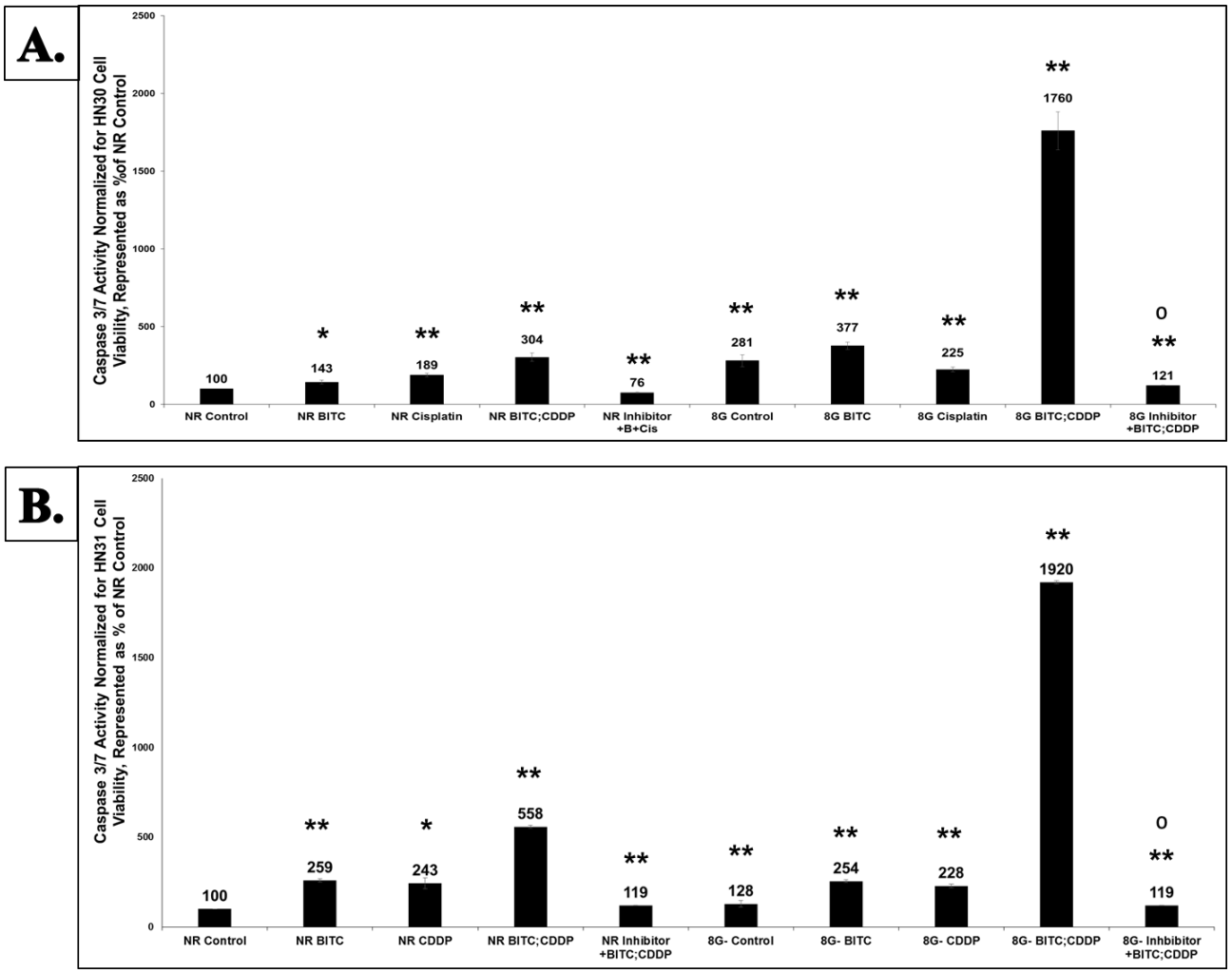

Figure 24. Apoptosis - Caspase 3/7 activity HN30 and HN31

The specificity of caspase-mediated apoptosis was confirmed using the caspase 3/7 inhibitor Ac-DEVD-CHO, which significantly reduced caspase activity in all treated groups while maintaining levels above untreated controls.

3.5.3 Antioxidant pre-treatment with glutathione blocks BITC-induced cytotoxicity

To investigate the role of oxidative stress in BITC-mediated cytotoxicity, HNSCC cell lines were pretreated with glutathione (GSH, 5 mM) prior to BITC exposure. Cell viability was assessed 24 hours after treatment.

Treatment with BITC alone resulted in a 30–50% reduction in cell viability across all tested cell lines compared to untreated controls ($p < 0.01$). In contrast, GSH pretreatment completely abrogated the cytotoxic effect of BITC, restoring cell viability to levels comparable to control conditions (**Figure 25**). These results indicate that BITC-induced cell death is strongly dependent on intracellular redox imbalance and reactive oxygen species (ROS) generation.

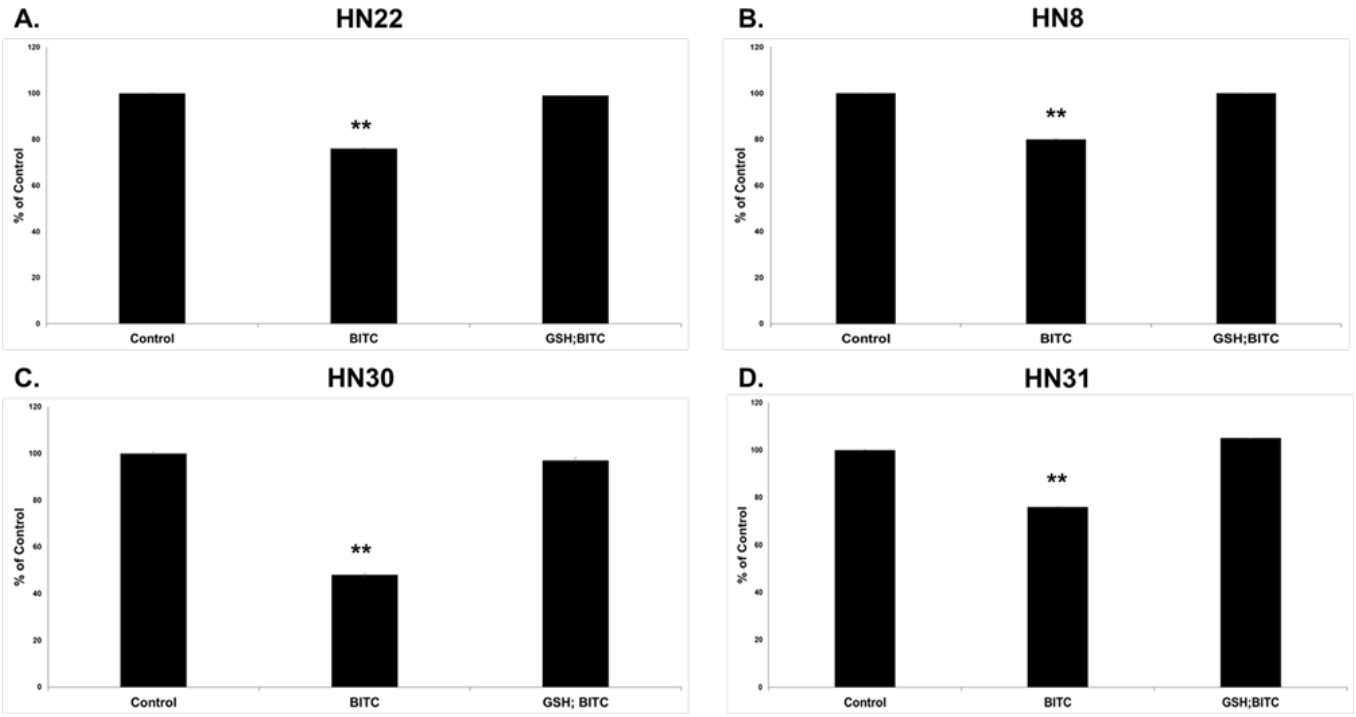

Figure 25. GSH Inhibits BITC induced cell death

3.6 Functional evaluation of Polydatin in HNSCC cell models

3.6.1 Polydatin selectively reduces viability of HNSCC cells compared to healthy fibroblasts

The cytotoxic effects of Polydatin (Pol) were evaluated in the HNSCC cell line HSC2 and compared with healthy gingival fibroblasts (hGF) to assess tumor selectivity. Cell

viability was measured using the MTT assay following 24-hour and 48-hour exposure to Pol at concentrations of 250 µM and 500 µM.

As shown in Figures 26 and 27, Pol treatment induced a dose-dependent reduction in cell viability in HSC2 tumor cells, whereas its effect on hGF cells was minimal. After 24 hours of treatment, hGF cells showed no significant reduction in viability at 250 µM, and only a modest decrease (19.3%) at 500 µM compared to controls. In contrast, HSC2 cells exhibited a marked decrease in viability, with reductions of 51.1% and 62.0% at 250 µM and 500 µM, respectively (Figure 26 A–B).

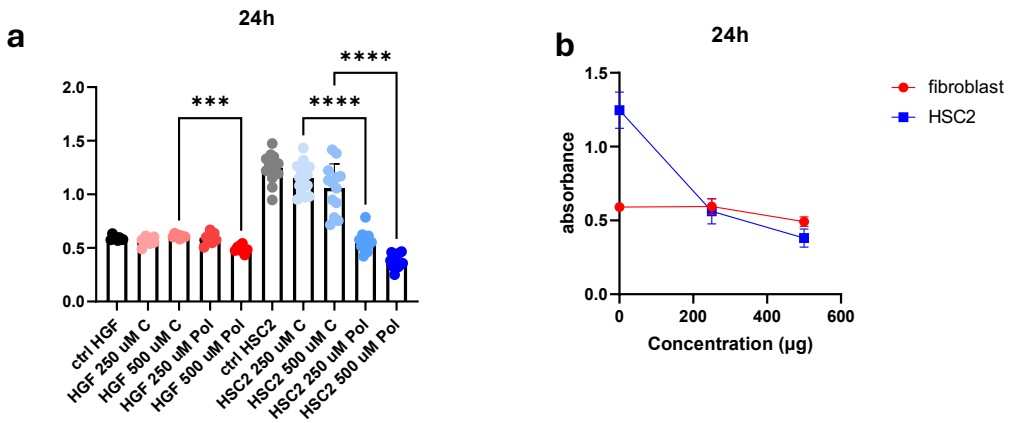

Figure 26. Dose-dependent reduction in cell viability in HSC2 tumor cells 24hrs after polydatin

After 48 hours of exposure, hGF cells remained largely unaffected by Pol treatment at both concentrations, while HSC2 cells continued to show a significant decrease in viability. Specifically, reductions of 31.3% and 62.8% were observed at 250 µM and 500 µM, respectively, relative to untreated controls (Figure 27A–B). These data demonstrate

that Polydatin exerts a selective cytotoxic effect on HNSCC cells, sparing non-tumor oral fibroblasts.

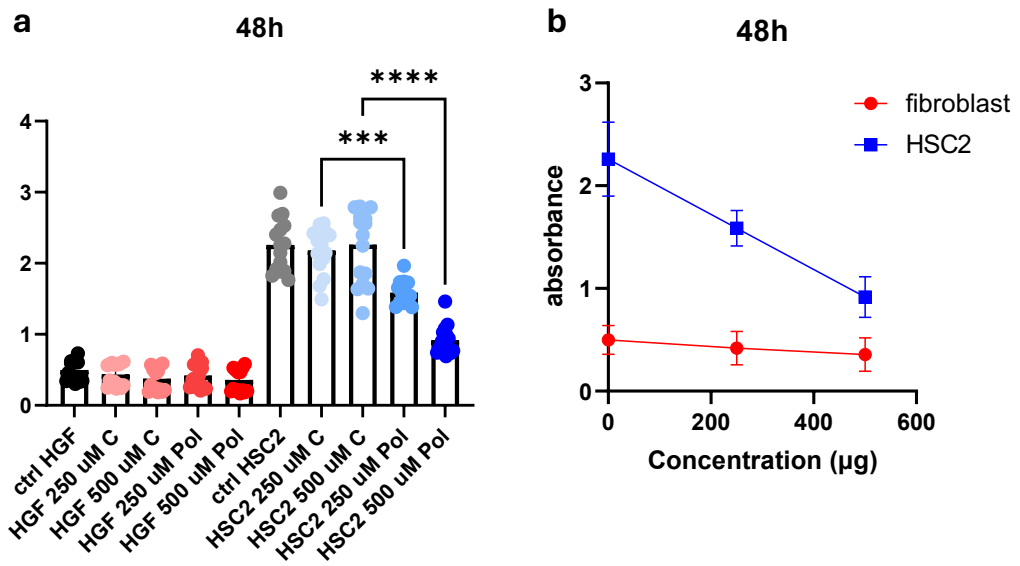

Figure 27. Dose-dependent reduction in cell viability in HSC2 tumor cells 48hrs after polydatin

3.6.2 Polydatin induces a senescence-associated transcriptional response in HNSCC cells

To investigate the molecular mechanisms underlying Pol-induced growth inhibition, the expression of genes involved in cell cycle regulation, survival, and apoptosis was analyzed by quantitative real-time PCR in HSC2 cells following treatment with 250 µM Pol.

As shown in Figure 28A, Pol treatment resulted in a significant upregulation of p21 (CDKN1A) compared to untreated controls. p21 is a cyclin-dependent kinase inhibitor that mediates cell cycle arrest and is commonly associated with the induction of cellular senescence. In contrast, Pol treatment did not significantly alter the Bcl2/Bax expression ratio (Figure 28B), indicating that short-term Pol exposure did not activate classical apoptotic pathways.

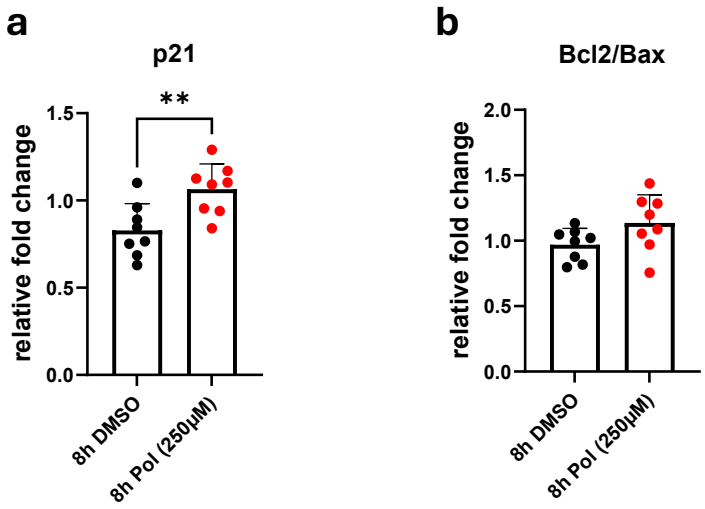

Figure 28. Relative gene expression after 8 h treatment with polydatin (250 µM).

These findings suggest that Polydatin-mediated growth inhibition in HNSCC cells is associated with the induction of a senescence-like transcriptional program, rather than apoptotic cell death.

3.6.3 Polydatin promotes antioxidant and stress-response pathways in HNSCC cells

Given the known role of oxidative stress in tumor cell fate, the expression of genes involved in the antioxidant response was evaluated following Pol treatment. Quantitative

PCR analysis demonstrated that exposure to 250 μM Pol for 8 hours significantly increased the expression of Nrf2 and Sod2 in HSC2 cells (Figures 29A–B).

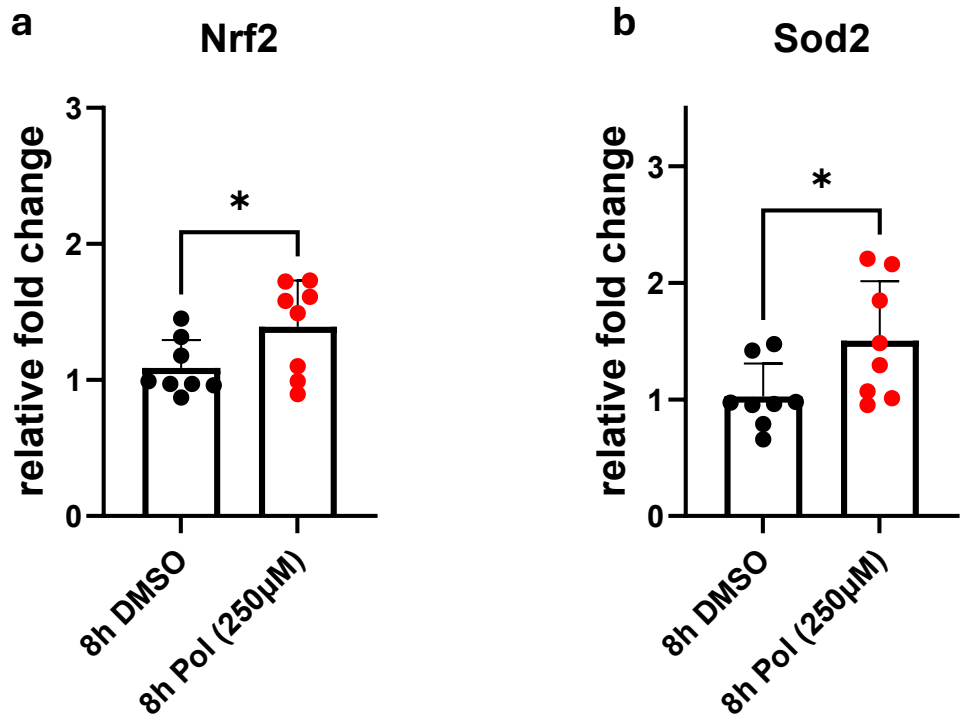

Figure 29. Relative expression of oxidative stress–related genes after 8 h treatment with polydatin

Nrf2 is a master regulator of cellular antioxidant defenses, while Sod2 encodes a mitochondrial enzyme critical for the detoxification of reactive oxygen species. The coordinated upregulation of these genes indicates activation of an Nrf2-mediated antioxidant response, which is consistent with a stress-adaptive, senescence-associated cellular state.

Together, these results indicate that Polydatin induces a non-apoptotic growth arrest in HNSCC cells, characterized by selective cytotoxicity toward tumor cells, upregulation of p21, and activation of antioxidant defense pathways.

Discussion

Head and neck squamous cell carcinoma (HNSCC) remains a major global health challenge, characterized by high incidence, poor long-term survival, and limited therapeutic options in advanced disease. [119] Despite improvements in surgical techniques, radiotherapy, and systemic treatments, survival rates have remained largely unchanged over the past decades, particularly in patients with locally advanced or recurrent disease. One of the main obstacles to therapeutic success is the marked inter-patient heterogeneity in treatment response, coupled with therapy-resistant tumor cell populations. [120]

Growing evidence indicates that cancer stem cells (CSCs) play a central role in therapeutic failure, disease recurrence, and metastasis in HNSCC. CSCs possess intrinsic properties of self-renewal, plasticity, and resistance to chemotherapy and radiotherapy, allowing them to survive conventional treatments and regenerate tumor bulk. Consequently, therapeutic strategies that fail to eradicate CSCs are unlikely to achieve durable clinical responses. [47] In this context, functional precision-medicine approaches capable of directly interrogating tumor-specific drug sensitivity represent a promising avenue to overcome treatment resistance.

ChemoID® as a functional precision-medicine tool in HNSCC

In the present study, we evaluated the clinical and biological relevance of the ChemoID® functional chemosensitivity assay in HNSCC by directly assessing drug responses in

CSC-enriched tumor populations. Our findings demonstrate a high degree of heterogeneity in chemosensitivity among patients with the same histological diagnosis, supporting the concept that empirical, guideline-based chemotherapy selection may be suboptimal for a substantial proportion of patients.

Importantly, the observed variability in drug response was independent of tumor anatomical site, as demonstrated by markedly different responses among tumors arising from the same oral subsites, including the tongue and retromolar trigone. These data reinforce the notion that HNSCC should not be treated as a biologically uniform entity and highlight the limitations of standardized treatment algorithms that do not account for patient-specific tumor biology.

While international guidelines identify cisplatin-based regimens as the cornerstone of systemic therapy for advanced HNSCC, [121-123] our results indicate that cisplatin monotherapy was not consistently the most effective treatment against CSCs in all patients. In several cases, alternative combination regimens, particularly those incorporating taxanes and fluoropyrimidines, achieved substantially higher CSC cytotoxicity. Notably, ChemoID® enabled identification of drug combinations capable of more than doubling CSC killing compared to cisplatin alone in individual patients, underscoring its potential clinical utility in optimizing treatment selection.

Beyond therapeutic efficacy, ChemoID® offers additional advantages in terms of toxicity reduction and cost-effectiveness. By excluding ineffective therapies upfront, the assay may help limit unnecessary systemic toxicity, reduce treatment-related morbidity, and avoid the economic burden associated with failed therapies. This aspect is particularly

relevant in elderly patients, in healthcare systems with limited resources, and in settings where access to targeted therapies or immunotherapies is restricted.

The representative clinical case presented in this study further supports the translational relevance of ChemoID®, illustrating how assay-guided chemotherapy selection correlated with significant radiological tumor regression in a patient deemed unsuitable for surgical intervention. While anecdotal, such cases provide proof-of-concept evidence that CSC-directed functional testing can inform clinically meaningful therapeutic decisions.

3D culture models and transcriptional plasticity in HNSCC

To better understand the biological underpinnings of CSC enrichment and therapy resistance, we performed transcriptomic profiling of patient-derived OSCC cultures grown under 2D and 3D conditions. Our results demonstrate that 3D culture systems impose a selective pressure that favors survival of a stress-resistant subpopulation with transcriptional features consistent with stemness, plasticity, and aggressive tumor behavior.

In contrast to 2D cultures, which were dominated by transcriptional programs related to extracellular matrix degradation, hyperproliferation, and replicative stress, 3D cultures activated pathways involved in cell migration, developmental signaling, and phenotypic adaptability. Overall, 3D cultures showed overexpression of genes related to pathways linked to cell proliferation, mitotic control, and migration, consistent with a condition that better mimics tumor aggressiveness and heterogeneity compared to 2D cell cultures. The enrichment of axon guidance pathways in 3D-grown tumor cells suggests

a shift toward neural-like signaling mechanisms, a phenomenon increasingly recognized as part of tumor cell plasticity[107]. Cellular plasticity is now considered a functional hallmark of cancer, allowing tumor cells to evade terminal differentiation and acquire new phenotypic states that enhance adaptability and survival. Tumor cells may dedifferentiate into progenitor-like cells, inhibit differentiation to maintain a partially undifferentiated phenotype, or even transdifferentiate into lineages of distinct origin[108]. Recent evidence shows that cancer cells can acquire neuronal characteristics, supporting a novel form of plasticity in which malignant cells adopt features typical of neural lineages [107]. Neurons are defined by the expression of lineage-specific genes, the ability to form long cytoplasmic projections (axons) guided by environmental cues, and their capacity to secrete molecules and propagate electrochemical signals. Analogously, tumor cells can exploit similar cytoskeletal mechanisms to promote migration and invasion [109]. The activation of axon guidance pathways observed in the 3D model may therefore reflect this neural-like reprogramming, whereby tumor cells adopt signaling and structural strategies reminiscent of neurons to enhance motility, invasion, and metastatic potential [107]. This finding reinforces the concept that 3D cultures better reproduce the biological complexity of tumors, including their capacity for phenotypic plasticity and microenvironmental adaptation, which are key determinants of malignancy and therapeutic resistance.

The activation of pathways such as TGF-β signaling, Reelin signaling, eNOS activation, and complement pathways in 3D cultures further supports the idea that CSC-enriched populations engage unconventional signaling networks to sustain survival, angiogenesis, and immune modulation.

The enrichment in TGF-β signaling further supports the involvement of developmental and migratory programs, often associated with epithelial–mesenchymal transition (EMT) and stem-like traits.[124]

According to recent research about Reelin's functions, it seems to be involved in processes such as cell proliferation, migration, and vascular development. [110] This suggests the potential of the cancer stem cells in increasing tumor aggressiveness, metastatic potential through unexpected pathways.

Additional enriched pathways related to angiogenesis, like eNOS activation [111,112] are consistent with adaptation to hypoxia and nutrient gradients in 3D microenvironments.

Furthermore, the Complement Activation has been shown to be related to cell dedifferentiation, proliferation, and migration, in addition to reducing apoptosis and enhancing tumor growth and increasing metastasis [113].

Taken together, these transcriptomic data validate the use of 3D culture systems as biologically relevant models for studying CSC behavior and therapeutic resistance in HNSCC. They also provide a mechanistic framework for interpreting the differential drug responses observed in functional chemosensitivity assays.

BITC as a chemosensitizing and radiosensitizing agent

Patients with HNSCC diagnosed at early stages (stages I/II) have been observed to achieve long-term survival when treated with single modality treatment, through either surgical resection or radiotherapy. However, patients with locally advanced HNSCC (stages III/IV) need most of the time a multi-modality treatment approach, including surgery, chemotherapy cocktails and radiotherapy. Neo-adjuvant or induction chemotherapy is considered an effective way for downstaging different types of cancer

in case of advanced or aggressive malignancies, data on application of this approach on HNSCC are limited and stil debated. [125,126]

In this context, the limited efficacy of standard chemotherapeutic regimens and the emergence of therapy-resistant tumor cell populations highlight the need for novel strategies capable of enhancing treatment response. We investigated the ability of the phytochemical BITC to act as a chemosensitizing agent in HNSCC, with the aim of improving the cytotoxic effects of conventional chemo-radiotherapy. Our results demonstrate that BITC significantly enhances the cytotoxic effects of chemotherapy and radiotherapy in therapy-resistant HNSCC cell lines by promoting ROS-dependent apoptotic cell death.

The ability of BITC to sensitize cancer cells to cisplatin and radiation appears to be tightly linked to intracellular redox imbalance. The rescue of cell viability following GSH pretreatment confirms that BITC-induced cytotoxicity depends on oxidative stress accumulation. GSH plays a central role in maintaining cellular redox homeostasis by neutralizing ROS and regenerating antioxidant molecules such as vitamins C and E.[127] Beyond its antioxidant function, GSH is critically involved in cancer-related processes, including apoptosis evasion and resistance to chemotherapy and radiotherapy.[128] BITC has been shown to conjugate with GSH through glutathione S-transferases, resulting in depletion of intracellular reduced GSH and consequent accumulation of ROS.[129] This redox imbalance promotes oxidative stress–mediated cytotoxicity.

These findings are particularly relevant in the context of CSC biology, as CSCs are known to maintain enhanced antioxidant capacity to survive genotoxic stress. By overwhelming this protective mechanism, BITC may help overcome one of the key barriers to effective

CSC eradication. Importantly, BITC is derived from dietary isothiocyanates found in cruciferous vegetables, compounds that have demonstrated safety and bioavailability in clinical settings.[130] This raises the intriguing possibility that BITC-based interventions could be integrated as low-toxicity adjuvants to conventional HNSCC therapy.

Polydatin as a metabolic modulator and senescence-inducing agent

In parallel, we investigated Polydatin, a natural polyphenolic compound, as a potential therapeutic agent targeting metabolic vulnerabilities in HNSCC. Our results showed a significant dose and time dependent reduction in cell viability in HSC2 cells after treatment with polydatin, while healthy gingival fibroblasts were only minimally affected by the treatment. Moreover, the results indicated that Pol exerted its action in HSC2 cells primarily through the induction of cellular senescence and the activation of the oxidant metabolism.

Cells in tumors, including HNSCC, exhibit elevated levels of oxidative stress and are highly dependent on glycolysis and altered mitochondrial dynamics for survival and proliferation [131]. Cancer cells respond to oxidative stress by modifying signaling pathways that influence ROS metabolism, and this process contributes to tumor progression [132-134]. Our results therefore supported the interesting hypothesis that Pol exploited this metabolic vulnerability of tumor cells by promoting oxidative metabolism, thus promoting senescence. Healthy cells, on the other hand, showed stable metabolic activity and were largely unaffected by Pol treatment. These data indicate that Pol predominantly targets cancer cells with minimal impact on healthy cells, demonstrating

a favorable toxicity profile, which is of particular interest for its potential clinical application.

We further investigated the effects of Pol on cell cycle regulation. p21 is a key cell cycle regulator that inhibits the G1–S transition[135], and has been associated with tumor progression and poor prognosis, including in HNSCC.[136-138]. Our data indicate that the early response of HNSCC cells to Pol is primarily mediated by p21-driven cell cycle arrest rather than apoptosis. This interpretation is supported by the absence of significant changes in the Bcl2/Bax ratio following short-term Pol exposure, suggesting that canonical apoptotic pathways are not initially activated. This mechanism differs from that reported in other tumor models, such as osteosarcoma, where Pol has been shown to induce apoptosis [139].

Beyond its effects on cell cycle control, Pol also modulated the oxidative stress response. We observed an upregulation of Nrf2 and Sod2, two key components of the antioxidant defense system. Activation of Nrf2, a master regulator of oxidative stress responses, [140] suggests that Pol acts as a metabolic modulator capable of altering redox homeostasis in HNSCC cells, in line with previous reports[141]. The increased expression of Sod2, a mitochondrial enzyme involved in detoxification of superoxide radicals, [142] further supports the hypothesis that Pol induces a metabolic shift in tumor cells. Specifically, Pol appears to redirect HNSCC cell metabolism away from glycolysis toward mitochondrial oxidative metabolism, a process that may contribute to growth arrest and senescence. [143]

Although Pol has demonstrated antitumor activity in several cancer types, including osteosarcoma,[141] breast,[144] and cervical cancer,[145] its role in HNSCC has remained largely unexplored. The ability of Pol to preferentially affect tumor cells while

sparing healthy cells highlights its favorable toxicity profile and supports its potential use as an adjuvant or preventive strategy in a tumor type characterized by high recurrence rates, metabolic plasticity, and therapeutic resistance. Further studies are warranted to assess the long-term effects of Pol and to elucidate the signaling networks involved, as well as potential synergistic interactions with radiotherapy or immunotherapy in translational settings.

Conclusions and future perspectives

Collectively, this work establishes a precision oncology framework for HNSCC that integrates functional CSC-directed chemosensitivity testing, transcriptional profiling in biologically relevant 3D models, and evaluation of bioactive compounds targeting tumor plasticity and redox balance. By addressing both inter-patient heterogeneity and intrinsic therapy resistance, this approach offers a rational strategy to improve therapeutic outcomes while minimizing toxicity.

Future studies should focus on prospective clinical validation of ChemoID® in HNSCC, longitudinal monitoring of CSC evolution during treatment, and exploration of combinatorial strategies integrating BITC, Polydatin, and standard therapies. Such efforts may ultimately contribute to more effective, personalized, and sustainable treatment paradigms for patients with head and neck cancer.

References

1. Johnson, D.E.; Burtness, B.; Leemans, C.R.; Lui, V.W.Y.; Bauman, J.E.; Grandis, J.R. Head and neck squamous cell carcinoma. *Nature Reviews Disease Primers* **2020**, *6*, 92, doi:10.1038/s41572-020-00224-3.
2. Ervik, M.; Lam, F.; Laversanne, M.; Colombet, M.; Ferlay, J.; Miranda-Filho, A.; Bray, F. Global Cancer Observatory: Cancer Over Time. Available online: https://gco.iarc.who.int/overtime (accessed on 08/22/25).
3. Caponio, V.C.A.; Zhurakivska, K.; Mascitti, M.; Togni, L.; Spirito, F.; Cirillo, N.; Lo Muzio, L.; Troiano, G. High-risk TP53 mutations predict poor primary treatment response of patients with head and neck squamous cell carcinoma. *Oral Dis* **2023**, doi:10.1111/odi.14698.
4. Society, A.C. *Cancer Facts & Figures 2025*; 2025.
5. Lop, J.; Venegas, M.D.P.; Pujol, A.; Sauter, B.; Vásquez, R.; Casasayas, M.; Quer, M.; León, X. Causes of long-term mortality in patients with head and neck squamous cell carcinomas. *Eur Arch Otorhinolaryngol* **2022**, *279*, 3657-3664, doi:10.1007/s00405-021-07211-8.
6. Conde-Lopez, C.; Marripati, D.; Elkabets, M.; Hess, J.; Kurth, I. Unravelling the Complexity of HNSCC Using Single-Cell Transcriptomics. *Cancers (Basel)* **2024**, *16*, doi:10.3390/cancers16193265.
7. Spirito, F.; Nocini, R.; Mori, G.; Albanese, M.; Georgakopoulou, E.A.; Sivaramakrishnan, G.; Khalil, B.; Špiljak, B.; Surya, V.; Mishra, D.; et al. The Potential of Oncolytic Virotherapy in the Treatment of Head and Neck Cancer: A Comprehensive Review. *International Journal of Molecular Sciences* **2024**, *25*, doi:10.3390/ijms252312990.
8. Fasano, M.; D'Onofrio, I.; Belfiore, M.P.; Angrisani, A.; Caliendo, V.; Della Corte, C.M.; Pirozzi, M.; Facchini, S.; Caterino, M.; Guida, C.; et al. Head and Neck Squamous Cell Carcinoma in Elderly Patients: Role of Radiotherapy and Chemotherapy. *Cancers* **2022**, *14*, 472.
9. Patel, S.; Carpenter, W.; Tyree, S.; Couch, M.; Weissler, M.; Hackman, T.; Hayes, D.; Shores, C.; Chera, B. Increasing Incidence of Oral Tongue Squamous Cell Carcinoma in Young White Women, Age 18 to 44 Years. *Journal of clinical oncology : official journal of the American Society of Clinical Oncology* **2011**, *29*, 1488-1494, doi:10.1200/JCO.2010.31.7883.
10. Barsouk, A.; Aluru, J.S.; Rawla, P.; Saginala, K.; Barsouk, A. Epidemiology, Risk Factors, and Prevention of Head and Neck Squamous Cell Carcinoma. *Med Sci (Basel)* **2023**, *11*, doi:10.3390/medsci11020042.
11. Luo, Z.; Huang, Y.; Ye, R.; Yin, M. Global Burden and Gender Disparities in Head and Neck Cancers Among Adults Aged 40-64, 1990-2021: A Systematic Analysis From the Global Burden of Disease Study 2021. *Cancer Rep (Hoboken)* **2025**, *8*, e70287, doi:10.1002/cnr2.70287.
12. Cheong, S.C.; Vatanasapt, P.; Yi-Hsin, Y.; Zain, R.B.; Kerr, A.R.; Johnson, N.W. Oral cancer in South East Asia:Current status and future directions. *Translational Research in Oral Oncology* **2017**, *2*, 2057178X17702921, doi:10.1177/2057178x17702921.
13. Oishi, N.; Orozco-Núñez, S.; Alba-García, J.R.; Gimeno-Coret, M.; Zapater, E. Survival and Prognostic Factors in Unresectable Head and Neck Cancer Patients. *J Clin Med* **2025**, *14*, doi:10.3390/jcm14155517.
14. AIOM. I numeri del cancro in Italia **2025**.

15. AIOM. I numeri del cancro in Italia 2022. **2022**.
16. Nokovitch, L.; Maquet, C.; Crampon, F.; Taihi, I.; Roussel, L.M.; Obongo, R.; Virard, F.; Fervers, B.; Deneuve, S. Oral Cavity Squamous Cell Carcinoma Risk Factors: State of the Art. *J Clin Med* **2023**, *12*, doi:10.3390/jcm12093264.
17. Jethwa, A.R.; Khariwala, S.S. Tobacco-related carcinogenesis in head and neck cancer. *Cancer Metastasis Rev* **2017**, *36*, 411-423, doi:10.1007/s10555-017-9689-6.
18. Li, Y.; Hecht, S.S. Carcinogenic components of tobacco and tobacco smoke: A 2022 update. *Food Chem Toxicol* **2022**, *165*, 113179, doi:10.1016/j.fct.2022.113179.
19. Xue, J.; Yang, S.; Seng, S. Mechanisms of Cancer Induction by Tobacco-Specific NNK and NNN. *Cancers* **2014**, *6*, 1138-1156.
20. Centers for Disease, C.; Prevention; National Center for Chronic Disease, P.; Health, P.; Office on, S.; Health. How Tobacco Smoke Causes Disease: The Biology and Behavioral Basis for Smoking-Attributable Disease. *A Report of the Surgeon General* **2010**, Cancer.
21. Sun, Q.; Jin, C. Cell signaling and epigenetic regulation of nicotine-induced carcinogenesis. *Environ Pollut* **2024**, *345*, 123426, doi:10.1016/j.envpol.2024.123426.
22. Schaal, C.; Chellappan, S.P. Nicotine-Mediated Cell Proliferation and Tumor Progression in Smoking-Related Cancers. *Molecular Cancer Research* **2014**, *12*, 14-23, doi:10.1158/1541-7786.Mcr-13-0541.
23. Vu, T.; Jin, L.; Datta, P.K. Effect of Cigarette Smoking on Epithelial to Mesenchymal Transition (EMT) in Lung Cancer. *J Clin Med* **2016**, *5*, doi:10.3390/jcm5040044.
24. Hecht, S.S.; Hatsukami, D.K. Smokeless tobacco and cigarette smoking: chemical mechanisms and cancer prevention. *Nature Reviews Cancer* **2022**, *22*, 143-155, doi:10.1038/s41568-021-00423-4.
25. Jun, S.; Park, H.; Kim, U.J.; Lee, H.A.; Park, B.; Lee, S.Y.; Jee, S.H.; Park, H. The Combined Effects of Alcohol Consumption and Smoking on Cancer Risk by Exposure Level: A Systematic Review and Meta-Analysis. *J Korean Med Sci* **2024**, *39*, e185, doi:10.3346/jkms.2024.39.e185.
26. Dal Maso, L.; Torelli, N.; Biancotto, E.; Di Maso, M.; Gini, A.; Franchin, G.; Levi, F.; La Vecchia, C.; Serraino, D.; Polesel, J. Combined effect of tobacco smoking and alcohol drinking in the risk of head and neck cancers: a re-analysis of case-control studies using bi-dimensional spline models. *Eur J Epidemiol* **2016**, *31*, 385-393, doi:10.1007/s10654-015-0028-3.
27. Feng, L.; Wang, L. Effects of alcohol on the morphological and structural changes in oral mucosa. *Pak J Med Sci* **2013**, *29*, 1046-1049, doi:10.12669/pjms.294.3696.
28. Mizumoto, A.; Ohashi, S.; Hirohashi, K.; Amanuma, Y.; Matsuda, T.; Muto, M. Molecular Mechanisms of Acetaldehyde-Mediated Carcinogenesis in Squamous Epithelium. *International Journal of Molecular Sciences* **2017**, *18*, 1943.
29. Hennessey, P.T.; Westra, W.H.; Califano, J.A. Human papillomavirus and head and neck squamous cell carcinoma: recent evidence and clinical implications. *J Dent Res* **2009**, *88*, 300-306, doi:10.1177/0022034509333371.
30. Jain, P.; Kumar, N.; Shetty, S.C.; Kalladka, S.S.; Ramesh, P.S.; Patil, P.; Kumar, M.; Rajendra, V.K.; Devegowda, D.; Shetty, V. Prevalence of Epstein Barr Virus and Herpes Simplex Virus Among Human Papillomavirus Negative Oral Cancer Patients: A Cross-Sectional Study from South India. *Indian J Otolaryngol Head Neck Surg* **2024**, *76*, 414-421, doi:10.1007/s12070-023-04174-6.
31. G, M.; Ravi, S.S.S.; Maheswary, D.; Leela, K.V.; Harikumar Lathakumari, R.; K, S.L. Role of Candida albicans in chronic inflammation and the development of oral squamous cell carcinoma. *Cancer Pathog Ther* **2025**, *3*, 402-410, doi:10.1016/j.cpt.2025.03.002.

32. Darnton-Hill, I. Public Health Aspects in the Prevention and Control of Vitamin Deficiencies. *Curr Dev Nutr* **2019**, *3*, nzz075, doi:10.1093/cdn/nzz075.
33. Haase, K.; Piwonski, I.; Stromberger, C.; Thieme, N.; Heiland, M.; Beck-Broichsitter, B.; Hofmann, V.M.; Kofla, G.; Sander, S.; Keilholz, U.; et al. Incidence and survival of HNSCC patients living with HIV compared with HIV-negative HNSCC patients. *Eur Arch Otorhinolaryngol* **2021**, *278*, 3941-3953, doi:10.1007/s00405-020-06573-9.
34. De Cecco, L.; Nicolau, M.; Giannoccaro, M.; Daidone, M.G.; Bossi, P.; Locati, L.; Licitra, L.; Canevari, S. Head and neck cancer subtypes with biological and clinical relevance: Meta-analysis of gene-expression data. *Oncotarget* **2015**, *6*, 9627-9642, doi:10.18632/oncotarget.3301.
35. Takes, R.P.; Rinaldo, A.; Silver, C.E.; Haigentz, M., Jr.; Woolgar, J.A.; Triantafyllou, A.; Mondin, V.; Paccagnella, D.; de Bree, R.; Shaha, A.R.; et al. Distant metastases from head and neck squamous cell carcinoma. Part I. Basic aspects. *Oral Oncol* **2012**, *48*, 775-779, doi:10.1016/j.oraloncology.2012.03.013.
36. Lee, A.M.; Weaver, A.N.; Acosta, P.; Harris, L.; Bowles, D.W. Review of Current and Future Medical Treatments in Head and Neck Squamous Cell Carcinoma. *Cancers* **2024**, *16*, 3488.
37. Liu, Z.; Chen, J.; Ren, Y.; Liu, S.; Ba, Y.; Zuo, A.; Luo, P.; Cheng, Q.; Xu, H.; Han, X. Multi-stage mechanisms of tumor metastasis and therapeutic strategies. *Signal Transduction and Targeted Therapy* **2024**, *9*, 270, doi:10.1038/s41392-024-01955-5.
38. Chen, Y.; Zhong, N.-N.; Cao, L.-M.; Liu, B.; Bu, L.-L. Surgical margins in head and neck squamous cell carcinoma: A narrative review. *International Journal of Surgery* **2024**, *110*.
39. Evans, M.; Bonomo, P.; Chan, P.C.; Chua, M.L.K.; Eriksen, J.G.; Hunter, K.; Jones, T.M.; Laskar, S.G.; Maroldi, R.; O'Sullivan, B.; et al. Post-operative radiotherapy for oral cavity squamous cell carcinoma: Review of the data guiding the selection and the delineation of post-operative target volumes. *Radiotherapy and Oncology* **2025**, *207*, 110880, doi:https://doi.org/10.1016/j.radonc.2025.110880.
40. Mohamad, I.; Glaun, M.D.E.; Prabhash, K.; Busheri, A.; Lai, S.Y.; Noronha, V.; Hosni, A. Current Treatment Strategies and Risk Stratification for Oral Carcinoma. *Am Soc Clin Oncol Educ Book* **2023**, *43*, e389810, doi:10.1200/EDBK_389810.
41. Sanabria, A.; Bradley, P.; de Bree, R.; Guntinas-Lichius, O.; Hamoir, M.; Kowalski, L.P.; Rodrigo, J.P.; Strojan, P.; Vander Poorten, V.; Ferlito, A. Deciding whether to do elective neck dissection in patients with salivary gland tumors with no evidence of neck lymph node metastasis. *Eur Ann Otorhinolaryngol Head Neck Dis* **2025**, *142*, 135-142, doi:10.1016/j.anorl.2025.02.001.
42. Pfister, D.G.; Spencer, S.; Adelstein, D.; Adkins, D.; Anzai, Y.; Brizel, D.M.; Bruce, J.Y.; Busse, P.M.; Caudell, J.J.; Cmelak, A.J.; et al. Head and Neck Cancers, Version 2.2020, NCCN Clinical Practice Guidelines in Oncology. *J Natl Compr Canc Netw* **2020**, *18*, 873-898, doi:10.6004/jnccn.2020.0031.
43. Bernier, J.; Cooper, J.S.; Pajak, T.F.; van Glabbeke, M.; Bourhis, J.; Forastiere, A.; Ozsahin, E.M.; Jacobs, J.R.; Jassem, J.; Ang, K.-K.; et al. Defining risk levels in locally advanced head and neck cancers: A comparative analysis of concurrent postoperative radiation plus chemotherapy trials of the EORTC (#22931) and RTOG (# 9501). *Head & Neck* **2005**, *27*, 843-850, doi:https://doi.org/10.1002/hed.20279.
44. Mordzińska-Rak, A.; Telejko, I.; Adamczuk, G.; Trombik, T.; Stepulak, A.; Błaszczak, E. Advancing Head and Neck Cancer Therapies: From Conventional Treatments to Emerging Strategies. *Biomedicines* **2025**, *13*, 1046.

45. Canning, M.; Guo, G.; Yu, M.; Myint, C.; Groves, M.W.; Byrd, J.K.; Cui, Y. Heterogeneity of the Head and Neck Squamous Cell Carcinoma Immune Landscape and Its Impact on Immunotherapy. *Front Cell Dev Biol* **2019**, *7*, 52, doi:10.3389/fcell.2019.00052.
46. Bianchi, G.; Ghobrial, I.M. Biological and Clinical Implications of Clonal Heterogeneity and Clonal Evolution in Multiple Myeloma. *Curr Cancer Ther Rev* **2014**, *10*, 70-79, doi:10.2174/1573394710021411241214O4.
47. Testa, U.; Pelosi, E.; Castelli, G. Cancer stem cell targeted therapies. *Ann Ist Super Sanita* **2020**, *56*, 336-350, doi:10.4415/ANN_20_03_12.
48. Reya, T.; Morrison, S.J.; Clarke, M.F.; Weissman, I.L. Stem cells, cancer, and cancer stem cells. *Nature* **2001**, *414*, 105-111, doi:10.1038/35102167.
49. Chu, X.; Tian, W.; Ning, J.; Xiao, G.; Zhou, Y.; Wang, Z.; Zhai, Z.; Tanzhu, G.; Yang, J.; Zhou, R. Cancer stem cells: advances in knowledge and implications for cancer therapy. *Signal Transduct Target Ther* **2024**, *9*, 170, doi:10.1038/s41392-024-01851-y.
50. Ghorbian, S. Cancer cell plasticity and therapeutic resistance: mechanisms, crosstalk, and translational perspectives. *Hereditas* **2025**, *162*, 188, doi:10.1186/s41065-025-00564-8.
51. Loh, J.-J.; Ma, S. Hallmarks of cancer stemness. *Cell Stem Cell* **2024**, *31*, 617-639, doi:https://doi.org/10.1016/j.stem.2024.04.004.
52. Lee, H.; Kim, B.; Park, J.; Park, S.; Yoo, G.; Yum, S.; Kang, W.; Lee, J.M.; Youn, H.; Youn, B. Cancer stem cells: landscape, challenges and emerging therapeutic innovations. *Signal Transduct Target Ther* **2025**, *10*, 248, doi:10.1038/s41392-025-02360-2.
53. Virchow, R. Editorial. Virchows Arch. Pathol. Anat. Physiol. Klin. Med. 3, 23. **1855**.
54. Till, J.E.; Mc, C.E. A direct measurement of the radiation sensitivity of normal mouse bone marrow cells. *Radiat Res* **1961**, *14*, 213-222.
55. Southam, C., Brunschwig, A., . Quantitative studies of autotransplantation of human cancer. . *Cancer* **1961**, 461-462.
56. Islam, F.; Qiao, B.; Smith, R.A.; Gopalan, V.; Lam, A.K. Cancer stem cell: fundamental experimental pathological concepts and updates. *Exp Mol Pathol* **2015**, *98*, 184-191, doi:10.1016/j.yexmp.2015.02.002.
57. Hamburger, A.W.; Salmon, S.E. Primary bioassay of human tumor stem cells. *Science* **1977**, *197*, 461-463, doi:10.1126/science.560061.
58. Lapidot, T.; Sirard, C.; Vormoor, J.; Murdoch, B.; Hoang, T.; Caceres-Cortes, J.; Minden, M.; Paterson, B.; Caligiuri, M.A.; Dick, J.E. A cell initiating human acute myeloid leukaemia after transplantation into SCID mice. *Nature* **1994**, *367*, 645-648, doi:10.1038/367645a0.
59. Bonnet, D.; Dick, J.E. Human acute myeloid leukemia is organized as a hierarchy that originates from a primitive hematopoietic cell. *Nat Med* **1997**, *3*, 730-737, doi:10.1038/nm0797-730.
60. Al-Hajj, M.; Wicha, M.S.; Benito-Hernandez, A.; Morrison, S.J.; Clarke, M.F. Prospective identification of tumorigenic breast cancer cells. *Proc Natl Acad Sci U S A* **2003**, *100*, 3983-3988, doi:10.1073/pnas.0530291100.
61. Singh, S.K.; Clarke, I.D.; Terasaki, M.; Bonn, V.E.; Hawkins, C.; Squire, J.; Dirks, P.B. Identification of a cancer stem cell in human brain tumors. *Cancer Res* **2003**, *63*, 5821-5828.
62. Todaro, M.; Alea, M.P.; Di Stefano, A.B.; Cammareri, P.; Vermeulen, L.; Iovino, F.; Tripodo, C.; Russo, A.; Gulotta, G.; Medema, J.P.; et al. Colon cancer stem cells dictate tumor growth and resist cell death by production of interleukin-4. *Cell Stem Cell* **2007**, *1*, 389-402, doi:10.1016/j.stem.2007.08.001.

63. O'Brien, C.A.; Pollett, A.; Gallinger, S.; Dick, J.E. A human colon cancer cell capable of initiating tumour growth in immunodeficient mice. *Nature* **2007**, *445*, 106-110, doi:10.1038/nature05372.
64. Kelly, P.N.; Dakic, A.; Adams, J.M.; Nutt, S.L.; Strasser, A. Tumor growth need not be driven by rare cancer stem cells. *Science* **2007**, *317*, 337, doi:10.1126/science.1142596.
65. Boiko, A.D.; Razorenova, O.V.; van de Rijn, M.; Swetter, S.M.; Johnson, D.L.; Ly, D.P.; Butler, P.D.; Yang, G.P.; Joshua, B.; Kaplan, M.J.; et al. Human melanoma-initiating cells express neural crest nerve growth factor receptor CD271. *Nature* **2010**, *466*, 133-137, doi:10.1038/nature09161.
66. Rosen, J.M.; Jordan, C.T. The increasing complexity of the cancer stem cell paradigm. *Science* **2009**, *324*, 1670-1673, doi:10.1126/science.1171837.
67. Walcher, L.; Kistenmacher, A.K.; Suo, H.; Kitte, R.; Dluczek, S.; Strauß, A.; Blaudszun, A.R.; Yevsa, T.; Fricke, S.; Kossatz-Boehlert, U. Cancer Stem Cells-Origins and Biomarkers: Perspectives for Targeted Personalized Therapies. *Front Immunol* **2020**, *11*, 1280, doi:10.3389/fimmu.2020.01280.
68. Thankamony, A.P.; Saxena, K.; Murali, R.; Jolly, M.K.; Nair, R. Cancer Stem Cell Plasticity - A Deadly Deal. *Front Mol Biosci* **2020**, *7*, 79, doi:10.3389/fmolb.2020.00079.
69. Peitzsch, C.; Nathansen, J.; Schniewind, S.I.; Schwarz, F.; Dubrovska, A. Cancer Stem Cells in Head and Neck Squamous Cell Carcinoma: Identification, Characterization and Clinical Implications. *Cancers (Basel)* **2019**, *11*, doi:10.3390/cancers11050616.
70. Baghai Naini, F.; Aminishakib, P.; Abdollahi, A.; Hodjat, M.; Mohammadpour, H.; Kardouni Khoozestani, N. Relative Expression of OCT4, SOX2 and NANOG in Oral Squamous Cell Carcinoma Versus Adjacent Non- Tumor Tissue. *Asian Pac J Cancer Prev* **2019**, *20*, 1649-1654, doi:10.31557/apjcp.2019.20.6.1649.
71. Pedregal-Mallo, D.; Hermida-Prado, F.; Granda-Díaz, R.; Montoro-Jiménez, I.; Allonca, E.; Pozo-Agundo, E.; Álvarez-Fernández, M.; Álvarez-Marcos, C.; García-Pedrero, J.M.; Rodrigo, J.P. Prognostic Significance of the Pluripotency Factors NANOG, SOX2, and OCT4 in Head and Neck Squamous Cell Carcinomas. *Cancers (Basel)* **2020**, *12*, doi:10.3390/cancers12071794.
72. Major, A.G.; Pitty, L.P.; Farah, C.S. Cancer stem cell markers in head and neck squamous cell carcinoma. *Stem Cells Int* **2013**, *2013*, 319489, doi:10.1155/2013/319489.
73. Acharya, S.K.; Shai, S.; Choon, Y.F.; Gunardi, I.; Hartanto, F.K.; Kadir, K.; Roychoudhury, A.; Amtha, R.; Vincent-Chong, V.K. Cancer Stem Cells in Oral Squamous Cell Carcinoma: A Narrative Review on Experimental Characteristics and Methodological Challenges. *Biomedicines* **2024**, *12*, 2111.
74. Szafarowski, T.; Sierdziński, J.; Ludwig, N.; Głuszko, A.; Filipowska, A.; Szczepański, M.J. Assessment of cancer stem cell marker expression in primary head and neck squamous cell carcinoma shows prognostic value for aldehyde dehydrogenase (ALDH1A1). *European Journal of Pharmacology* **2020**, *867*, 172837, doi:https://doi.org/10.1016/j.ejphar.2019.172837.
75. Li, C.; Wu, J.J.; Hynes, M.; Dosch, J.; Sarkar, B.; Welling, T.H.; Pasca di Magliano, M.; Simeone, D.M. c-Met Is a Marker of Pancreatic Cancer Stem Cells and Therapeutic Target. *Gastroenterology* **2011**, *141*, 2218-2227.e2215, doi:https://doi.org/10.1053/j.gastro.2011.08.009.
76. Nwokolo, G.C.; Ganesan, T.S.; Pors, K.; Falconer, R.A.; Smarakan, S. Cancer stem cells in focus: Deciphering the dynamic functional landscape of stemness in cancer.

Biochimica et Biophysica Acta (BBA) - Reviews on Cancer **2025**, *1880*, 189440, doi:https://doi.org/10.1016/j.bbcan.2025.189440.

77. Cao, J.; Bhatnagar, S.; Wang, J.; Qi, X.; Prabha, S.; Panyam, J. Cancer stem cells and strategies for targeted drug delivery. *Drug Deliv Transl Res* **2021**, *11*, 1779-1805, doi:10.1007/s13346-020-00863-9.
78. Edmondson, R.; Broglie, J.J.; Adcock, A.F.; Yang, L. Three-dimensional cell culture systems and their applications in drug discovery and cell-based biosensors. *Assay Drug Dev Technol* **2014**, *12*, 207-218, doi:10.1089/adt.2014.573.
79. Sattar, T.; Nazir, I.; Jabbar, M.; Malik, J.; Afzal, S.; Hanif, S.; Mosaddad, S.A.; Hussain, A.; Tebyaniyan, H. Current innovations in head and neck cancer: From diagnostics to therapeutics. *Oncol Res* **2025**, *33*, 1019-1032, doi:10.32604/or.2025.060601.
80. Rivera, C. Essentials of oral cancer. *Int J Clin Exp Pathol* **2015**, *8*, 11884-11894.
81. Okamoto, O.K.; Perez, J.F. Targeting cancer stem cells with monoclonal antibodies: a new perspective in cancer therapy and diagnosis. *Expert Rev Mol Diagn* **2008**, *8*, 387-393, doi:10.1586/14737159.8.4.387.
82. Rajan, P.; Srinivasan, R. Targeting cancer stem cells in cancer prevention and therapy. *Stem Cell Rev* **2008**, *4*, 211-216, doi:10.1007/s12015-008-9037-x.
83. Ranjan, T.; Howard, C.M.; Yu, A.; Xu, L.; Aziz, K.; Jho, D.; Leonardo, J.; Hameed, M.A.; Karlovits, S.M.; Wegner, R.E.; et al. Cancer Stem Cell Chemotherapeutics Assay for Prospective Treatment of Recurrent Glioblastoma and Progressive Anaplastic Glioma: A Single-Institution Case Series. *Transl Oncol* **2020**, *13*, 100755, doi:10.1016/j.tranon.2020.100755.
84. Howard, C.M.; Valluri, J.; Alberico, A.; Julien, T.; Mazagri, R.; Marsh, R.; Alastair, H.; Cortese, A.; Griswold, M.; Wang, W.; et al. Analysis of Chemopredictive Assay for Targeting Cancer Stem Cells in Glioblastoma Patients. *Transl Oncol* **2017**, *10*, 241-254, doi:10.1016/j.tranon.2017.01.008.
85. Cortese, A.; Pantaleo, G.; Amato, M.; Lawrence, L.; Mayes, V.; Brown, L.; Sarno, M.R.; Valluri, J.; Claudio, P.P. A new complementary procedure for patients affected by head and neck cancer: Chemo-predictive assay. *Int J Surg Case Rep* **2016**, *26*, 42-46, doi:10.1016/j.ijscr.2016.07.013.
86. Batlle, E.; Clevers, H. Cancer stem cells revisited. *Nat Med* **2017**, *23*, 1124-1134, doi:10.1038/nm.4409.
87. Shibata, M.; Hoque, M.O. Targeting Cancer Stem Cells: A Strategy for Effective Eradication of Cancer. *Cancers (Basel)* **2019**, *11*, doi:10.3390/cancers11050732.
88. Spirito, F.; Claudio, P.P.; Howard, C.M.; Valluri, J.; Denning, K.L.; Muzio, L.L.; Cortese, A. A New and Effective Procedure for Advanced Oral Cancer Therapy: The Potential of a Cancer Stem Cell Assay in Guiding Chemotherapy. *Transl Med UniSa* **2023**, *25*, 16-27, doi:10.37825/2239-9747.1042.
89. Zhao, W.; Luo, Q.; Yuan, B.; Duan, H.; Jiang, S. Unraveling resistance to immune checkpoint inhibitors in HNSCC: from mechanisms to combination therapies. *Cancer Drug Resistance* **2025**, *8*, 63, doi:10.20517/cdr.2025.153.
90. Dioguardi, M.; Ballini, A.; Sovereto, D.; Spirito, F.; Cazzolla, A.P.; Aiuto, R.; Crincoli, V.; Caloro, G.A.; Lo Muzio, L. Application of the Extracts of Punica granatum in Oral Cancer: Scoping Review. *Dent J (Basel)* **2022**, *10*, doi:10.3390/dj10120234.
91. Ballini, A.; Zhurakivska, K.; Troiano, G.; Muzio, L.L.; Caponio, V.C.A.; Spirito, F.; Porro, R.; Rella, M.; Cantore, S.; Arrigoni, R.; et al. Dietary Polyphenols against Oxidative Stress in Head and Neck Cancer: What's New, What's Next. *Journal of Cancer* **2024**, *15*, 293-308, doi:10.7150/jca.90545.

92. Aljabali, A.A.A.; Obeid, M.A.; Bashatwah, R.M.; Qnais, E.; Gammoh, O.; Alqudah, A.; Mishra, V.; Mishra, Y.; Khan, M.A.; Parvez, S.; et al. Phytochemicals in Cancer Therapy: A Structured Review of Mechanisms, Challenges, and Progress in Personalized Treatment. *Chem Biodivers* **2025**, *22*, e202402479, doi:10.1002/cbdv.202402479.
93. Shuvalov, O.; Kirdeeva, Y.; Daks, A.; Fedorova, O.; Parfenyev, S.; Simon, H.U.; Barlev, N.A. Phytochemicals Target Multiple Metabolic Pathways in Cancer. *Antioxidants (Basel)* **2023**, *12*, doi:10.3390/antiox12112012.
94. Kattel, S.; Antonious, G.F. Glucosinolates in Cruciferous Vegetables: Genetic and Environmental Regulation, Metabolic Pathways, and Cancer-Preventive Mechanisms. *International Journal of Plant Biology* **2025**, *16*, 58.
95. Hoch, C.C.; Shoykhet, M.; Weiser, T.; Griesbaum, L.; Petry, J.; Hachani, K.; Multhoff, G.; Bashiri Dezfouli, A.; Wollenberg, B. Isothiocyanates in medicine: A comprehensive review on phenylethyl-, allyl-, and benzyl-isothiocyanates. *Pharmacological Research* **2024**, *201*, 107107, doi:https://doi.org/10.1016/j.phrs.2024.107107.
96. Mitsiogianni, M.; Koutsidis, G.; Mavroudis, N.; Trafalis, D.T.; Botaitis, S.; Franco, R.; Zoumpourlis, V.; Amery, T.; Galanis, A.; Pappa, A.; et al. The Role of Isothiocyanates as Cancer Chemo-Preventive, Chemo-Therapeutic and Anti-Melanoma Agents. *Antioxidants (Basel)* **2019**, *8*, doi:10.3390/antiox8040106.
97. Shoaib, S.; Khan, F.B.; Alsharif, M.A.; Malik, M.S.; Ahmed, S.A.; Jamous, Y.F.; Uddin, S.; Tan, C.S.; Ardianto, C.; Tufail, S.; et al. Reviewing the Prospective Pharmacological Potential of Isothiocyanates in Fight against Female-Specific Cancers. *Cancers (Basel)* **2023**, *15*, doi:10.3390/cancers15082390.
98. Wolf, M.A.; Claudio, P.P. Benzyl isothiocyanate inhibits HNSCC cell migration and invasion, and sensitizes HNSCC cells to cisplatin. *Nutr Cancer* **2014**, *66*, 285-294, doi:10.1080/01635581.2014.868912.
99. Lin, J.F.; Tsai, T.F.; Yang, S.C.; Lin, Y.C.; Chen, H.E.; Chou, K.Y.; Hwang, T.I. Benzyl isothiocyanate induces reactive oxygen species-initiated autophagy and apoptosis in human prostate cancer cells. *Oncotarget* **2017**, *8*, 20220-20234, doi:10.18632/oncotarget.15643.
100. Zhao, G.; Yang, L.; Zhong, W.; Hu, Y.; Tan, Y.; Ren, Z.; Ban, Q.; Yang, C.S.; Wang, Y.; Wang, Z. Polydatin, A Glycoside of Resveratrol, Is Better Than Resveratrol in Alleviating Non-alcoholic Fatty Liver Disease in Mice Fed a High-Fructose Diet. *Front Nutr* **2022**, *9*, 857879, doi:10.3389/fnut.2022.857879.
101. Karami, A.; Fakhri, S.; Kooshki, L.; Khan, H. Polydatin: Pharmacological Mechanisms, Therapeutic Targets, Biological Activities, and Health Benefits. *Molecules* **2022**, *27*, doi:10.3390/molecules27196474.
102. Liu, G.; Yao, X.; Hou, Y.; Deng, W.; Zhang, L.; Li, S.; Huang, P.; Chang, W.; Huang, H.; Shi, L.; et al. Metabolomic and transcriptomic profiling of HNSCC identifies AMIGO2 as a therapeutic target modulating tumor microenvironment. *NPJ Precis Oncol* **2025**, *9*, 358, doi:10.1038/s41698-025-01132-z.
103. Kelly, S.E.; Di Benedetto, A.; Greco, A.; Howard, C.M.; Sollars, V.E.; Primerano, D.A.; Valluri, J.V.; Claudio, P.P. Rapid selection and proliferation of CD133+ cells from cancer cell lines: chemotherapeutic implications. *PLoS One* **2010**, *5*, e10035, doi:10.1371/journal.pone.0010035.
104. Winkler, J.; Abisoye-Ogunniyan, A.; Metcalf, K.J.; Werb, Z. Concepts of extracellular matrix remodelling in tumour progression and metastasis. *Nature Communications* **2020**, *11*, 5120, doi:10.1038/s41467-020-18794-x.

105. Kapałczyńska, M.; Kolenda, T.; Przybyła, W.; Zajączkowska, M.; Teresiak, A.; Filas, V.; Ibbs, M.; Bliźniak, R.; Łuczewski, Ł.; Lamperska, K. 2D and 3D cell cultures - a comparison of different types of cancer cell cultures. *Arch Med Sci* **2018**, *14*, 910-919, doi:10.5114/aoms.2016.63743.
106. Tufail, M.; Jiang, C.-H.; Li, N. Wnt signaling in cancer: from biomarkers to targeted therapies and clinical translation. *Molecular Cancer* **2025**, *24*, 107, doi:10.1186/s12943-025-02306-w.
107. Bloomer, H.; Dame, H.B.; Parker, S.R.; Oudin, M.J. Neuronal mimicry in tumors: lessons from neuroscience to tackle cancer. *Cancer and Metastasis Reviews* **2025**, *44*, 31, doi:10.1007/s10555-025-10249-3.
108. Hanahan, D. Hallmarks of Cancer: New Dimensions. *Cancer Discov* **2022**, *12*, 31-46, doi:10.1158/2159-8290.CD-21-1059.
109. Zang, Y.; Chaudhari, K.; Bashaw, G.J. New insights into the molecular mechanisms of axon guidance receptor regulation and signaling. *Curr Top Dev Biol* **2021**, *142*, 147-196, doi:10.1016/bs.ctdb.2020.11.008.
110. Hsu, C.-Y.; Ismaeel, G.L.; Kadhim, O.; Hadi, Z.D.; Alubiady, M.H.S.; Alasheqi, M.Q.; Ali, M.S.; Ramadan, M.F.; Al-Abdeen, S.H.Z.; Muzammil, K.; et al. Beyond the brain: Reelin's emerging role in cancer pathways. *Pathology - Research and Practice* **2025**, *269*, 155901, doi:https://doi.org/10.1016/j.prp.2025.155901.
111. Gao, W.; Wang, Y.; Yu, S.; Wang, Z.; Ma, T.; Chan, A.M.; Chiu, P.K.; Ng, C.F.; Wu, D.; Chan, F.L. Endothelial nitric oxide synthase (eNOS)-NO signaling axis functions to promote the growth of prostate cancer stem-like cells. *Stem Cell Res Ther* **2022**, *13*, 188, doi:10.1186/s13287-022-02864-6.
112. Ying, L.; Hofseth, L.J. An Emerging Role for Endothelial Nitric Oxide Synthase in Chronic Inflammation and Cancer. *Cancer Research* **2007**, *67*, 1407-1410, doi:10.1158/0008-5472.Can-06-2149.
113. Afshar-Kharghan, V. The role of the complement system in cancer. *J Clin Invest* **2017**, *127*, 780-789, doi:10.1172/jci90962.
114. Clijsters, L.; Hoencamp, C.; Calis, J.J.A.; Marzio, A.; Handgraaf, S.M.; Cuitino, M.C.; Rosenberg, B.R.; Leone, G.; Pagano, M. Cyclin F Controls Cell-Cycle Transcriptional Outputs by Directing the Degradation of the Three Activator E2Fs. *Mol Cell* **2019**, *74*, 1264-1277.e1267, doi:10.1016/j.molcel.2019.04.010.
115. Teng, Y.; Wang, X.; Wang, Y.; Ma, D. Wnt/β-catenin signaling regulates cancer stem cells in lung cancer A549 cells. *Biochemical and Biophysical Research Communications* **2010**, *392*, 373-379, doi:https://doi.org/10.1016/j.bbrc.2010.01.028.
116. Liu, W.; Lu, X.; Shi, P.; Yang, G.; Zhou, Z.; Li, W.; Mao, X.; Jiang, D.; Chen, C. TNF-α increases breast cancer stem-like cells through up-regulating TAZ expression via the non-canonical NF-κB pathway. *Scientific Reports* **2020**, *10*, 1804, doi:10.1038/s41598-020-58642-y.
117. Lee, S.H.; Hong, H.S.; Liu, Z.X.; Kim, R.H.; Kang, M.K.; Park, N.-H.; Shin, K.-H. TNFα enhances cancer stem cell-like phenotype via Notch-Hes1 activation in oral squamous cell carcinoma cells. *Biochemical and Biophysical Research Communications* **2012**, *424*, 58-64, doi:https://doi.org/10.1016/j.bbrc.2012.06.065.
118. Sari, I.N.; Phi, L.T.H.; Jun, N.; Wijaya, Y.T.; Lee, S.; Kwon, H.Y. Hedgehog Signaling in Cancer: A Prospective Therapeutic Target for Eradicating Cancer Stem Cells. *Cells* **2018**, *7*, doi:10.3390/cells7110208.
119. Sung, H.; Ferlay, J.; Siegel, R.L.; Laversanne, M.; Soerjomataram, I.; Jemal, A.; Bray, F. Global Cancer Statistics 2020: GLOBOCAN Estimates of Incidence and Mortality

Worldwide for 36 Cancers in 185 Countries. *CA Cancer J Clin* **2021**, *71*, 209-249, doi:10.3322/caac.21660.
120. de Morais, E.F.; Almangush, A.; Salo, T.; da Silva, S.D.; Kujan, O.; Coletta, R.D. Emerging histopathological parameters in the prognosis of oral squamous cell carcinomas. *Histol Histopathol* **2023**, 18634, doi:10.14670/HH-18-634.
121. Hennequin, C.; Guillerm, S.; Quero, L. Combination of chemotherapy and radiotherapy: A thirty years evolution. *Cancer Radiother* **2019**, *23*, 662-665, doi:10.1016/j.canrad.2019.07.157.
122. Szturz, P.; Cristina, V.; Herrera Gomez, R.G.; Bourhis, J.; Simon, C.; Vermorken, J.B. Cisplatin Eligibility Issues and Alternative Regimens in Locoregionally Advanced Head and Neck Cancer: Recommendations for Clinical Practice. *Front Oncol* **2019**, *9*, 464, doi:10.3389/fonc.2019.00464.
123. Carlsson, L.; Bratman, S.V.; Siu, L.L.; Spreafico, A. The Cisplatin Total Dose and Concomitant Radiation in Locoregionally Advanced Head and Neck Cancer: Any Recent Evidence for Dose Efficacy? *Curr Treat Options Oncol* **2017**, *18*, 39, doi:10.1007/s11864-017-0482-0.
124. Pickup, M.; Novitskiy, S.; Moses, H.L. The roles of TGFβ in the tumour microenvironment. *Nat Rev Cancer* **2013**, *13*, 788-799, doi:10.1038/nrc3603.
125. Cai, W.L.; Helou, V.; Carlson, K.M.; Mazul, A.L.; Zandberg, D.P.; Spector, M.E.; Zevallos, J.P.; Ferris, R.L.; Contrera, K.J. Trends in the Use of Neoadjuvant Systemic Therapy for Head and Neck Squamous Cell Carcinoma. *JAMA Network Open* **2025**, *8*, e2539778-e2539778, doi:10.1001/jamanetworkopen.2025.39778.
126. Kende, P.; Mathur, Y.; Varte, V.; Tayal, S.; Patyal, N.; Landge, J. The efficacy of neoadjuvant chemotherapy as compared to upfront surgery for the management of oral squamous cell carcinoma: a systematic review and meta-analysis. *International Journal of Oral and Maxillofacial Surgery* **2024**, *53*, 1-10, doi:https://doi.org/10.1016/j.ijom.2023.03.007.
127. Georgiou-Siafis, S.K.; Tsiftsoglou, A.S. The Key Role of GSH in Keeping the Redox Balance in Mammalian Cells: Mechanisms and Significance of GSH in Detoxification via Formation of Conjugates. *Antioxidants (Basel)* **2023**, *12*, doi:10.3390/antiox12111953.
128. Gu, X.; Mu, C.; Zheng, R.; Zhang, Z.; Zhang, Q.; Liang, T. The Cancer Antioxidant Regulation System in Therapeutic Resistance. *Antioxidants (Basel)* **2024**, *13*, doi:10.3390/antiox13070778.
129. Meyer, D.J.; Crease, D.J.; Ketterer, B. Forward and reverse catalysis and product sequestration by human glutathione S-transferases in the reaction of GSH with dietary aralkyl isothiocyanates. *Biochemical Journal* **1995**, *306*, 565-569, doi:10.1042/bj3060565.
130. Singh, S.V.; Singh, K. Cancer chemoprevention with dietary isothiocyanates mature for clinical translational research. *Carcinogenesis* **2012**, *33*, 1833-1842, doi:10.1093/carcin/bgs216.
131. Jiang, H.; Zhou, L.; Zhang, H.; Yu, Z. Bioinformatic analysis of glycolysis and lactate metabolism genes in head and neck squamous cell carcinoma. *Scientific Reports* **2025**, *15*, 10781, doi:10.1038/s41598-025-94843-z.
132. Fanelli, G.; Alloisio, G.; Lelli, V.; Marini, S.; Rinalducci, S.; Gioia, M. Mechano-induced cell metabolism disrupts the oxidative stress homeostasis of SAOS-2 osteosarcoma cells. *Front Mol Biosci* **2023**, *10*, 1297826, doi:10.3389/fmolb.2023.1297826.

133. Van Loenhout, J.; Peeters, M.; Bogaerts, A.; Smits, E.; Deben, C. Oxidative Stress-Inducing Anticancer Therapies: Taking a Closer Look at Their Immunomodulating Effects. *Antioxidants (Basel)* **2020**, *9*, doi:10.3390/antiox9121188.
134. Gorrini, C.; Harris, I.S.; Mak, T.W. Modulation of oxidative stress as an anticancer strategy. *Nat Rev Drug Discov* **2013**, *12*, 931-947, doi:10.1038/nrd4002.
135. Abbas, T.; Dutta, A. p21 in cancer: intricate networks and multiple activities. *Nat Rev Cancer* **2009**, *9*, 400-414, doi:10.1038/nrc2657.
136. Ooi, L.C.; Ho, V.; Zhu, J.Z.; Lim, S.; Chung, L.; Abubakar, A.; Rutland, T.; Chua, W.; Ng, W.; Lee, M.; et al. p21 as a Predictor and Prognostic Indicator of Clinical Outcome in Rectal Cancer Patients. *International Journal of Molecular Sciences* **2024**, *25*, 725.
137. Fromowitz, F.B.; Viola, M.V.; Chao, S.; Oravez, S.; Mishriki, Y.; Finkel, G.; Grimson, R.; Lundy, J. ras p21 expression in the progression of breast cancer. *Hum Pathol* **1987**, *18*, 1268-1275, doi:10.1016/s0046-8177(87)80412-4.
138. Huang, Y.; Li, Z.; Zhong, Q.; Li, G.; Zhang, Y.; Huang, Z. Association of TBX2 and P21 expression with clinicopathological features and survival of laryngeal squamous cell carcinoma. *Int J Clin Exp Med* **2014**, *7*, 5394-5402.
139. Xu, G.; Kuang, G.; Jiang, W.; Jiang, R.; Jiang, D. Polydatin promotes apoptosis through upregulation the ratio of Bax/Bcl-2 and inhibits proliferation by attenuating the β-catenin signaling in human osteosarcoma cells. *Am J Transl Res* **2016**, *8*, 922-931.
140. Xue, D.; Zhou, X.; Qiu, J. Emerging role of NRF2 in ROS-mediated tumor chemoresistance. *Biomed Pharmacother* **2020**, *131*, 110676, doi:10.1016/j.biopha.2020.110676.
141. Cimmino, A.; Gioia, M.; Clementi, M.E.; Faraoni, I.; Marini, S.; Ciaccio, C. Polydatin-Induced Shift of Redox Balance and Its Anti-Cancer Impact on Human Osteosarcoma Cells. *Curr Issues Mol Biol* **2024**, *47*, doi:10.3390/cimb47010021.
142. Kim, Y.S.; Gupta Vallur, P.; Phaëton, R.; Mythreye, K.; Hempel, N. Insights into the Dichotomous Regulation of SOD2 in Cancer. *Antioxidants* **2017**, *6*, 86.
143. Raj, S.; Kumar, A.; Kumar, D. Regulation of Glycolysis in Head and Neck Cancer. *Adv Exp Med Biol* **2021**, *1280*, 219-230, doi:10.1007/978-3-030-51652-9_15.
144. Chen, S.; Tao, J.; Zhong, F.; Jiao, Y.; Xu, J.; Shen, Q.; Wang, H.; Fan, S.; Zhang, Y. Polydatin down-regulates the phosphorylation level of Creb and induces apoptosis in human breast cancer cell. *PLoS One* **2017**, *12*, e0176501, doi:10.1371/journal.pone.0176501.
145. Bai, L.; Ma, Y.; Wang, X.; Feng, Q.; Zhang, Z.; Wang, S.; Zhang, H.; Lu, X.; Xu, Y.; Zhao, E.; et al. Polydatin Inhibits Cell Viability, Migration, and Invasion Through Suppressing the c-Myc Expression in Human Cervical Cancer. *Front Cell Dev Biol* **2021**, *9*, 587218, doi:10.3389/fcell.2021.587218.